

**Activation of hypoxia-inducible factor signaling
modulates the RNA protein interactome in
*Caenorhabditis elegans***

Inaugural-Dissertation

zur

Erlangung des Doktorgrades

der Mathematisch-Naturwissenschaftlichen Fakultät

der Universität zu Köln

vorgelegt von

Reza Esmailie

aus Hamburg, Deutschland

Köln 2020

Erster Gutachter:

Prof. Dr. Roman-Ulrich Müller

Zweiter Gutachter:

Prof. Dr. Günter Schwarz

Vorsitzender der Prüfungskommission:

Prof. Dr. Björn Schumacher

Tag der mündlichen Prüfung: 30.10.2020

Table of Content

List of Figures	IV
List of Tables.....	V
Abbreviations.....	VI
1 Abstract.....	1
2 Zusammenfassung	2
3 Introduction.....	3
3.1 The kidney and its function.....	3
3.2 Acute kidney injury	4
3.3 Preconditioning.....	5
3.4 Hypoxia signaling	6
3.5 RNA binding proteins.....	8
3.6 Methods for the identification of RBPs.....	9
3.7 RBP target identification	10
3.8 <i>C. elegans</i> as a model organism	11
3.9 Hypoxia signaling in <i>C. elegans</i>	13
3.10 Aims	14
4 Materials and Methods	15
4.1 Materials.....	15
4.1.1 Used materials.....	15
4.1.2 Devices	16
4.1.3 Chemicals and reagents	18
4.1.4 Kits.....	20
4.1.5 Buffers.....	21
4.1.6 Software.....	23
4.1.7 Beads used	24
4.1.8 Antibodies	24
4.1.9 Worm strains.....	25
4.1.10 RNAi used	25
4.1.11 Oligonucleotides used	25
4.2 Methods.....	26
4.2.1 Worm maintenance	26
4.2.2 Molecular techniques	30

4.2.3	Mass Spectrometry	35
5	Results.....	39
5.1	RNA Interactome Capture of wild-type and <i>vhl-1(ok161)</i>	39
5.1.1	<i>vhl-1(ok161)</i> modulates the length of <i>C. elegans</i>	39
5.1.2	Establishing RNA Interactome Capture in <i>C. elegans</i>	40
5.1.3	Analyses of RNA and protein amounts reveal functioning RIC	42
5.1.4	Mass spectrometry based identification of RNA associated proteins	43
5.1.5	RNA interactome capture data analysis and quality control	46
5.1.6	Classification of proteins identified in RNA interactome capture	48
5.1.7	Annotation enrichment analysis of proteins identified in RIC	50
5.2	Identification of novel RBPs.....	52
5.2.1	Comparative analysis of published RNA interactomes.....	52
5.2.2	Comparison of RIC with novel techniques	53
5.2.3	The identification of 270 novel RBPs in <i>C. elegans</i>	55
5.3	Proteome analysis of wild-type and <i>vhl-1(ok161)</i>	55
5.3.1	Proteome data analysis and quality check.....	55
5.3.2	Proteome analysis reveals activation of the hypoxia signaling pathway in <i>vhl-1(ok161)</i> mutant worms	56
5.3.3	Annotation enrichment analysis of the proteome	57
5.4	Analysis of the mode of regulation of RBPs in wild-type and <i>vhl-1(ok161)</i> ..	58
5.4.1	The hypoxia signaling pathway regulates the abundance of RBPs.....	58
5.4.2	Analysis of RBPs identified exclusively in wild-type or <i>vhl-1(ok161)</i> RIC..	59
5.4.3	Identification of the mode of regulation of RBPs in wild-type and <i>vhl-1(ok161)</i> RIC	61
5.5	Hypoxia-signaling associated RBPs have an impact on <i>C. elegans</i> lifespan	64
5.5.1	Establishing the lifespan machine in <i>C. elegans</i>	64
5.5.2	Lifespan analysis of long-lived mutants	65
5.5.3	Lifespan analysis of worms fed on RNAi in the lifespan machine set-up	67
5.5.4	Knockdown of RBPs regulates <i>C. elegans</i> lifespan	68
5.5.5	CRISPR-Cas9 based Genome editing in <i>C. elegans</i>	69
6	Discussion	71
6.1	<i>vhl-1(ok161)</i> mutant phenotype and its impact in RIC.....	71
6.2	The complexity of RIC protocols.....	72

6.3	Interspecies data comparison.....	73
6.4	The impact of hypoxia signaling on the RBP landscape.....	75
6.5	The <i>C. elegans</i> lifespan machine	77
6.6	RBPs involved in <i>C. elegans</i> lifespan	79
6.7	Future perspectives to elucidate RBPs in AKI	80
7	Conclusion	81
8	References	82
9	Publications	98
9.1	Publications in academic journals.....	98
9.2	International conferences	98
10	Acknowledgment	100
11	Erklärung	101
12	Curriculum vitae.....	102

List of Figures

Figure 1: The anatomy of a human kidney.....	3
Figure 2: Acute kidney injury - the vicious circle.	5
Figure 3: Hypoxia signaling pathway.	7
Figure 4: RBPs involved in post-transcription.....	8
Figure 5: The advantages of <i>C. elegans</i>	12
Figure 6: <i>vhl-1(ok161)</i> mutants are shorter and contain less RNA and protein.....	40
Figure 7: Experimental workflow of RIC.....	41
Figure 8: Silver staining revealed efficient crosslinking in RIC.....	43
Figure 9: Normalization and imputation of wild-type and <i>vhl-1(ok161)</i> proteome.	45
Figure 10: RBPome sample analysis.....	47
Figure 11: Volcano plot of wild-type and <i>vhl-1(ok161)</i> RBPome.....	48
Figure 12: Classification of the wild-type and <i>vhl-1(ok161)</i> RBPome.	49
Figure 13: GO-term enrichment of RIC proteins.	50
Figure 14: Comparison of the GO terms <i>RNA binding</i> and <i>DNA binding</i>	51
Figure 15: Domain enrichment of RIC proteins.....	52
Figure 16: Comparisons of Class I and Class II RBPs with previously published RIC datasets.....	53
Figure 17: Comparisons of Class I and Class II RBPs with novel techniques and predicted RBPs.....	54
Figure 18: Identification of novel RBPs.....	55
Figure 19: PCA and heat map analysis of wild-type and <i>vhl-1(ok161)</i> proteome.....	56
Figure 20: Analysis of <i>HIF-1</i> and its target genes in wild-type and <i>vhl-1(ok161)</i> proteome.	57
Figure 21: GO-term enrichment analysis of wild-type and <i>vhl-1(ok161)</i> proteome... ..	58
Figure 22: Identification of RBPs in the proteome of wild-type and <i>vhl-1(ok161)</i>	59
Figure 23: RBPs measured exclusively in either wild-type or <i>vhl-1(ok161)</i> analysed in their proteomes.....	60
Figure 24: Identification of mode of regulation of RBPs in wild-type and <i>vhl-1(ok161)</i>	62
Figure 25: Overview of the lifespan machine.....	65
Figure 26: Automated lifespan analysis of <i>C. elegans</i> mutants.	66
Figure 27: Lifespan analysis of <i>C. elegans</i> feed on RNAi.....	67
Figure 28: Lifespan analysis of RBP knockdown in <i>C. elegans</i>	68
Figure 29: Genome editing using CRISPR-Cas9.....	70

List of Tables

Table 1: List of materials used.	15
Table 2: List of devices used.....	16
Table 3: List of chemicals and reagents used.	18
Table 4: List of Kits used.....	20
Table 5: List of buffers used.....	21
Table 6: List of Software used.....	23
Table 7: List of used beads.	24
Table 8: List of antibodies used.	24
Table 9: List of worm strains used.	25
Table 10: List of RNAi used.	25
Table 11: List of oligonucleotides used.	25
Table 12: Summary of Lifespan results.....	29
Table 13: Pipetting scheme for genotyping PCR.	30
Table 14: Genotyping PCR program.....	30
Table 15: Agarose gel ingredients.....	31
Table 16: CRISPR-Cas9 injection mix.	32
Table 17: Sequencing mix.....	32
Table 18: Sequencing reaction cycling conditions.	33
Table 19: Overview of samples analysed by mass spectrometry.....	44
Table 20: Overview of RBPs above and below the 95% prediction interval.....	63

Abbreviations

μl	Microliter
4SU	4-thiouridine
6SG	6-thio-guanosine
ACN	Acetonitrile
AKI	Acute kidney injury
BSA	Bovine serum albumin
CAA	Chloroacetamide
<i>C. elegans</i>	<i>Caenorhabditis elegans</i>
CKD	Chronic kidney disease
CL	Crosslinked
CLIP	Crosslinking and immunoprecipitation
CoCl ₂	Cobalt(II) chloride
CRISPR	Clustered regularly interspaced short palindromic repeats
DMSO	Dimethyl sulfoxide
DNA	Deoxyribonucleic acid
dNTP	Deoxyribonucleotide triphosphate
dsRNA	Double-stranded RNA
DTT	Dithiothreitol
EDTA	Ethylenediaminetetraacetic acid
ESRD	End-stage renal disease
EtOH	Ethanol
EV	Empty vector
FC	Fold change
FDR	False discovery rate
fp	Forward primer
FUDR	5-Fluoro-2'-deoxyuridine
GFP	Green fluorescent protein
GO	Gene ontology
h	Hour
HCl	Hydrochloric acid
HDR	Homology-dependent repair
HIF	Hypoxia-inducible factor
HRE	Hypoxia response element

HRP	Horseradish peroxidase
HuR	Human antigen R
iBAQ	Intensity based absolute quantification
IPC	Ischemic preconditioning
IPTG	Isopropyl- β -D-thiogalacto-pyranosid
IREs	iron-responsive elements
KCl	Potassium chloride
KDIGO	Kidney disease: Improving global outcomes
kg	Kilogram
KH_2PO_4	Monopotassium phosphate
KIM-1	Kidney injury molecule-1
l	Liter
LDS	Lithiumdodecyl sulphate
LED	Light-emitting diode
LFQ	Label-free quantitation
LiCl	Lithium chloride
MgCl_2	Magnesium chloride
MgSO_4	Magnesium sulfate
ml	Mililiter
mm	Millimeter
mRNA	Messenger RNA
ncRNA	Non-coding RNA
NGAL	Neutrophil gelatinase-associated lipocalin
NGM	Nematode growth medium
NHEJ	Nonhomologous end-joining
O_2	Oxygen
OOPS	Orthogonal organic phase separation
p Value	Probability
PCA	Principal component analysis
PCR	Polymerase chain reaction
PHD	Prolyl 4-hydroxylase
PTB	Polypyrimidine tract-binding protein
PTex	Phenol toluol extraction
PUF	Pumilio

RBD	RNA binding domain
RBP	RNA binding protein
RIC	RNA interactome capture
RIP	RNP immunoprecipitation
RNA	Ribonucleic acid
RNAi	RNA interference
RNP	Ribonucleoprotein
rp	Reverse primer
rpm	Revolutions per minute
RRM	RNA recognition motif
rRNA	Ribosomal RNA
SDS	Sodium dodecyl sulfate
SEM	Standard error of the mean
snoRNA	Small nucleolar RNA
snRNA	Small nuclear RNAs
ssODN	Single-stranded oligodeoxynucleotide
ssRNA	Single-stranded RNAs
TEAB	Triethylammonium bicarbonate
Tris	Tris(hydroxymethyl)aminomethane
tRNA	Transfer RNA
UTR	Untranslated region
UV	Ultraviolet
VHL	Von Hippel-Lindau
WT	Wild-type
XRNAX	Protein-crosslinked RNA extraction

1 Abstract

Acute kidney injury (AKI) shows a rising incidence especially in the elderly above the age of 65. AKI does not only lead to an acute impairment of renal function but also comes with a strongly increased risk of adverse outcome including mortality. Since there are no therapies for AKI prevention measures this would be of utmost importance. However, clinically established specific interventions protecting the kidney are not available. Prevention of kidney damage can be addressed by the concept of preconditioning which exploits the fact that damaging stimuli at a sublethal dose can activate cellular protection programs that increase resistance to future stressors. One of these preconditioning protocols is based on the activation of the hypoxia signaling pathway which has been shown to prevent AKI in animal models. However, the underlying mechanisms are still unknown hampering translation to the clinical setting. A recent study highlighted the importance of RNA binding proteins (RBPs) and hinted towards differences in RNA-protein binding upon exposure to hypoxia. In the last decade, the list of known and putative RBPs has been increasing in size and complexity across species. Thanks to the development of techniques that allow crosslinking of RNA to interacting proteins followed by both RNA pulldown and mass spectrometry (RNA interactome capture). However, little is still known about the molecular function of many RBPs and their global dynamics in different conditions. In this study, we chose *C. elegans* as a model organism to further dissect the complex biological question of (1) how hypoxia-inducible factor signaling modulates the RNA protein interactome and (2) how these RBPs may impact on stress resistance. Performing RNA interactome capture in wild-type and *vhl-1* mutant worms we identified 1354 RBPs 270 out of which had not been described before. Among these, we found 30 RBPs to be overrepresented in *vhl-1* mutant and 50 RBPs in wild-type worms. A comparison of the proteome in both strains showed that all but one of these are not differentially regulated on the level of protein abundance pointing towards differences in RNA-binding capacity. Lifespan extension in the nematode reflects increased stress resistance. To enable screening of this phenotype after knockdown of RBP candidates in *C. elegans*, we established the automated lifespan machine. Using this approach, we could show longevity induced by knockdown several of these RBPs. Our results will significantly add to the understanding of the RBPome in the nematode and its modulation by HIF-signaling.

2 Zusammenfassung

Die Inzidenz für eine akute Nierenschädigung (AKI) steigt insbesondere bei älteren Menschen über 65 Jahren. AKI führt nicht nur zu einer akuten Beeinträchtigung der Nierenfunktion, sondern birgt auch ein stark erhöhtes Risiko für Mortalität. Da es keine Therapien für AKI gibt, wären Präventionsmaßnahmen von größter Bedeutung. Die Prävention von Organschäden wird durch das Konzept der Präkonditionierung angegangen, bei dem die Tatsache ausgenutzt wird, dass schädliche Reize bei einer subletalen Dosis zelluläre Schutzprogramme aktivieren können, die dann die Resistenz gegen zukünftige Stressfaktoren erhöhen. Einer dieser Präkonditionierung Protokolle beruht auf die Aktivierung des Hypoxie-Signalwegs. Die zugrunde liegenden Mechanismen sind jedoch noch unbekannt, was eine Translation in die Klinik bislang verhindert hat. Eine Studie aus unserer Gruppe unter Verwendung von Zellkulturen deutet auf Unterschiede in der Bindung von RNA-Bindungsproteinen (RBPs) an mRNA während Hypoxie hin. In den letzten zehn Jahren hat die Liste der bekannten und mutmaßlichen RBPs an Größe und Komplexität zugenommen. Das gelang durch die Entwicklung von Techniken, die die Vernetzung von RNA mit RBPs ermöglichen, gefolgt von RNA-Pulldown und Massenspektrometrie (RNA-Interaktom-Capture). In dieser Studie haben wir *C. elegans* als Modellorganismus ausgewählt, um die komplexe biologische Frage weiter zu untersuchen: (1) wie durch Hypoxie induzierbare Faktorsignale das RNA-Protein-Interaktom moduliert wird und (2) wie diese RBPs die Stressresistenz beeinflussen können. Bei der Durchführung des RNA-Interaktom-Captures in Wildtyp und *vhl-1* Mutanten Würmern identifizierten wir 1354 RBPs von denen 270 zuvor noch nicht beschrieben worden waren. Zusätzlich fanden wir 30 RBPs, die in der *vhl-1* Mutante und 50 RBPs in Wildtypischen Würmern überrepräsentiert waren. Ein Vergleich des Proteoms in beiden Stämmen zeigte, dass alle bis auf ein RBP nicht unterschiedlich auf der Ebene der Proteinhäufigkeit reguliert sind, was auf Unterschiede in der RNA-Bindungskapazität hinweist. Um ein Screening der Lebensspanne nach dem Herunterregulieren von RBP-Kandidaten in *C. elegans* zu ermöglichen, haben wir die automatisierte Lebensdauer-Maschine etabliert. Mit diesem Ansatz konnten wir eine Langlebigkeit nachweisen, die durch das Herunterregulieren mehrerer dieser RBPs verursacht wurde. Unsere Ergebnisse werden das Verständnis des RBPome im Nematoden und seine Modulation durch HIF-Signalisierung erheblich verbessern.

3 Introduction

3.1 The kidney and its function

Human kidneys are a pair of organs located beneath the rib cage in the posterior abdomen. They have the size of a fist and weigh on average 135 g - 162 g (Rao and Wagner 1972). Every kidney contains about one million nephrons (Puelles et al. 2011). The nephrons are located in the renal cortex and renal medulla (Figure 1). Each nephron is divided into the renal glomerulum and the renal tubule. The renal tubule consists of the proximal convoluted tubule, the loop of Henle, the distal convoluted tubule and the collecting duct (Figure 1) (Wallace 1998).

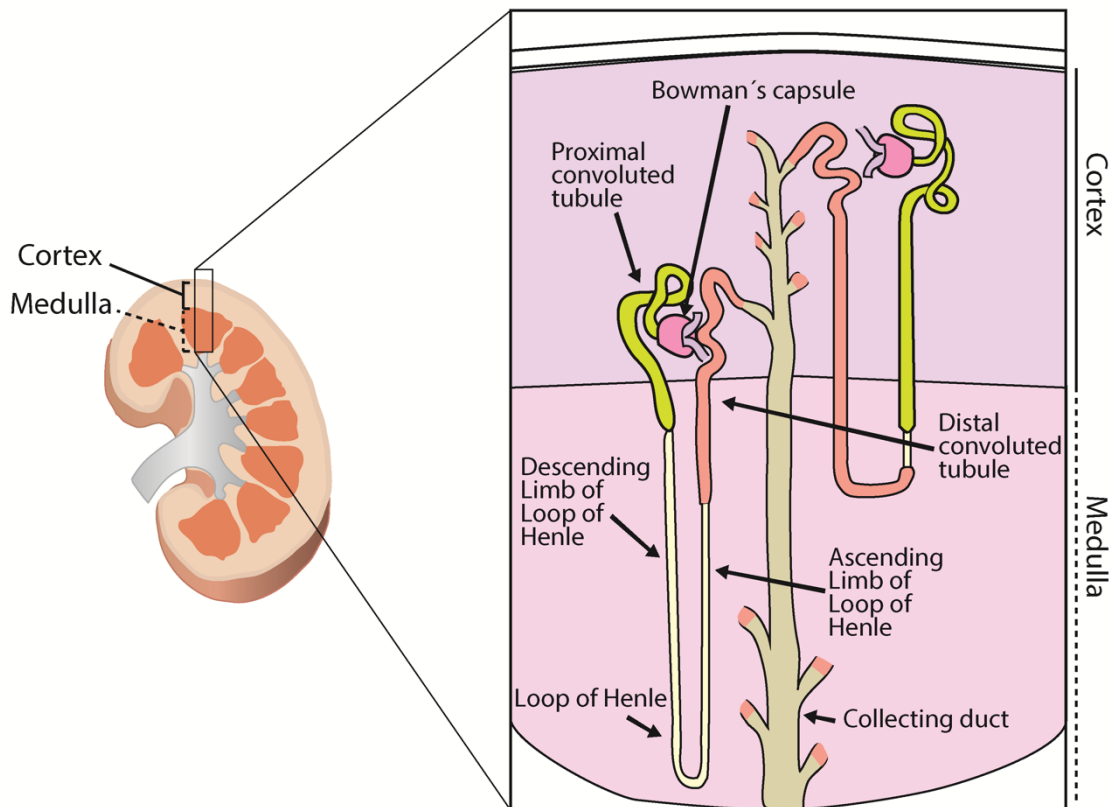


Figure 1: The anatomy of a human kidney.

Cross-section of a human kidney (left) cortex and medulla is indicated. The black box marks the region which is viewed in detail (right). On the right side, a nephron is depicted with all parts needed for filtration, reabsorption and secretion involving the glomerulus, the proximal convoluted tubule, loop of Henle (descending and ascending limb), distal convoluted tubule and collecting duct.

Filtration of the blood takes place in the glomerulum. Water and solutes are filtered in a size and charge-dependent fashion and collected in the Bowmans capsule, while proteins above approximately 50 kD are retained in the blood. Along the renal tubule reabsorption and secretion of electrolytes, substances and water, on different

sections in various amounts takes place. The kidneys filter about 180 liters of fluid (primary urine) per day resulting in about 1.5 liter urine output after reabsorption. Besides the important filtration function, the kidney participates in hormone secretion, blood pressure regulation and bone physiology (Coffman 2014). As a consequence, end-stage renal disease is only compatible with life due to the availability of renal replacement therapies like dialysis or kidney transplantation. However, even a mild loss of kidney function leads to significantly increased cardiovascular morbidity and a decrease in life expectancy.

3.2 Acute kidney injury

Acute kidney injury (AKI) causes an acute loss of renal function. With increased age, there is a higher risk to develop AKI (Xue et al. 2006). Since we live in a society with demographic changes that lead to our population getting older and older the incidence of AKI is rising. Further, AKI is a major independent risk factor for cardiovascular morbidity and mortality (Go et al. 2004). The etiology of AKI can be divided into prerenal, intrarenal and postrenal AKI (Farrar 2018). Prerenal AKI is caused by decreased renal perfusion or blood flow and is – due to its functional nature and as long as intrarenal damage has not occurred yet – usually rapidly reversible upon improving perfusion. Intrarenal AKI refers to actual damage to renal cells as a consequence of prolonged ischemia or toxic injury. Postrenal AKI is defined as an acute obstruction to urinary flow. In the following, I will primarily focus on actual intrarenal AKI which – in the majority of cases – is caused by tubular damage and acute tubular necrosis. According to “Kidney disease: Improving global outcomes” (KDIGO), AKI is defined by the following criteria. Firstly, an increase in serum creatinine by 0.3 mg/dL or more within 48 hours. Secondly, an increase in serum creatinine to 1.5 times or more to baseline, within the prior seven days. Thirdly, if urine volume is less than 0.5 mL/kg/h for at least 6 hours (“KDIGO for AKI” 2012). AKI is associated with adverse outcomes including the need for renal-replacement therapy, prolonged treatment in the intensive care unit and increased cardiovascular morbidity and mortality (P. K. Moore et al. 2018). Consequently, prevention and treatment of AKI would be highly beneficial. Unfortunately, there are no therapeutic strategies and targeted preventive options have not been established in the clinical setting. One problem is the fact, that AKI does not hurt making early detection per se difficult and no established biomarker of early damage is available. Besides

increased mortality and morbidity directly due to AKI, acute renal damage also increases the risk of chronic kidney disease (CKD) (Chawla and Kimmel 2012). CKD is known to be a major independent risk factor of cardiovascular mortality. Furthermore, patients with CKD are at increased risk of AKI leading to the situation of a vicious circle (Figure 2). This is – at least partly - due to a decrease in cellular stress resistance which is particularly important in elderly individuals. It would thus be crucial to find ways to activate the body's own protection and stress resistance mechanisms to prevent damage. Such an enhancement of intrinsic stress resistance mechanisms is the aim of preconditioning algorithms.

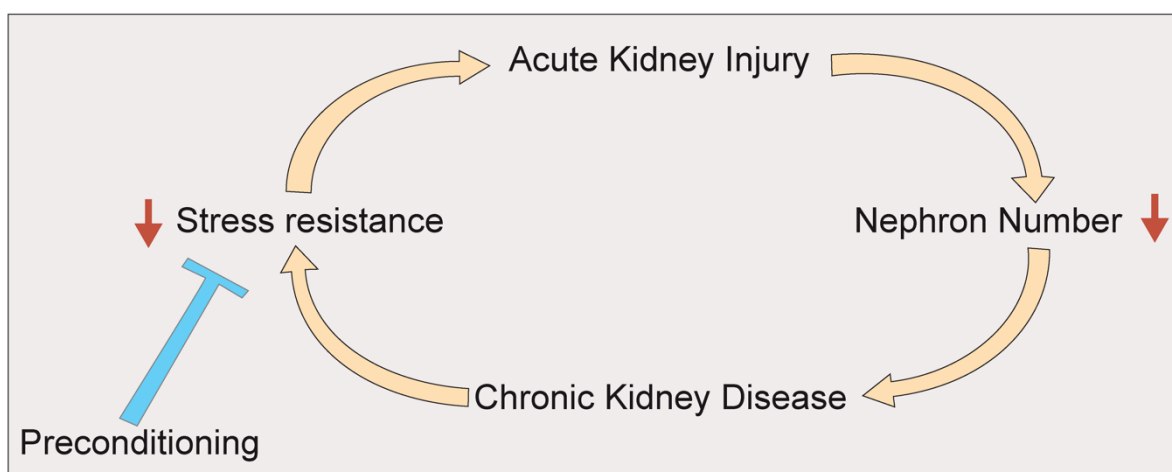


Figure 2: Acute kidney injury - the vicious circle.

Acute injury leads to a loss of functional kidney tissue reducing the nephron number. As a consequence chronic kidney disease develops going along with a reduced tolerance to future stressors. This makes the elderly patient more prone to further episodes of acute kidney injury causing a vicious circle. Considering the lack of therapeutic options, preconditioning protocols are a promising strategy to increase stress resistance and prevent AKI.

3.3 Preconditioning

Preconditioning strategies are based on the concept of hormesis. Exposing cells, tissues or organisms to a sublethal dose of a stressor induces programs capable of preparing the cell to counteracting greater stress stimuli in the future. Importantly, these mechanisms are conserved in evolution and lead – activated either by environmental stimuli or genetic intervention – to lifespan extension in organisms as diverse as worms to humans (Costa et al. 2019; Hwangbo et al. 2020). It has been shown that different regimens of dietary restriction can extend the lifespan of numerous organisms including yeast, flies, worms, fish and rodents (Fontana et al. 2010). Moreover, dietary restriction can significantly reduce the damage to various

organs such as heart, brain and kidney upon ischemia-reperfusion (Chandrasekar et al. 2001; J. R. Mitchell et al. 2010; Yu and Mattson 1999). Similar to dietary restriction, several publications could demonstrate that hypoxia signaling can extend the lifespan of flies and worms (Mehta et al. 2009; Müller et al. 2009; Vigne and Frelin 2007). Hypoxia describes the state of insufficient or low oxygen supply in organs or tissues that leads to the activation of the hypoxia signaling pathway. This signaling pathway can also be activated by drugs, ischemic reperfusion or gas (Eltzschig and Eckle 2011; Li et al. 2012; Pockock and Nicholls 1998; Provenzano et al. 2016). Induction of the hypoxia signaling pathway by prolyl 4-hydroxylases (PHDs) inhibitors was able to ameliorate post-ischemic renal injury (X.-L. Zhang et al. 2011). Another preconditioning algorithm linked to hypoxia is ischemic preconditioning (IPC). IPC has been shown to protect against ischemia-reperfusion injury (Endre 2011; Joo et al. 2006). Taken together, the hypoxia signaling pathway is a promising target for strategies preventing AKI.

3.4 Hypoxia signaling

The hypoxia signaling pathway is predominantly controlled by a group of transcription factors termed hypoxia-inducible factors (HIF). HIF proteins are heterodimers and consist of an unstable alpha (α) subunit and a stable beta (β) subunit (Kaelin and Ratcliffe 2008). There are three HIF α proteins (HIF-1, HIF-2, HIF-3) encoded in the human genome. During normoxia, the HIF α subunit is hydroxylated by PHDs on two proline residues (HIF-1 α : Pro402 and 564; HIF-2 α : Pro405 and Pro531) (Strowitzki et al. 2019). Hydroxylated HIF α is then recognized and bound by the tumour suppressor pVHL (von Hippel-Lindau protein). pVHL is the substrate recognition subunit of an E3 ubiquitin ligase that mediates HIF α polyubiquitination and subsequent proteasomal degradation (Kaelin 2005). The enzymatic activity of PHDs is dependent on the presence of oxygen (Epstein et al. 2001). Upon hypoxia, HIF α is no longer hydroxylated and bound by pVHL. HIF α gets stabilized and translocates into the nucleus where it dimerizes with HIF β . The HIF heterodimer binds to the hypoxia response elements (HRE) and activates the transcription of target genes involved in angiogenesis, cell proliferation and survival (Figure 3) (Harris 2002; Kaelin and Ratcliffe 2008).

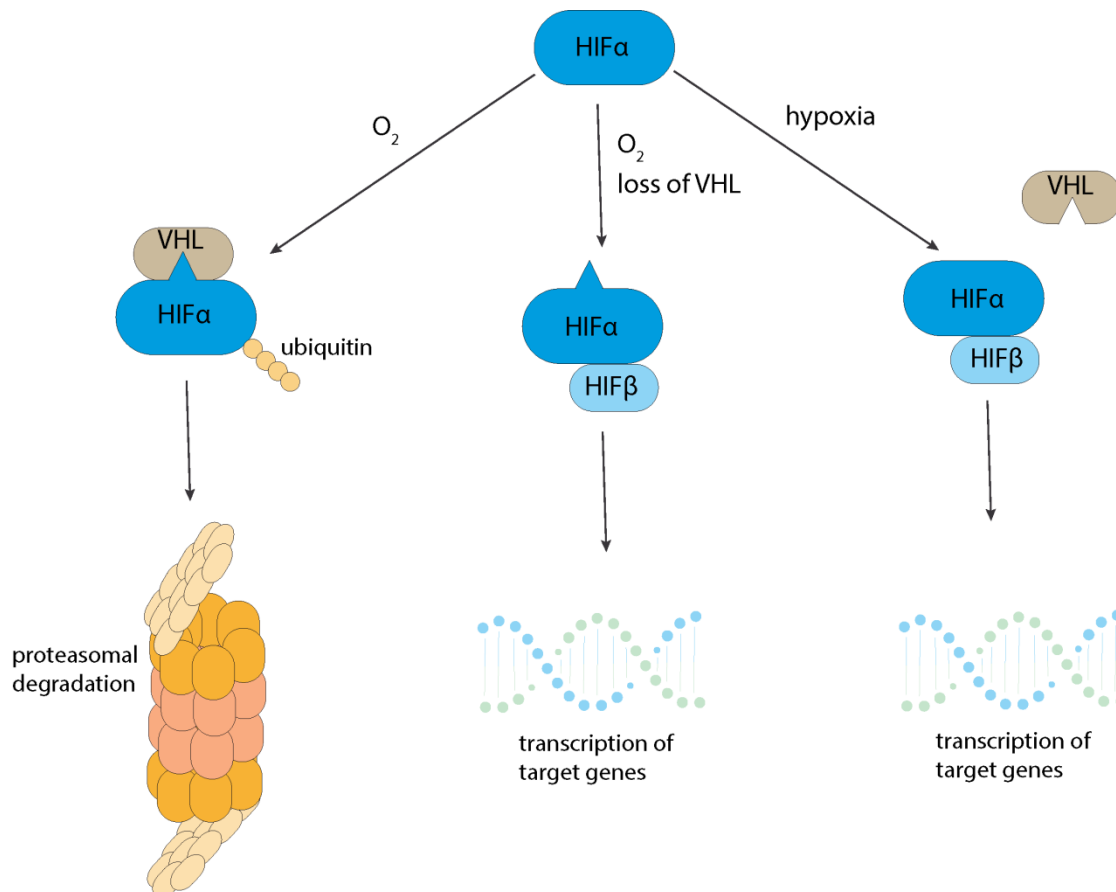


Figure 3: Hypoxia signaling pathway.

In the presence of oxygen (O_2) pVHL binds to HIF α and mediates its ubiquitination followed by its proteasomal degradation (left panel). Loss of VHL leads to a stabilization of HIF α (middle panel). Similarly, during hypoxia, pVHL is unable to bind HIF α . HIF α gets stabilized, translocates into the nucleus and dimerizes with HIF β leading to the activation of their target genes (right panel).

Besides the regulation of HIF on the protein level, HIF mRNA can also be regulated suggesting a role for RBPs. In human cells treated with $CoCl_2$ (hypoxia mimetic) HIF1 α protein was further increased upon knockdown of the RBP RBM38 and decreased upon overexpression. RBM38 can bind to HIF1 α 5' and 3'UTRs and thereby regulate HIF1 α mRNA translation (Cho et al. 2015). Another RBP known to bind HIF1 α mRNA is polypyrimidine tract-binding protein (PTB). PTB primarily binds to the HIF1 α 3'UTR leading to an increase in HIF-1 α translation after hypoxia (Galbán et al. 2008). HIF1 α mRNA regulation by PTB depends on another RBP, human antigen R (HuR). There is evidence that both PTB and HuR need to bind to HIF1 α mRNA to promote its translation (Masuda et al. 2009). HuR is a well-known RBP with many RNA targets besides HIF1 α , known for the induction of renal fibrosis and inflammation (Brennan and Steitz 2001; Feigerlová and Battaglia-Hsu 2017; Galbán et al. 2008). On the one hand, these studies show that RBPs can have a

direct impact on hypoxia signaling. On the other hand, it would be extremely interesting to determine how hypoxia signaling changes the RBP landscape.

3.5 RNA binding proteins

RNA binding proteins play an important role in cellular biology and explicitly in the posttranslational regulation of gene expression. Gene expression starts with the transcription of DNA to synthesize RNA molecules and ends with the translation of RNA molecules into protein followed by protein turnover. The central steps for transcription and translation are initiation, elongation, and termination (Cramer 2019; M. J. Moore 2005; Orphanides and Reinberg 2002). Every step of gene expression is tightly controlled and regulated (Figure 4).

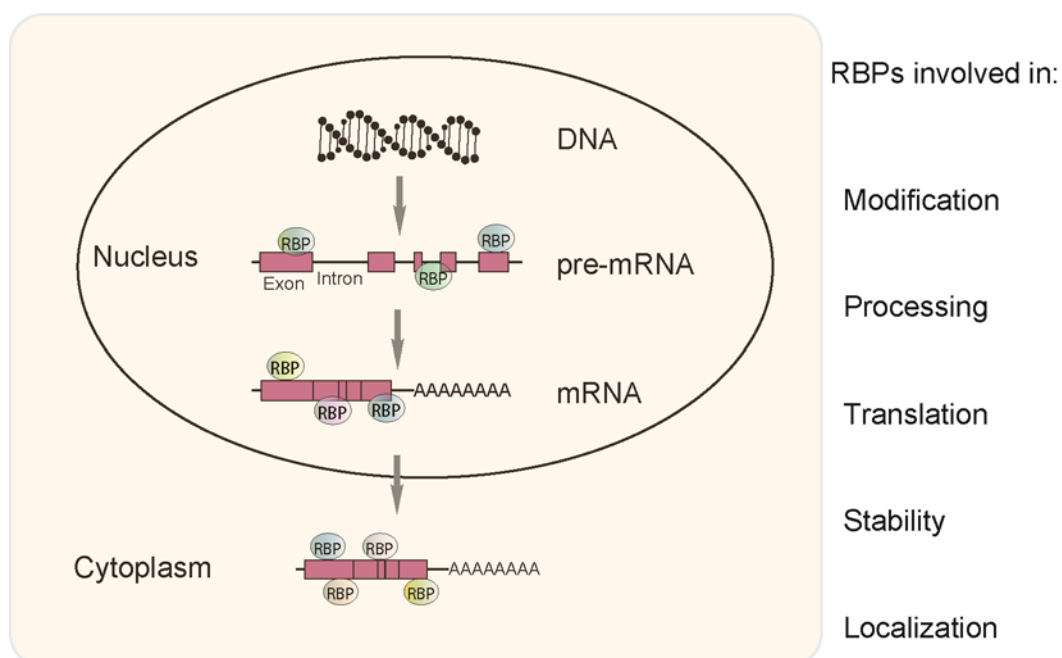


Figure 4: RBPs involved in post-transcription.

DNA is transcribed resulting in pre-mRNA for protein coding genes. These pre-mRNAs contain exons and introns. Splicing of the pre-mRNA results in the actual mRNA. The mRNA is exported out of the nucleus into the cytoplasm. There it can be transported, stored, translated or degraded. RBPs are involved in each post-transcriptional regulation step and determine the fate of the RNA.

RBPs bind RNA throughout all the steps of its production and maturation in the different cellular compartments; they regulate RNA translation, modification, localization, processing and stability which makes them key regulators of numerous cellular functions (Figure 4) (Halbeisen et al. 2008; Hasan et al. 2014; S. R. Lee and Lykke-Andersen 2013; Wilkie et al. 2003). To bind RNA, most RBPs contain multiple

RNA binding domains (RBD). Among the classical RBDs are the RNA recognition motif (RRM), the DEAD motif, the Pumilio/FBF (PUF) domain and the zinc finger domains (Cléry et al. 2008; Hall 2005; Rocak and Linder 2004; Zamore et al. 1997). With the help of computational biology, RBPs are identified by sequence analysis based on these RBDs leading to an increase in the number of RBPs (Kazan et al. 2010; Tamburino et al. 2013). In addition, the number of RBPs without a classical RBD (termed “enigmRBPs”) is rising (Beckmann et al. 2015). The continued increase in the number of RBPs, especially enigmRBPs, is due to the recent development of improved methods for studying RNA-protein interactions.

3.6 Methods for the identification of RBPs

In the last century, the development of high-throughput approaches has given the field of RBPs and their identification a boost, so that many new methods have emerged. In the past, these methods used either immobilized RNA probes or arrayed proteins (Butter et al. 2009; Scherrer et al. 2010). More recently RNA Interactome Capture (RIC) was developed to identify RBPs in a systematic, unbiased approach (Baltz et al. 2012; Castello et al. 2012). RIC is based on covalently linking RNA with RBPs by crosslinking using UV light. For RIC, the standard approach to crosslink RNA with RBPs is the usage of UV-C wavelength (254 nm). UV-C leads to the formation of covalent links between adjacent bases RNA and amino acids such as Phe, Trp, Tyr, Cys and Lys. In contrast, the use of the photoactivatable ribonucleosides 4-thiouridine (4SU) or 6-thio-guanosine (6SG) enables crosslinking with UV-A (Castello et al. 2012) and allows for pulse-chase experiments. Independent from the actual strategy used for crosslinking, polyadenylated RNA is captured using oligo(dT) beads. Co-precipitated proteins are released from the beads followed by RNase treatment and identification / quantification of the proteins by mass spectrometry (Baltz et al. 2012; Castello et al. 2012). By now, RIC has been applied to a growing number of samples derived from various organisms, e.g. yeast, worms, plants, mouse and humans. Due to technical challenges most experiments were performed using cultured cells rather than tissue or whole organisms (Hentze et al. 2018). Interestingly, the broad usage of RIC revealed that there are many RBPs (enigmRBPs) that lack a classical RNA binding motif and have no known relation to RNA biology (Beckmann et al. 2015; Hentze et al. 2018). These enigmRBPs are involved in biological roles such as metabolism, cell-cycle progression, antiviral

response, spindle organization and protein metabolism (Hentze et al. 2018). Although RIC allows the identification of the mRNA bound RBPs it will fail to provide a comprehensive identification of proteins interacting with non-polyadenylated RNA. Thus, different methods were developed for the identification of RBPs bound to all RNA species. Just recently, at about the same time, three methods were published based on organic extraction protocols instead of polyA pulldown, called Phenol Toluol extraction (PTex), protein-crosslinked RNA extraction (XRNAX) and orthogonal organic phase separation (OOPS) (Queiroz et al. 2019; Trendel et al. 2019; Urdaneta et al. 2019). These methods – since they are rather based on physical properties of RNA-protein complexes than sequence-recognition - do now allow for a comprehensive identification of proteins interacting with all kinds of RNA molecules. The principle of these methods is based on the purification of RBPs using acidic phenol phase separation. Protein–RNA adducts will be separated from free protein and RNA. However, noticeable differences between these methods downstream of the RBP extraction makes it difficult to compare their data (Smith et al. 2020). Taken together, the increasing number of RBPs identified in the last decade is based on highly improved methodologies paired with sensitive protein identification by MS and the fact that these methods have been applied to a growing number of cell types and species.

3.7 RBP target identification

The first approaches to identify RNA targets of RBPs emerged in 1979. Lerner and Steitz demonstrated that using antibodies against the spliceosomal Sm proteins allows the precipitation of small nuclear RNA molecules (Lerner and Steitz 1979). This method was the basis to further development and is now known as RNP immunoprecipitation (RIP) assay (Niranjanakumari et al. 2002). RIP typically uses formaldehyde which crosslinks - besides RNA-protein complexes - also protein-protein interactions. Using conditions in the RIP assay preserving RNP, it is well applicable to identify RNA targets of an entire RNP but is unsuitable to study direct RNA-protein interaction. To overcome this issue, crosslinking and immunoprecipitation (CLIP) were developed that identify RNA targets of a specific RBP (Ule et al. 2003). To date, there are more than 15 different versions of the protocol published to improve the efficiency of the protocol steps (F. C. Y. Lee and Ule 2018). To name just the most significant changes HITS-CLIP and CLIP-seq

introduced high-throughput sequencing (Licatalosi et al. 2008; Yeo et al. 2009). Furthermore, both PAR-CLIP and iCLIP resolve the position of the crosslinked sites at nucleotide resolution (Hafner et al. 2010; König et al. 2010). Moreover, in one of the most recent improvements of the protocol, enhanced CLIP (eCLIP), the amplification of the library could be decreased resulting in an increase in usable read fraction (Van Nostrand et al. 2016). However, the basis of all approaches remains the combination of an efficient crosslinking technology with protein immunoprecipitation. High-throughput sequencing is then used to identify the actual RNA targets. Since immunoprecipitation of RBPs is required the model organism has to be chosen according to antibody availability or availability of techniques that facilitate genetic modification to tag specific RBPs.

3.8 *C. elegans* as a model organism

In the beginning, *C. elegans* was used in the laboratory of Sydney Brenner to study development and the nervous system (Brenner 1974; White et al. 1986). The worm's relatively simple nervous system with 302 neurons compared to over 100 billion in humans, despite the small number, represents most of the nerve cells identified in other organisms. Also, the cuticle is transparent, which makes it possible to observe the cells in the living worm (White et al. 1986). *C. elegans* quickly became a well-established model organism due to many features such as easy cultivation on agar-plates, feeding on bacteria and its short lifecycle (Figure 5) (Edgar and Wood 1977). The lifecycle of the worms starts with a fertilized egg. After hatching the worm passes four larval stages (L1-L4) through molting until it reaches adulthood. A key feature of *C. elegans* is their eutely, the defined somatic cell numbers for hermaphrodites are 959 cells and for males 1031 cells (Sulston et al. 1980; Sulston and Horvitz 1977). These first discoveries were the basis for insight into the genetic regulation of organ development and programmed cell death. For these discoveries, the Nobel Prize in Physiology or Medicine was awarded to Sydney Brenner, H. Robert Horvitz and John E. Sulston in 2002. Another major discovery using *C. elegans* was RNA interference. Thanks to the development of RNAi every gene in the worm can be knocked down using simple techniques (Fire et al. 1998). The easy application of RNAi by feeding the worms with bacteria expressing RNAi or by soaking them in double-stranded RNA (dsRNA) solution is a major advantage to other organisms (Figure 5).

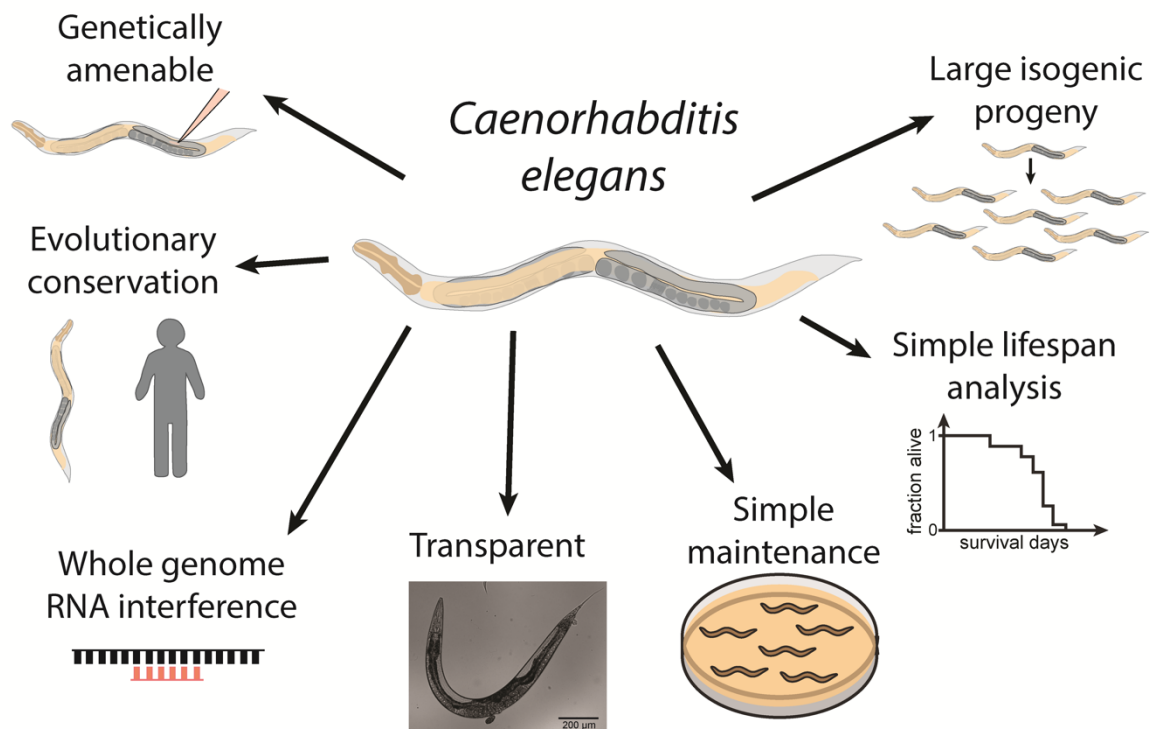


Figure 5: The advantages of *C. elegans*.

C. elegans quickly developed into an established model organism due to many advantages summarized here. They are genetically amenable, many genes and pathways are conserved up to human and commercial available RNAi libraries cover most of the genome (black strand mRNA and red strand RNAi). Also *C. elegans* is transparent. Image taken by using Nomarski microscopy with a magnification of 5x. Scale bar represents 200 µm. The worms are very cost effective because they are simple to maintain. Lifespan experiments can be done easily. They are very suitable for experiments where many animals are needed because they have large isogenic progeny.

RNAi uses dsRNA which is processed into single-stranded RNAs (ssRNAs). First, the dsRNA is processed into ssRNA by an endoribonuclease called Dicer. Then the ssRNA gets in complex with TSN-1 and VIG-1 and together they build the RNA-induced silencing complex (RISC). The ssRNA directs the RISC to the specific mRNA determined by sequence complementary. Once bound the mRNA will be cleaved and degraded (Grishok 2005). Using commercially available RNAi libraries genome-wide RNAi screening is feasible (Kamath and Ahringer 2003). The discovery of RNAi was rewarded with another Nobel Prize in Physiology or Medicine in 2006 to Craig Mello and Andrew Fire. A third Nobel Prize for research using the nematode went to Martin Chalfie who shared the Nobel Prize in Chemistry in 2008. He contributed to the development of green fluorescent protein (GFP) as a tool for visualizing biological structures in living organisms by inserting the GFP gene into *C. elegans*. The DNA transformation in *C. elegans* can be achieved by germline microinjection or by

bombardment with microparticles (Mello et al. 1991; Praitis et al. 2001). In addition, many signaling pathways have been uncovered in *C. elegans* which are conserved in humans including the hypoxia signaling pathway.

3.9 Hypoxia signaling in *C. elegans*

The hypoxia signaling pathway was originally decrypted in the worm. A protein was identified which regulates *HIF-1* through prolyl hydroxylation (Epstein et al. 2001). The gene that encoded this protein is called *egl-9* or better known as *PHD* in humans. Nowadays it is also known that the *C. elegans* genome encodes one *VHL* gene (*vhl-1*) and a HIF- α homolog (*hif-1*). VHL role as a substrate-recognition subunit of an E3 ubiquitin ligase regulating HIF is entirely conserved (Epstein et al. 2001; Jiang et al. 2001). Further studies showed, that the activation of *HIF* mediates longevity in *C. elegans* (Mehta et al. 2009; Müller et al. 2009). This longevity caused by *HIF* is independent of the insulin/IGF-1/FOXO pathway. The insulin/IGF-1/FOXO pathway was the first lifespan pathway that was discovered in the worms (Kenyon et al. 1993). Today, many other pathways and genes were found to be involved in the lifespan of *C. elegans* including TOR signaling, Sirtuins and AMP-activated protein kinase (Uno and Nishida 2016). That makes *C. elegans* suitable for lifespan analysis.

3.10 Aims

AKI can lead to ESRD and loss of kidney function. Possible approaches to prevent AKI are addressed by the concept of preconditioning protocols. These protocols are based on activating innate stress response pathways to protect renal tissue against AKI. One of these preconditioning protocols relies on the activation of the hypoxia signaling pathway. However, none of the preconditioning protocols have yet made their way into a clinical setting. To increase the understanding of the molecular mechanisms behind hypoxic preconditioning, we set out to further elucidate the hypoxia signaling pathway focussing on RBPs in a simple model organism. Thus, the overall aim of the thesis was to investigate the impact of the hypoxia signaling pathway on the global RBP landscape. Since we had successfully used *vhl-1(ok161)* mutant worms previously as a model to constitutively activate *HIF*, *C. elegans* was our choice of model organism to address this complex biological question.

Hence, to investigate the impact of the hypoxia signaling pathway on the global RBP landscape, we focused our work on the following objectives:

- To conduct RIC in wild-type and *vhl-1(ok161)* mutant worms
- To describe a comprehensive RBPome based on these data
- To identify novel RBPs
- To analyse the impact of hypoxia signaling on RNA-protein interactions
- To characterize the role of RBPs identified in lifespan regulation
- To create worm strains allowing for the identification of the RNA targets of these RBPs

4 Materials and Methods

4.1 Materials

4.1.1 Used materials

Table 1: List of materials used.

Materials	Product Number	Company
Blotting Paper / Grade BF 4	FT-2-521-110170G	Sartorius
Bis-Tris gel, 4% to 12% 1.0 mm, Mini Protein Gel, 12-well	10247002	Thermo Fischer Scientific
Carl Roth™ Opaque Blue Disposable Antistatic Polystyrene Weighing Trays	10057602	Fischer Scientific
Centrifuge tubes, Falcon® (15 ml)	734-0451	VWR
Centrifuge tubes, Falcon® (50 ml)	734-0448	VWR
CryoPure Tube 1.0ml white	72.377	Sarstedt
Empty Gel Cassette Combs, mini, 1.0 mm, 10 well	NC3010	Thermo Fischer Scientific
Empty Gel Cassettes, mini, 1.0 mm	NC2010	Thermo Fischer Scientific
Microtubes (1.5 ml)	72.690.001	Sarstedt
Femtotips®, injection capillary, sterile, set of 20	930000035	Eppendorf
Immobilon-P PVDF membrane	T831.1	Roth
Lid chain, flat	65.989.002	Sarstedt
Micro tube 1.5ml	72.690.001	Sarstedt
MicroAmp™ Fast Optical 96-Well Reaction Plate, 0.1 mL	4346907	Thermo Fischer Scientific
Microscope Slide 76 x 26 mm	11102	Engelbrecht
Multiply®-µStrip 0.2ml chain	72.985.002	Sarstedt
Parafilm M laboratory film	PM996	Bemis
Pasteur pipettes	612-1701	VWR
Petri dish 60x15mm with cams	82.1194.500	Sarstedt
Petri dish 92x16mm with cams	82.1473.001	Sarstedt
Polypropylene Bottle (250 ml)	334205	Beckman Coulter

Polypropylene Bottle (1000 ml)	A98812	Beckman Coulter
Platinum Wire 0.2 mm diameter/ 99.9%	900543	CHEMPUR
Pipette bulbs	612-2693	VWR
Peha-soft® nitrile white powder-free	9422083	Hartmann
PIPETMAN Classic	P1000 (F123602), P10 (F144802), P200 (F123601), P20 (F123600)	Gilson
Rotilabo® disposable weighing pans, opaque blue, anti-static (100 ml)	2150.1	Roth
Rotilabo® disposable weighing pans, opaque blue, anti-static (330 ml)	2159.2	Roth
Safe Lock Tubes 1.5 ml	0030120086	Eppendorf
Semi-micro cuvette, PS	67.742	Sarstedt
Strippettes (5 ml)	4051	Corning
Strippettes (10 ml)	4101	Corning
Strippettes (25 ml)	4251	Corning
Yellow Bevelled Tip 10 µl (Sterile), Racked	S1111-3810-C	Starlab
Yellow Bevelled Tip 1000 µl (Sterile), Racked	S1111-6811-C	Starlab
Yellow Bevelled Tip 200 µl (Sterile), Racked	S1111-1816-C	Starlab

4.1.2 Devices

Table 2: List of devices used.

Instrument	Product Number	Company
Centrifuge 5810/ 5810 R	5811000620	Eppendorf
Drying / heating oven	T 6030 300	Heraeus

EnSpire Multimode Plate Reader	2300-0000	Perkin Elmer
Ertical floor-standing autoclaves Systec V-Series	V-150	Systec
Fusion solo Chemiluminator	60-FU-SOLO	PeqLab
Gas burner Fuego SCS pro	8.204.000	Wild-tec
Horizontal Electrophoresis system size S	40-0708	PeqLab
Homogeniser	432-3750	VWR
Horizontal Electrophoresis system size L	40-1214	PeqLab
LED light source	KL 1500 LCD	Schott
Magnet	12321D	Thermo Fischer Scientific
Mediaclave 10/30	-	Integra
Mediajet, Petri Dish Filler	-	Integra
Minicentrifuge	521-2844	VWR
Microcentrifuge	5409000210	Eppendorf
Microscope Axio Zoom.V16	495010-0001-000	Zeiss
Microscope Observer.A1	-	Zeiss
micro injector (FemtoJet)	5252000013	Eppendorf
MIR Cooled Incubators	MIR-154-PE	Phcbi
NanoDrop Spectrophotometer	1000	PeqLab
Precision balance PCB	PCB 1000-2	Kern
Reax top Vortex	541-10000-00	heidolph
Scanner Perfection V800	B11B223401	Epson

Sonicator/Bioruptor Pico	B01060010	Diagenode
Sonopuls	3665	Bandelin
Spectrophotometer	80-3003-75	Biochrom
Stereomicroscope	MDG35	Leica
Tissue grinder, 7 ml	357424	Wheaton
Thermal Cycler	S100	Biorad
ThermoShaker	846-051-500	Analytikjena
Tube roll mixer SRT6	9.728 810	Häberle
UV Transilluminator	Ti5	Biometra
Vortex Reax top	541-10000-00	Heidolph
Waterbath WNB 22	WNB 22	Memmert
XCell SureLock™ Mini-Cell Electrophoresis System	EI0001	Thermo Fischer Scientific

4.1.3 Chemicals and reagents

Table 3: List of chemicals and reagents used.

Chemicals/Reagents	Product Number	Company
Agar	11396.03	Serva
Agarose	A9539	Sigma
Ampicillin	RO/K0291.000100	Roth
Ampuwa (Water)	7610894	Fresenius
Bacto Peptone	211820	BD
Bovine Serum Albumin (BSA)	A7030	Sigma
Bromphenol blue	A2331	Applichem
Calcium chloride	5239.1	Roth
Carbenicillin	6344.2	Roth
Cholesterol	C8667-5G	Sigma

cOmplete™, EDTA-free Protease Inhibitor Cocktail (PIM)	11873580001	Merck
dNTP set 100 mM	R0181	Thermo Fischer
Dithiothreiol (DTT)	6908	Applichem
Ethanol	9065	Roth
Ethidium Bromide Solution (1%)	2218.1	Roth
Ethylenediaminetetraacetic acid disodium salt dihydrate (EDTA)	E5134	Sigma
Gene Ruler 1 KB DNA Ladder	SM0311	Thermo Fischer Scientific
Gene Ruler 50 bp DNA Ladder	SM0372	Thermo Fischer Scientific
Glycerol	3783	Roth
GoTaq G2 Flexi DNA Polymerase	M7801	Promega
GoTaq® Reaction Buffers	M7911	Promega
Halocarbon oil 700	H8898-50ML	Sigma
Hydrochloride acid 2 N	T134	Roth
Incidin Plus	3011520	Ecolab
Isopropyl-β-D-thiogalactopyranosid (IPTG)	730-1497	VWR
LB-Agar	X965	Roth
LB-Medium	X964	Roth
Lithium chloride (LiCl)	L9650-500G	Merck
Lithiumdodecyl sulphate (LDS)	CN25.1	Roth
Loading Dye Solution 6x	R0611	ThermoFischer Scientific
Magnesium chloride (MgCl ₂)	KK36.1	Roth
Magnesium sulfate heptahydrate (MgSO ₄ ·7H ₂ O)	105886	Merck

Methanol	4627	Roth
Monopotassium phosphate (KH ₂ PO ₄)	3904.1	Roth
Nystatin (10 mg/ml)	475914	Calbiochem
PageRuler plus Prestained Protein Ladder	26619	Thermo Fischer
Potassium chloride (KCL)	6781.1	Roth
Pure acetic acid 99% - 100%	7332	Roth
RNase-free Water Ultra Pure	10977-035	Invitrogen
Sodium Azide	S2002	Sigma
Sodium Chloride	S5886	Sigma
Sodium dodecyl sulfate (SDS)	CN30	Roth
Sodium hydroxide solution 2N	T135	Roth
Tris Hydrochloride (HCl)	9090.3	Sigma
Trizma (Tris base)	93352-100G	Merck
TRIzol Reagent	15596018	Thermo Fischer
Tween-20	3472	Caesae&Lorentz
5-Fluoro-2'-deoxyuridine (FUDR)	F0503	Merck

4.1.4 Kits

Table 4: List of Kits used.

Kit/Assay	Product Number	Company
Pierce™ BCA Protein Assay Kit	23225	Thermo Fischer
Direct-zol RNA Miniprep	R2051	Zymo Research
Pierce™ Silver Stain Kit	24612	Thermo Fischer

4.1.5 Buffers

Table 5: List of buffers used.

Buffer	Composition
NP40 Washing buffer	50 mM Tris pH 7.5 140 mM LiCl 2 mM EDTA pH 8 0.5% NP40 0.5 mM DTT
Laemmli 2X	150 mM TrisHCl pH 6,8 4% SDS 20% Glycerol 0.002% Bromophenol blue 0.1 M DTT
Lysis Buffer	100 mM Tris pH 7.5 500 mM LiCl 10 mM EDTA pH 8 1% LiDS 5 mM DTT 1 Tablet Protease inhibitor per 50 ml
S Medium	1 l S Basal 10 ml 1 M potassium citrate pH 6 10 ml trace metals solution 3 ml 1 M CaCl ₂ 3 ml 1M MgSO ₄ 1 ml Cholesterol
S Basal	5.85 g NaCl 1 g K ₂ HPO ₄ 6 g KH ₂ PO ₄ 1 ml Cholesterol H ₂ O to 1 l
Trace metals solution	1.86 g disodium EDTA 0.69 g FeSO ₄ *7 H ₂ O 0.2 g MnCl ₂ *4 H ₂ O

	0.29 g ZnSO ₄ *7 H ₂ O 0.025 g CuSO ₄ *5 H ₂ O H ₂ O to 1 l
Bleach solution	0.4 N NaOH 7.5% NaClO
TAE Buffer	22 mM Tris 10 mM Acetic acid 1 mM Na ₂ EDTA 2*H ₂ O 0.0005% Ethidium bromide
Western blot Running Buffer	25 mM Tris 192 mM Glycine 0.1% (W/V) SDS pH 6.8
Western blot Transfer Buffer	25 mM Tris 188 mM Glycine 0.1% (W/V) SDS
Western blot Wash Buffer	30 mM Tris 300 mM NaCl 0.3% (V/V) Tween20 pH 7.5
Freezing solution	100 mM NaCl 50 mM KH ₂ PO ₄ 3.26 M Glycerol 300 M MgSO ₄
NGM Agar Plate	2.5 mM Bacto Peptone 53 mM NaCl 52 mM Serva Agar H ₂ O autoclave 1 mM CaCl ₂ 1 mM MgSO ₄ 0.013 mM Cholesterol 25 mM KPO ₄

	100 units/ml Nystatin
RNAi Plates	2.5 mM Bacto Peptone 53 mM NaCl 52 mM Serva Agar autoclave 1 mM CaCl ₂ 1 mM MgSO ₄ 0.013 mM Cholesterol 25 mM KPO ₄ 100 units/ml Nystatin 100 µg/ml Carbenicillin 4 mM IPTG
M9 buffer	1 mM MgSO ₄ 22 mM K ₂ HPO ₄ 52 mM Na ₂ HPO ₄ 85 mM NaCl in H ₂ O
LB medium	4 g LB Medium in 200 mL H ₂ O
Base solution	0.025 N NaOH 0.2 mM EDTA pH 12
Neutralization solution	40 mM Tris-HCl pH 5
ECL Detecting Solution	100 mM Tris 1.25 mM Luminol 0.20 mM Coumeric acid 0.75 % (V/V) H ₂ O ₂ pH 8.5

4.1.6 Software

Table 6: List of Software used.

Software	Version	Provider
Perseus	1.6.2.2	https://maxquant.net/perseus/

Graph pad prism	6.07	https://www.graphpad.com/
Fiji	2020-02-25 15:47	https://imagej.net/Fiji
Excel	Microsoft Office Professional Plus 2016	https://www.office.com/?omkt=de-DE
MaxQuant	1.5.3.8	https://www.maxquant.org/
R	3.4.4	https://www.r-project.org/

4.1.7 Beads used

Table 7: List of used beads.

Beads	Catalog Number	Provider	Usage
Dynabeads™ Oligo(dT) ₂₅	61005	Thermo Fischer	RNA interactome capture
Dynabeads™ Protein G	10004D	Thermo Fischer	Immunoprecipitation
Sera-Mag Carboxylate- Modified Magnetic Particles (Hydrophylic)	24152105050250	GE Healthcare	Mass Spectrometry
Sera-Mag Carboxylate- Modified Magnetic Particles (Hydrophobic)	44152105050250	GE Healthcare	Mass Spectrometry

4.1.8 Antibodies

Table 8: List of antibodies used.

Antigen	Catalog Number	Provider	Dilution	Usage
FLAG	F3165-1MG	Merck	1:50 1:10000	Immunoprecipitation Western Blot
IgG Mouse	115-035-003	Dianova	1:30000	Western Blot

4.1.9 Worm strains

Table 9: List of worm strains used.

Strain Name	Genotype	Source
WTN2	-	CGC
TMB032	<i>vhl-1(ok161) X</i>	Nephrolab
CB1370	<i>daf-2(e1370) III</i>	CGC
TMB087	<i>pqn-53::3xFLAG</i>	Nephrolab

4.1.10 RNAi used

Table 10: List of RNAi used.

RNAi against	Sequence Name	Source
<i>EV</i>	-	Nephrolab
<i>GFP</i>	-	Nephrolab
<i>daf-2</i>	<i>Y55D5A.5</i>	Nephrolab
<i>daf-16</i>	<i>R13H8.1</i>	Nephrolab
<i>atad-3</i>	<i>F54B3.3</i>	Ahringer library
<i>C46F11.4</i>	<i>C46F11.4</i>	Ahringer library
<i>R148.5</i>	<i>R148.5</i>	Ahringer library
<i>cdk-11.1</i>	<i>B0495.2</i>	Ahringer library
<i>F42G8.10</i>	<i>F42G8.10</i>	Ahringer library
<i>M28.5</i>	<i>M28.5</i>	Ahringer library

4.1.11 Oligonucleotides used

Table 11: List of oligonucleotides used.

Primer name	Sequence (5'→3')	Usage

<i>dpy-10</i> ssODN	CACTTGAACCTTCAATACGGCAAGAT GAGAATGACTGGAAACCGTACCGCA TGCGGTGCCTATGGTAGCGGAGCT TCACATGGCTTCAGACCAACAGCCT AT	CRISPR-Cas9 injection mix
<i>dpy-10</i> crRNA	GCUACCAUAGGCACCACGAG	CRISPR-Cas9 injection mix
<i>pqn-53</i> ssODN	GTTCAATATCGTCCAGTCCAATACGT CACTGATCAGGTTGTCAACTCTCGT GGTCGTGGATTCCGTGCCTTCGATT ATAAAGACCACGATGGAGACTATAA AGATCATGACATTGACTACAAGGAT GACGACGACAAGTGATTTTCATCAAC TCGTACACAATCAAGGATACTCAG	CRISPR-Cas9 injection mix
<i>pqn-53</i> crRNA	CATCAACTCGTACACAATCAAGG	CRISPR-Cas9 injection mix
<i>pqn-53</i> fp	GTTCAATATCGTCCAGTCCAATACG	Genotyping PCR/ Sequencing
<i>pqn-53</i> rp	GAGTATGGCGGAGTATTTTATTAAC ATGG	Genotyping PCR/ Sequencing
<i>vhl-1</i> fp	TCATAAACCGCTGTCAATCG	Genotyping PCR
<i>vhl-1</i> rp	AAAACGACCGTATGGGGAAT	Genotyping PCR
<i>vhl-1</i> fp	ATCATCCATGGGTTGCTAGG	Genotyping PCR
L4440 fp	CAGTGAGCGAGGAAGCAA	RNAi sequencing
L4440 rp	AAAACGACGGCCAGTGAG	RNAi sequencing

4.2 Methods

4.2.1 Worm maintenance

4.2.1.1 Culturing of *C. elegans*

Worms were cultured on NGM agar plates seeded with *E. coli* strain OP50 at 20°C using standard techniques as described before (Brenner 1974).

4.2.1.2 Culturing of *Escherichia coli* bacteria

Escherichia coli (*E. coli*) bacteria were cultured in LB medium overnight on a shaker at 37°C and seeded on NGM agar plates. For the *C. elegans* liquid culture, bacteria were harvested when an OD of 0.8 was measured in 1 liter LB medium to have them

in the exponential phase. For long term storage 800 µl of a bacteria overnight culture were mixed with 200 µl Glycerol in a 1 ml cryotube and stored at -80°C.

4.2.1.3 Freezing worms

Starved L1 larvae were frozen at -80°C for storage. 2 ml of freezing solution mixed with 2 ml of M9 buffer were used to wash the worms from the plates, the larvae were then aliquoted in cryotubes (1 ml) and stored at -80°C.

4.2.1.4 Egg prep

Axenization is a method commonly used to remove bacterial and fungal contaminations and to synchronize a nematode population. Adult gravid worms were collected either from plates or from liquid culture and were washed in M9 buffer. The worms were then incubated with Bleach solution until complete lysis (approx. 5 min confirmed under a stereo microscope). After adding M9 buffer to partly neutralize the solution, the mixture was centrifuged at 400 x g for 2 minutes. The supernatant was discarded and the pellet containing the isolated eggs was washed three times with M9 buffer. After washing the eggs were either transferred on OP50 seeded NGM dishes, or on non-seeded dishes for L1 synchronization or directly added to a liquid culture.

4.2.1.5 Worm lysis for genotyping

A single worm was transferred to 11 µl of base solution and incubated at 95°C for 30 minutes. To stop the lysis 11 µl of neutralization solution was added and the lysate was stored at -20 °C.

4.2.1.6 Feeding RNAi expressing bacteria

RNAi by feeding is commonly used to down-regulate gene expression in nematodes (Fire et al. 2007). The RNAi expressing bacteria, *E. coli* strain HT115 was cultured in LB medium containing 100 µg/ml ampicillin and 10 µg/ml tetracycline at 37°C, shaking. The bacteria were then seeded on RNAi NGM agar plates containing 1 mM IPTG and 100 µg/ml Carbenicillin. IPTG induces the activation of the two inverted T7 promoters and by this the expression of double-stranded RNA (Timmons et al. 2001). As a technical control for each RNAi experiment, worms ubiquitously expressing *p_{sur}*-

5::GFP were fed with bacteria expressing empty vector RNAi and GFP RNAi, and visually screened at a fluorescence microscope (Axio Zoom) for GFP levels.

4.2.1.7 *C. elegans* Lifespan Machine

Setup

The Lifespan Machine is a scanner-based system able to observe and compute the lifespan of *C. elegans* (Stroustrup et al. 2013). This machine consists of hardware and software parts. The hardware parts are modified flatbed scanners and glass plates including rubber mask. In our laboratory, 10 Epson v800 scanners were set up. Differently than what described by Stroustrup et al. 2013, we installed two long lateral fans on each scanner instead of eight small fans. The rubber masks used on each scanner were made for 60 mm dishes at a size to harbor 14 dishes (Figure 24). The software part consists of the acquisition server, the analysis server and the website. For the acquisition server, we used the version 2.3 (from <http://lifespanmachine.org.eu/lsm/>) on a laptop with a Linux operating system. To increase the calculation speed the analysis software was run simultaneously on multiple computers with windows 10 as the operating system. The lifespan machine website is the interface between the acquisition server and the analysis server. It manages the data storage and schedules data processes.

Experiments

For each lifespan experiment, 35 young adult worms were transferred to 60 mm NGM or RNAi plates containing 150 μ M Fluorodeoxyuridine (FUdR) to inhibit reproduction. For each strain at least 3 plates were used. The plates were put upside down without the lids on the scanner glass plates, sealed by the rubber mask to prevent desiccation. The glass plates were then placed in the scanner, and a first scan was taken to make sure the plates and the worms were scanned correctly. With this scan, the position of each plate was defined and the complete experiment could then be started. The scan interval was set to 30 minutes. After the first three scans were finished the masking which splits the acquired images into per plate pictures was applied. Following the worm detection could be started. When all worms were dead the storyboard was created. The storyboard visualizes each worm detected on the plates over time. At this step, each worm image was manually checked and was

censored when there was any discrepancy (usually not a worm or worm was still alive). The final death events of the worms were collected in a table.

Analysis

The lifespan machine results are summarized in a table containing all information collected during the complete experiment. This information comprises device name, experiment name, plate name and location, strain name, age at death, and censored worms. To visualize the data in a graph we used the following information: strain name and age at death. The graph was generated using the graph pad prism software version 5.04. All of the lifespans performed in this work are summarized in Table 12.

Table 12: Summary of Lifespan results.

Figure	Strain	RNAi Strain used	Number of Worms	Mean lifespan in days
Figure 26 A	wild-type	-	349	20
Figure 26 B	wild-type	-	58	16.5
Figure 26 B	<i>vhl-1(ok161)</i>	-	84	20
Figure 26 C	wild-type	-	70	21
Figure 26 C	<i>daf-2(e1370)</i>	-	242	46
Figure 27 A	wild-type	<i>empty vector</i>	88	16.5
Figure 27 A	wild-type	<i>daf-2</i>	163	27.5
Figure 27 B	wild-type	<i>empty vector</i>	115	18.5
Figure 27 B	wild-type	<i>daf-16</i>	36	11
Figure 28 A	wild-type	<i>Empty vector</i>	69	17.14
Figure 28 A	wild-type	<i>daf-2</i>	65	28.10
Figure 28 A	wild-type	<i>atad-3</i>	66	21.66
Figure 28 A	wild-type	<i>C46F11.4</i>	59	21.66
Figure 28 A	wild-type	<i>R148.5</i>	77	20.83
Figure 28 A	wild-type	<i>F42G8.10</i>	51	23.35
Figure 28 A	wild-type	<i>M28.5</i>	57	19.94
Figure 28 A	wild-type	<i>cdk-11.1</i>	54	20.16
Figure 28 A	wild-type	<i>tat-5</i>	54	16.79
Figure 28 A	wild-type	<i>pfd-5</i>	53	17.18

4.2.2 Molecular techniques

4.2.2.1 Genotyping PCR

The desired DNA fragments were amplified by PCR. For the genotyping of *vhl-1(ok161)* mutants, three primer approach was used whereas for *pqn-53::3xFlag* worms two primer approach were used. The following protocol was performed:

Table 13: Pipetting scheme for genotyping PCR.

ddH ₂ O	13.35 μ l
5xGotaq Buffer	5 μ l
25 mM dNTPs	0.2 μ l
25 mM MgCl ₂	1.5 μ l
5 μ M Primer 1	1.25 μ l
5 μ M Primer 2	1.25 μ l
5 μ M Primer 3 or ddH ₂ O	1.25 μ l
Worm lysate	1 μ l
Gotaq 5 u/ μ l	0.2 μ l
Total volume	25 μ l

The following PCR program was used on a standard thermocycler:

Table 14: Genotyping PCR program.

95°C	95 min.	
95°C	30 sec.	x 30 Cycles
55°C	30 sec.	
72°C	45 sec.	
72°C	5 min.	
10°C	∞	

4.2.2.2 Gel electrophoresis

Table 15: Agarose gel ingredients.

2% Gel	
Agarose	2 g
TAE-buffer	100 ml
Ethidium bromide 1%	1 μ l

The products of the genotyping PCRs were analysed by electrophoresis on 2% agarose gel. The size was estimated using the appropriate DNA ladder.

4.2.2.3 *C. elegans* genome editing using CRISPR-Cas9

The CRISPR-Cas9 protocol was performed as already described (Paix et al. 2017). Briefly, the strategy consists of a guide RNA (crRNA) that will guide Cas9 protein to the target sequence and a repair template (single-stranded oligodeoxynucleotide (ssODN)) containing homology arms corresponding to the gene and a FLAG tag. We designed a crRNA and an ssODN for the *pqn-53* gene. The *pqn-53* ssODN consists of the nucleotide sequence corresponding to a triple FLAG (3xFLAG) tag. The 3xFLAG tag sequence is flanked 5' and 3' by 30 nucleotide long homology arms corresponding to parts of the *pqn-53* gene sequence. Besides, *dpy-10* gene guide RNA and DNA repair template were designed to allow the identification of successfully injected hermaphrodites. The injection was performed as described before (Evans 2006). Briefly, five worms day one adults were placed on a coverslip with a 2% agarose pad on it, and were covered with a layer of Halocarbon oil to prevent drying during the process. The injection needle was filled with the CRISPR-Cas9 mix and positioned to inject worms. Injections were performed on a microscope (Observer.A1) connected to an electronic microinjector (FemtoJet) with a magnification of 40x.

Table 16: CRISPR-Cas9 injection mix.

Cas9 (10 µg/µl)	5 µl
tracrRNA (4 µg/µl)	5 µl
<i>dpy-10</i> crRNA (8 µg/µl)	0.3 µl
<i>dpy-10</i> ssODN (500 ng/µl)	0.3 µl
<i>pqn-53</i> crRNA (8 µg/µl)	0.5 µl
<i>pqn-53</i> ssODN (500 ng/µl)	1 µl
KCl (1 M)	0.3 µl
HEPES pH 7.4	0.3 µl
H ₂ O	7.3 µl

For each construct, 50 worms were injected in one of the two gonads and afterward placed on a single plate seeded with OP50, and incubated at 20 °C for several days. After 2 days, the plates were screened for the presence of roller and dumpy phenotypes in the F1 generation, caused by editing events in the gene *dpy-10* and an indication of successful injection. The F1 worms from the selected plates were singled on new plates and grown till they laid eggs. Next, the genotyping PCR was performed on the F1 generation and the F2 worms were selected based on the results of the PCR. After the F2 generation laid eggs they were genotyped and FLAG tag homozygous worms were isolated. Sanger sequencing was used to screen and confirm the integration of the triple FLAG tag after CRISPR based genome editing. For that reason, the following reaction was performed.

Table 17: Sequencing mix.

BigDye® Terminator	0.25 µl
BigDye™ Terminator buffer	2.25 µl
<i>pqn-53</i> fp or <i>pqn-53</i> rp (1:1000 of 100 pmol/µl)	2 µl
Worm lysate	1 µl
ddH ₂ O	4.5 µl

Table 18: Sequencing reaction cycling conditions.

Temperature (°C)	Time	
96	60 sec	
96	10 sec	
55	5 sec	40 cycles
60	4 min	
10	∞	

The samples were then submitted to the Cologne Center for Genomics (CCG).

4.2.2.4 Western blot

Western blot analysis was used to confirm the integration, expression and size of triple FLAG after CRISPR injection. First, 50 worms were picked into 1 ml lysis buffer and sonicated (Sonopuls) ten times for 30 seconds. Afterward, 2xLaemmli buffer was added and the sample was incubated for 5 minutes at 95°C. 30 µl of the samples were loaded on a 4 to 12% Bis-Tris polyacrylamide gel and the gel was run at 200 V constant for 60 minutes. The PVDF membrane was activated before by incubation for 30 seconds in methanol. Meanwhile, the gel and the two filter papers were soaked in transfer buffer. Next, the gel was transferred into a transfer chamber where a sandwich was built with the following order from bottom to top: filter paper, PVDF membrane, Gel, filter paper. The transfer was run at 12 V for 60 minutes. The membrane was incubated with a blocking solution (4% BSA in wash buffer) for one hour. Then the membrane was washed three times with wash buffer and incubated for 1 hour with the first antibody (1:10000) recognizing the FLAG tag. After another washing round of three times the membrane was incubated for 1 hour with the horseradish peroxidase (HRP) labeled secondary antibody (1:30000) recognizing the FLAG tag. Finally, the membrane was washed three times and overlaid with 100 µl Femto Luminol buffer. That leads to oxidizing luminol in the presence of HRP resulting in chemiluminescence. The chemiluminescence was visualized using a chemiluminescence imaging system (Fusion solo).

4.2.2.5 RNA interactome capture (RIC)

For each liquid culture, 300.000 worms were grown in 300 ml of growth medium. The growth medium was prepared by resuspending an OP50 bacterial pellet obtained from 1 liter OD 0.8 bacteria culture in S Medium. Isolated eggs were added to the mixture, and incubated at 20°C, shaking at 120 rpm for 72 hours. Young adult worms were harvested and washed three times in M9 buffer. After settling down in a 50 ml tube on ice, the supernatant was discarded and the worms were transferred to an empty NGM plate. Half of the worms (150.000) were irradiated with UV-C (254 nm) at 300mJ/cm² (Stratalinker 1800). Afterwards the worms were collected in M9 buffer and resuspended in lysis buffer. The non-crosslinked worms (150.000) were directly resuspended in lysis buffer. Worm lysates were prepared using a dounce homogenizer performing fifty strokes for each sample and checking at the stereomicroscope for complete homogenization. The lysates were directly used for RNA interactome capture and a fraction of the same lysate for proteome analysis. A total of 18 samples were created (Table 19). RIC was performed as previously described (Ignarski et al. 2019), and adapted to *C. elegans*. The lysate was incubated with 2 ml oligo(dT) magnetic beads, rotating for 1 hour at 4°C. The beads were collected on a magnet and the supernatants were saved for two additional rounds of depletion. Beads were then washed three times with 10 ml lysis buffer, three times with 10 ml washing buffer and once with 10 ml washing buffer without NP40. After the last wash the beads were resuspended in 300 µl elution buffer and incubated at 80°C for 2 minutes. The protocol was repeated three times in total and the three eluted fractions were combined. An aliquot from each sample was taken to measure RNA concentration. To remove RNA before mass spectrometry and silver gel analysis, the combined fractions were treated with 10 U/ml RNase I and 125 U/ml Benzonase at 37°C for 3 hours. After that, 2% of each eluate was loaded together with 0.01% of the lysate (taken after homogenizing) on a 4 to 12% Bis-Tris gel. The gel was run at 200 V constant for 60 minutes and was incubated afterwards with silver staining. RNA concentration was measured using a Qubit™ RNA HS Assay Kit. Protein concentration was measured using BCA assay. Protocols were performed as described in the manual (PierceSilver Stain Kit, Qubit™ RNA HS Assay Kit, PierceBCA Protein-Assay).

4.2.3 Mass Spectrometry

4.2.3.1 Protein preparation for mass spectrometry

All protein samples origin from RIC and the whole worm lysate samples were prepared for mass spectrometry using carboxylate modified paramagnetic beads (SP3) according to the published protocol (Hughes et al., 2014). Briefly, samples were reduced in 5 mM dithiothreitol (DTT) incubating at 55°C for 30 min. Reduced cysteine residues were alkylated by adding chloroacetamide (CAA) to 40 mM for 30 minutes at room temperature in the dark. The samples were then centrifuged for 10 minutes at 20,000 x g and the supernatants were transferred to a new tube. Hydrophilic and hydrophobic Sera-Mag carboxylate-modified magnetic particles (GE Healthcare) were combined 1:1, washed two times with 10 volumes of water and resuspended at a concentration of 10 µg/µl with water. 2 µl of the beads mix was added to the samples and acetonitrile (ACN) was added to a final percentage of 50%. The mixture was incubated at room temperature for 8 minutes and placed on a magnetic rack for 2 minutes. Supernatants were removed and the beads were washed twice with 200 µl of 70% Ethanol (EtOH) and once with 100% ACN. The beads were air dried and reconstituted in 5 µl 50mM triethylammonium bicarbonate (TEAB) containing 0.5 µg trypsin and 0.5 µg LysC. Proteins were digested for 16 hours at 37°C. The beads were resuspended by pipetting up and down and ACN was added to 95 % final. The mixture was incubated at room temperature for 8 minutes and placed on a magnetic rack for 3 minutes. Supernatants were removed and the beads were washed twice with 200 µl of 100% ACN. Peptides were eluted from the beads by the addition 9 µl 4% dimethyl sulfoxide (DMSO) and sonication for 5 minutes. Samples were placed on a magnetic rack and the supernatants were transferred to new tubes. This step was repeated once to ensure the complete removal of magnetic beads. Peptides were acidified by the addition of 1 µl 10% formic acid and stored at -20 °C until LC-MS analysis.

4.2.3.2 LC-MS Acquisition

All samples were analysed on a Q Exactive Plus Orbitrap (Thermo Scientific) mass spectrometer that was coupled to an EASY nLC LC (Thermo Scientific). Peptides were loaded onto an in-house packed analytical column (50 cm — 75 μ m I.D., filled with 2.7 μ m Poroshell EC120 C18, Agilent) that was operated at a constant flow rate of 250 nl/min at 50°C. Depending on the experiment type, one of three different chromatographic gradients was used. 240 min: 4-5% solvent B (0.1% formic acid in 80% acetonitrile) within 1.0 min, 5-28% solvent B within 200.0 min, 28-50% solvent B within 28.0 min, 50-95% solvent B within 1.0 min, 150 min: 3-5% solvent B (0.1% formic acid in 80% acetonitrile) within 1.0 min, 5-30% solvent B within 119.0 min, 30-50% solvent B within 19.0 min, 50-95% solvent B within 1.0 min 90 min: 3-5% solvent B (0.1% formic acid in 80% acetonitrile) within 1.0 min, 5-30% solvent B within 65.0 min, 30-50% solvent B within 13.0 min, 50-95% solvent B within 1.0 min. All gradients included final wash and column equilibration steps. Depending on gradient length, peptide precursors were dynamically excluded for 40.0 s, 25 s or 15 sec. MS1 survey scans were acquired from 300-1750 m/z at a resolution of 70,000. The top 10 most abundant peptides were isolated within a 1.8 Th window and subjected to HCD fragmentation at a normalized collision energy of 27%. The AGC target was set to 5e5 charges, allowing maximum injection times of 60 ms (240 min and 150 min gradients) or 100 ms (90 min gradient). Product ions were detected in the Orbitrap at a resolution of 17,500.

4.2.3.3 Data analysis and statistics

Protein identification: all mass spectrometric raw data were processed with MaxQuant (version 1.5.3.8) using default parameters. Briefly, MS2 spectra were searched against the Uniprot CAEEL.fasta database (downloaded the 16.6.2017), including a list of common contaminants. False discovery rates on protein and PSM levels were estimated by the target-decoy approach to 1% (Protein FDR) and 1% (PSM FDR) respectively. The minimal peptide length was set to 7 amino acids and carbamidomethylation at cysteine residues was considered as a fixed modification. Oxidation (M) and Acetyl (Protein N-term) were included as variable modifications. The match-between runs option was enabled.

Statistical analysis of both the whole worm proteome and the RNA interactome raw data was performed with the Perseus software (Tyanova et al., 2016), version 1.6.2.2. iBAQ intensities were used in this analysis and \log_2 transformed. Filtering of proteins only identified by site, reverse proteins and potential contaminants was performed.

RNA interactome: Two samples were identified as outliers based on the number of proteins measured, which were higher than in crosslinked samples and the results of PCA and hierarchical clustering (Figure 10). Indicating that these samples possibly contaminated during processing e.g. with the whole worm lysates and therefore excluded from further analyses “T-test was performed for *vhl-1(ok161)* crosslinked (n=3) versus non-crosslinked samples (n=2) and WT crosslinked (n=3) versus non-crosslinked samples (n=2) using $FDR < 0.05$ and $s_0 = 0.5$.

Whole Proteome: First, proteins measured at least 3 times out of 6 replicates in total (WT and *vhl-1(ok161)*) were filtered. Second, the protein amount of wild-type and *vhl-1(ok161)* mutant worms were normalized by subtracting the median and adding $x + (\text{highest median}) + 1$. Third, missing values were imputed by replacing them from a normal distribution (width 0.3, downshift 1.8) and significantly regulated proteins were identified using a t-test ($FDR < 0.05$, $s_0 = 0.5$).

Categorical annotation and enrichment analysis: The UniProt IDs were annotated using Perseus software for Gene Ontology (GO), PFAM and SMART. Gene set enrichment analysis of the combined Class I and II RIC of *vhl-1(ok161)* and WT was calculated using a Fisher exact test (Perseus standard settings, $FDR < 0.05$ (Tyanova et al., 2016)), and the total number of proteins identified in both RIC and Proteome experiments was used as background.

Correlation analysis WT vs. *vhl-1(ok161)* RNA interactome: The linear regression of \log_2 fold change of WT versus *vhl-1(ok161)* was calculated with R (version 3.4.4) using the method *deming()* from the R package *deming* (version 1.4 (<https://cran.r-project.org/web/packages/deming/index.html>)) which applies the method of total least squares. This results in the formula $y = 0.7806137 + 1.095646 \cdot x$ with a \log_2 fold change of *vhl-1(ok161)* on the x-axis and values of WT on the y-axis. To get the proteins that are more enriched in *vhl-1(ok161)* or WT, we calculated the linear equations that define the upper and lower boundary of the interval in which 95% of all measurements lie, in other words, the 95% prediction interval. This interval is defined by multiplying the standard deviation of the regression (1.562865) by 1.96 and

adding or subtracting this value to the intercept of the regression line for the upper and lower boundary, respectively. The linear equation for the upper boundary is $y = 3.843829 + 1.095646 \cdot x$, the equation for the lower boundary is $y = -2.282602 + 1.095646 \cdot x$.

4.2.3.4 Data and Software Availability

The mass spectrometry data (Raw data and MaxQuant (version 1.5.3.8) output) have been deposited at the ProteomeXchange Consortium (<http://www.ebi.ac.uk/pride>) via the PRIDE (Perez-Riverol et al., 2019) partner repository with the dataset identifier PXD014469. An interactive online repository was created and is provided at http://shiny.cecad.uni-koeln.de:3838/celegans_rbpome (Esmailie et al. 2019).

5 Results

5.1 RNA Interactome Capture of wild-type and *vhl-1(ok161)*

5.1.1 *vhl-1(ok161)* modulates the length of *C. elegans*

Stabilization of HIF-1 is central to hypoxia signaling and results in the transcription of many target genes. Although the hypoxia signaling pathway is well studied its impact on the global RBPome is elusive. In this study, we used *C. elegans* as a model to analyse the impact of hypoxia signaling on RBPs. We used *vhl-1* mutant worms (*vhl-1(ok161)*) as a model to constitutively activate HIF. Phenotypic analysis of the first larval stage of *C. elegans* revealed that *vhl-1(ok161)* mutants are shorter compared to the wild-type worms (Figure 6A). Quantification of the length confirmed the observed shorter length of *vhl-1(ok161)* mutants compared to wild-type worms (Figure 6B). A previous study performing developmental studies in *vhl-1(ok161)* mutant worms observed the length phenotype likewise in larvae and showed that it persists in the adult stage (Wen et al. 2015). Further studies from our lab revealed that *vhl-1(ok161)* shorter length is dependent on HIF-1 activation (data not shown). Consequently, before performing RIC in wild-type and *vhl-1(ok161)* mutant worms we analysed their RNA content. Using 500 worms for each strain we observed reduced RNA amount per worm in *vhl-1(ok161)* mutant compared to wild-type (Figure 6C). The RIC method is based on the pulldown of poly-adenylated RNA and the mass spectrometric analysis of the bound proteins. Therefore we also analysed the protein amount of the worms. Again, the analysis revealed that the protein amount of *vhl-1(ok161)* mutant worms compared to wild-type is reduced (Figure 6D). As a result, the RIC experiment needs to be adjusted for the fact that the same number of *vhl-1(ok161)* mutant worms contain less RNA and protein compared to wild-type worms.

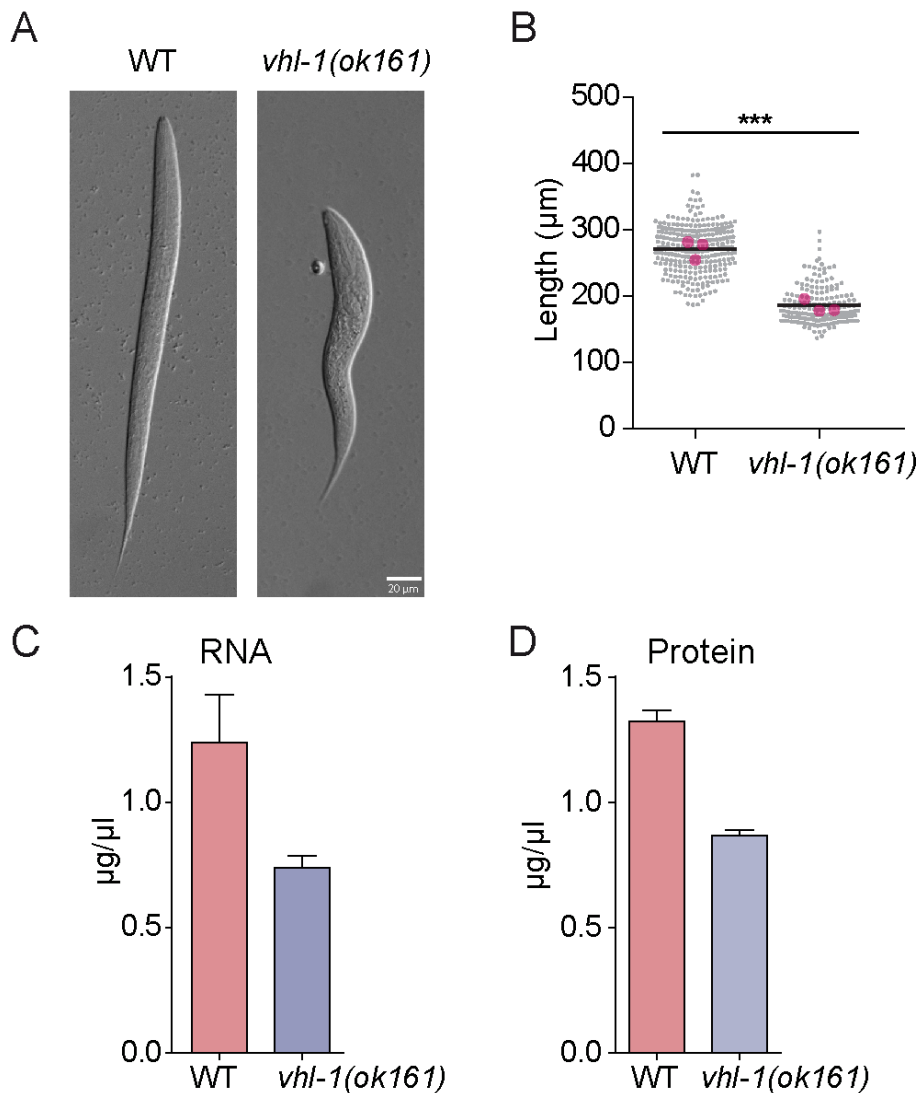


Figure 6: *vhl-1(ok161)* mutants are shorter and contain less RNA and protein.

A. Representative images of L1 worms of wild-type (WT) and *vhl-1(ok161)* using Nomarski microscopy with a magnification of 40x. Scale bar represents 20 μm . **B.** Quantification of the length from wild-type and *vhl-1(ok161)* worms using WormSizer. Three biological replicates are shown whereas each dot represents the length of a single worm, magenta dots represent the mean of a single biological replicate and the black bar shows the mean of the three biological replicates (n = 276 for WT, n = 177 for *vhl-1(ok161)*). Significance was calculated by comparing the mean value of three biological replicates (p = 0.0022). **C.** Measurement of RNA obtained from 500 wild-type (red bar) or *vhl-1(ok161)* (blue bar) worms dissolved in 700 μl TRIzol using Qbit assay. **D.** Measurement of protein obtained from 500 wild-type (red bar) or *vhl-1(ok161)* (blue bar) worms dissolved in 1 ml lysis buffer using BCA.

5.1.2 Establishing RNA Interactome Capture in *C. elegans*

To investigate whether the hypoxia signaling pathway modulates the RNA- protein interactome we established RIC in *C. elegans*. To obtain sufficient material performing RIC we grew wild-type and *vhl-1(ok161)* mutant worms in liquid culture.

For each biological replicate, 300.000 worms were used and split into two samples containing 150.000 worms each. When the worms reached the young adult stage they were harvested and the crucial step of crosslinking RNA and protein was conducted. Crosslinking was performed for one of the two samples per condition using a UV wavelength of 254 nm. The other sample serves as a negative control and is termed “non-crosslinked” from now on. Comparison of the crosslinked samples against the non-crosslinked samples after RIC allows for the identification of bona-fide RBPs. The crosslinked and non-crosslinked samples were collected and stored frozen. After the collection of the biological replicates, all samples were mechanically homogenized. Next, the RNA was captured from the worm lysate by adding oligo-dT beads followed by several stringent washing steps. Following the elution of the ribonucleoprotein (RNP) complexes, the protocol was repeated twice and the pooled elution was RNase digested (For detailed experimental procedures see Methods). Finally, the proteins were digested according to the published protocol using carboxylate modified paramagnetic beads (Hughes et al. 2014) and loaded on a mass spectrometer (Figure 7). Furthermore, after oligo-dT capture RNA and protein measurements were performed. This will show the presence of RNA and protein at that specific step and thereby confirms the efficacy of the RIC setup in wild-type and *vhl-1(ok161)* mutant worms.

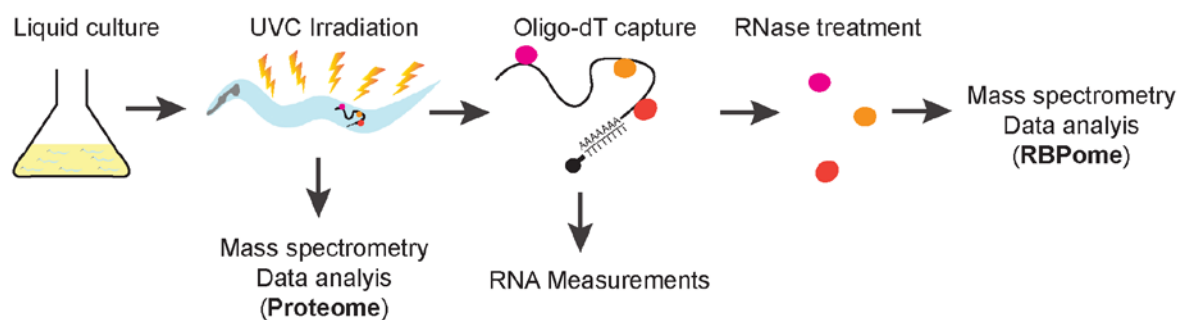


Figure 7: Experimental workflow of RIC.

Wild-type and *vhl-1(ok161)* mutant worms were grown at 20°C in liquid culture until they reached the young adult stage. Worms were harvested and RNA and proteins (red, orange and magenta dots) were crosslinked using a UV wavelength of 254 nm. Afterwards, the worms were mixed with lysis buffer and mechanically homogenized. 10% of the lysate was used for mass spectrometry to analyse the proteome. 90% of the lysate was incubated with oligo-dT beads followed by washing steps. 10% of the bead suspension was used for RNA measurements. The rest was RNase digested and used for mass spectrometry to analyse the RBPome. For the detailed experimental procedure see Methods. See also Esmailie et al. 2019.

5.1.3 Analyses of RNA and protein amounts reveal functioning RIC

We used the wild-type and *vhl-1(ok161)* mutant worm strains for the RIC. Previously, we found that the same number of *vhl-1(ok161)* mutant worms contain lower amounts of RNA and protein compared to wild-type. Since we used the same worm number for RIC saturation of the beads was crucial at this step. To confirm this, we measured the RNA amount of the samples obtained after oligo-dT capture and before RNase treatment (Figure 8A). Here, we analysed the crosslinked and non-crosslinked samples of wild-type and *vhl-1(ok161)* mutants, respectively. Notably, there was no difference in RNA amount between non-crosslinked and crosslinked samples of either wild-type or *vhl-1(ok161)* mutant worms. In contrast to the RNA content in whole worms (Figure 6C), there was an equal amount of RNA in wild-type and *vhl-1(ok161)* mutant worm samples after pulldown indicating saturation. Saturation of the beads compensates the reduced content of RNA in *vhl-1(ok161)* mutant worms leading to an equal amount of RNA after pulldown (Figure 8A). Also, we determined the amount of proteins in the RIC samples after RNase treatment. In crosslinked samples, we would expect more protein compared to the non-crosslinked samples. Since the RIC protocol contains harsh washing steps all non-crosslinked proteins disengage from RNA and are washed off the oligo-dT beads. To determine the protein amounts in the samples we performed silver staining of a polyacrylamide gel loaded with 0.1% of total lysates of wild-type and *vhl-1(ok161)* before (Input) and after the RIC experiment (10% of pooled eluates) (Figure 8B). The silver staining revealed that all samples, wild-type and *vhl-1(ok161)*, both crosslinked and non-crosslinked had similar amounts of protein in the input samples. However, as expected, the bands distributed between 40 kDa and 130 kDa on the polyacrylamide gel from the eluate samples showed a higher intensity in crosslinked samples compared to non-crosslinked samples in both wild-type and *vhl-1(ok161)* mutant worms. This result is consistent with previous studies that performed RIC showing enrichment of proteins in UVC crosslinked samples compared to non-crosslinked samples (Castello et al. 2012; Ignarski et al. 2019; Kwon et al. 2013; Liepelt et al. 2016). The measurement of RNA and protein amounts revealed effective crosslinking of RNA with protein and enriched pulldown of proteins in crosslinked samples. After all samples had passed this quality control step, we moved on to mass spectrometry measurements for the identification and quantification of RBPs in both conditions.

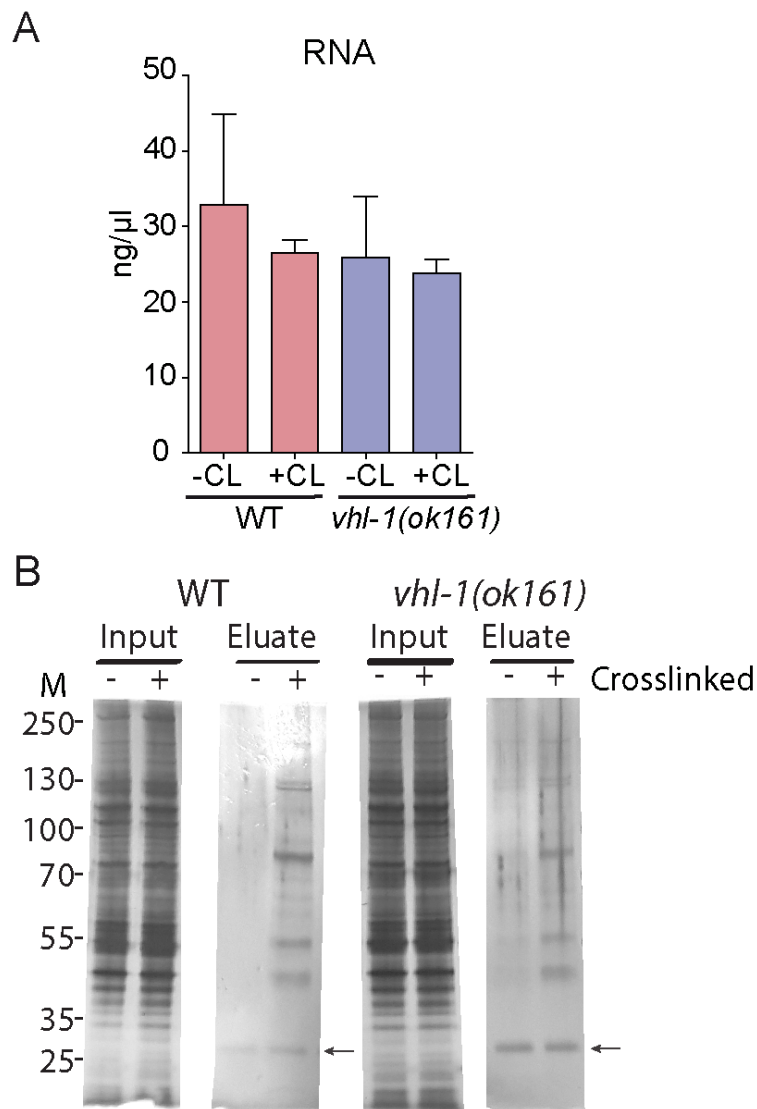


Figure 8: Silver staining revealed efficient crosslinking in RIC.

A. RNA measurement of RIC samples after precipitation. RNA was measured from wild-type (red bars) and *vhl-1(ok161)* (blue bars) crosslinked (+CL) and non-crosslinked (-CL) samples. Data are represented as mean \pm SEM of three biological replicates. **B.** Image of a silver stained polyacrylamide gel loaded with RIC input and eluate samples after RNase treatment of wild-type and *vhl-1(ok161)* worms. Non-crosslinked samples are denoted by - and crosslinked samples are marked with +. The arrow indicates the RNase I band in the RNase I treated eluates. The protein ladder (M) indicates the protein size ranging from 25 kDa to 250 kDa. See also Esmailie et al. 2019.

5.1.4 Mass spectrometry based identification of RNA associated proteins

From the RIC we had 3 biological replicates of crosslinked and non-crosslinked samples from wild-type and *vhl-1(ok161)* mutant worms. Also, we used the whole lysate for proteomics of 3 biological replicates from wild-type and *vhl-1(ok161)* mutant worms. Together we loaded 18 samples on the mass spectrometer in total (Table 19).

Table 19: Overview of samples analysed by mass spectrometry.

	wild-type	<i>vhl-1(ok161)</i>
Crosslinked samples	3*	3*
Non-crosslinked samples	3*	3*
Proteome samples	3*	3*

*Biological replicate per genotype

To compare these datasets to each other we analysed the mass spectrometry data of all samples together and processed them using the Perseus software package (For details see Methods). In total, we identified 6350 proteins. For further analysis we chose intensity-based absolute quantification (iBAQ) values instead of label-free quantitation (LFQ) values since we expected large differences regarding the number of proteins measured between crosslinked and non-crosslinked samples. This would have caused the LFQ-based normalization to exclude a large number of hits since the LFQ approach uses the whole dataset for normalization whereas iBAQ does not. After logarithmization of the iBAQ values into \log_2 values, we first checked the whole worm proteome. For the proteome analysis we removed proteins if they were not measured at least in 3 samples out of 6 (wild-type and *vhl-1(ok161)*). This filtering step resulted in 5759 proteins identified. For the identification of significantly regulated proteins of *vhl-1(ok161)* mutants compared to wild-type, we used a t-test with an $FDR \leq 0.05$ and $s0 = 0.5$. This resulted in 162 proteins that were significantly regulated in *vhl-1(ok161)* mutants compared to wild-type. $s0$ is a feature in Perseus that – on top of p-values - takes the protein fold changes into account, i.e. proteins with a good p-value but minimal fold change will not reach the threshold. Further analysis of the whole worm proteome of wild-type and *vhl-1(ok161)* revealed that there is a shift of proteins in direction to wild-type in the volcano plot (Figure 9A), indicating that there was more protein in the wild-type samples compared to *vhl-1(ok161)* mutants potentially due to the higher protein content. The higher protein amount in the sample is explained by the higher protein amount in a single wild-type worm compared to *vhl-1(ok161)* (see Figure 6D).

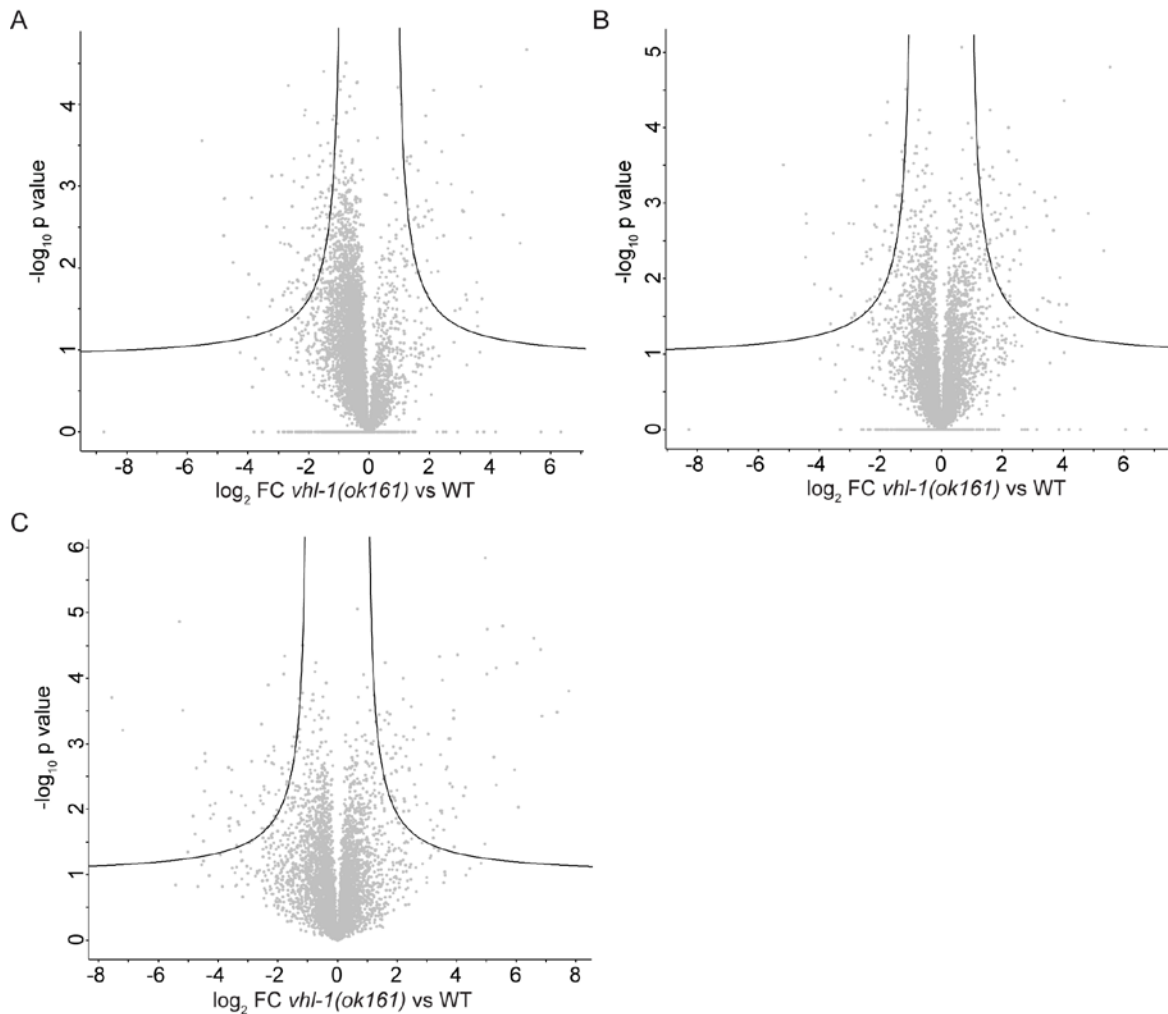


Figure 9: Normalization and imputation of wild-type and *vhl-1(ok161)* proteome.

Volcano plots showing \log_2 FC change of *vhl-1(ok161)* proteome compared to the wild-type proteome (x-axis) against the $-\log_{10}$ p-value of the *vhl-1(ok161)* proteome compared to the wild-type proteome (y-axis). **A.** Shows the proteome of *vhl-1(ok161)* versus wild-type. **B.** Shows the proteome of *vhl-1(ok161)* versus wild-type after normalization. **C.** Shows the proteome of *vhl-1(ok161)* versus wild-type after normalization and imputation.

To balance the protein amount of wild-type and *vhl-1(ok161)* mutant worms the median was subtracted and $x+(\text{highest median})+1$ was added. After normalization of the proteome data, there was no shift of proteins in direction to wild-type observed in the volcano plot (Figure 9B). We noticed that many proteins were measured either only in wild-type or *vhl-1(ok161)*. These proteins are not visualized in the volcano plots. To overcome this problem we replaced the missing values with values from the normal distribution (Figure 9C). After analysis of the whole worm proteome, we checked the RBPome. To analyse the RBPome we removed all proteins that were measured in the proteome but not measured in at least 1 sample out of 12 (crosslinked and non-crosslinked samples from wild-type and *vhl-1(ok161)*). The total

number of 6162 identified proteins was reduced after filtering to 2520 identified proteins for the RBPome.

5.1.5 RNA interactome capture data analysis and quality control

We identified 2520 proteins in the RBPome of 3 biological replicates including both genotypes wild-type and *vhl-1(ok161)* and both non-crosslinked and crosslinked samples. To further investigate the quality of the RIC data we performed a Principal Component Analysis (PCA). The PCA indicated a clear separation of crosslinked and non-crosslinked samples except for two non-crosslinked samples. These samples contained one replicate, which did not cluster with the other non-crosslinked samples of their genotype (Figure 10A). Heat map analysis confirmed the results of the PCA showing wild-type and *vhl-1(ok161)* non-crosslinked samples not clustering together (Figure 10B). Further analysis of the two samples showed that the number of identified proteins is much higher compared to their corresponding crosslinked samples (Figure 10C, indicated in red). Since the method is based on the enrichment of proteins in crosslinked samples a higher amount of proteins in the non-crosslinked sample is unexpected. A comparison of all RIC samples shows a high number of proteins identified exclusively in the two outliers (Figure 10C, Unique Proteins). These two samples were excluded from further analyses. To check how the exclusion of the two samples impacted the rest of the samples, we analysed the PCA and heat map without these samples. In the PCA, the genotype and the state of crosslinking primarily determine the separation of the individual samples as expected (Figure 10D). In line with the PCA, the heat map showed a clear separation of UVC treated samples to non UVC treated samples (Figure 10E). Together the PCA and heat map analysis showed that the strongest component is the crosslinking status followed by the genotype.

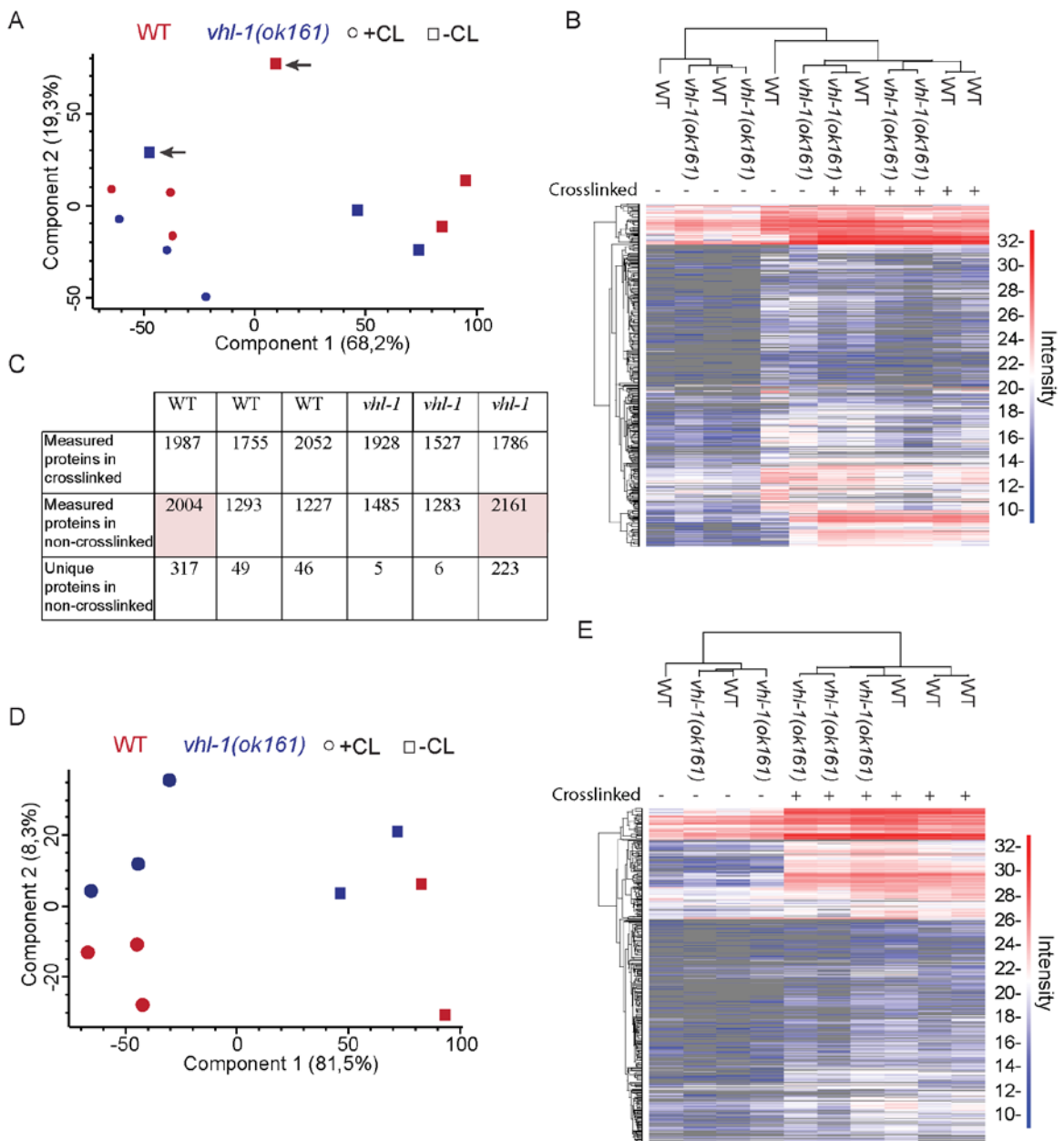


Figure 10: RBPome sample analysis.

A. PCA of the RIC dataset. Wild-type samples are shown in red, *vhl-1(ok161)* samples in blue, non-crosslinked samples depicted by a square and crosslinked samples shown in a dot. **B.** Heat map analysis of the RIC dataset. Wild-type and *vhl-1(ok161)* non-crosslinked and crosslinked samples are shown. The iBAQ intensity scale starts from 10 (blue) over 21 (white) to 32 (red). **C.** Table showing the number of proteins measured in the RIC for each crosslinked and non-crosslinked sample of WT and *vhl-1(ok161)*. Also, the unique proteins compared to any of the other RIC samples are shown for the non-crosslinked samples of WT and *vhl-1(ok161)*. Samples in columns marked in red were excluded from further analysis. **D.** PCA of the RIC dataset without outliers. Colour and symbol code as in A. **E.** Heatmap analysis of the RIC dataset without outliers. Wild-type and *vhl-1(ok161)* non-crosslinked and crosslinked samples are shown. Intensity scale described in B. See also Esmailie et al. 2019.

5.1.6 Classification of proteins identified in RNA interactome capture

For the identification of significantly regulated proteins and to further increase the evidence that the proteins identified were indeed RBPs we used - as for the whole worm proteome - a t-test with an $FDR \leq 0.05$ and $s_0 = 0.5$ to compare crosslinked to non-crosslinked samples (Figures 11A and B). The volcano plots for both wild-type and *vhl-1(ok161)* show a clear enrichment regarding the number of proteins in direction to the crosslinked samples. This indicates an increased protein content in the crosslinked sample as shown before by the silver staining (Figure 8B) and the number of identified proteins in mass spectrometry (Figure 10C). We identified 721 proteins significantly enriched in crosslinked samples compared to non-crosslinked samples in wild-type (Figure 11A, red marked dots) and 530 in *vhl-1(ok161)* (Figure 11B, blue marked dots). Proteins in which calculation of an FDR was impossible due to missing values in one condition are not shown here.

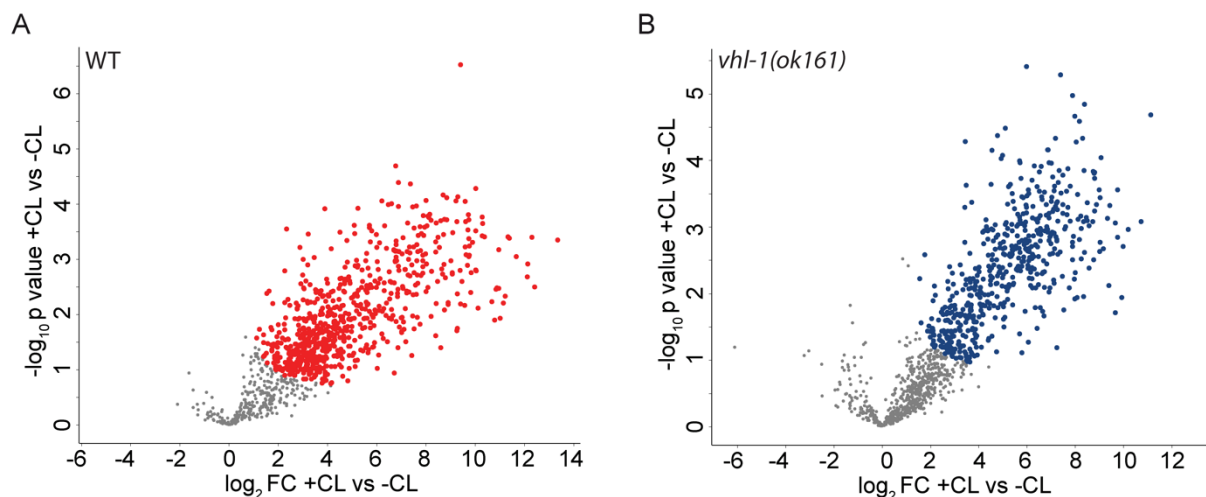


Figure 11: Volcano plot of wild-type and *vhl-1(ok161)* RBPome.

A. Wild-type non-crosslinked versus crosslinked \log_2 FC was plotted against the wild-type non-crosslinked versus crosslinked $-\log_{10}$ p-value. Proteins with an FDR lower than 0.05 are marked in red. **B.** *vhl-1(ok161)* non-crosslinked versus crosslinked \log_2 FC was plotted against the *vhl-1(ok161)* non-crosslinked versus crosslinked $-\log_{10}$ p-value. Proteins with an FDR lower than 0.05 are marked in blue. See also Esmailie et al. 2019.

We defined those proteins identified in mass spectrometry with an $FDR \leq 0.05$ as RBPs. Nevertheless, proteins measured only in crosslinked samples and absent in non-crosslinked samples have no FDR. Therefore, we defined another criterion to include these missing proteins. We distinguish RBPs defined by the two criteria as Class I and Class II RBPs (Figure 12A). Class I describes proteins measured exclusively three times (out of three replicates) in the crosslinked samples and never

in the corresponding non-crosslinked sample. Class II proteins are defined by an FDR < 0.05. In addition to Class I and Class II we created another Class based on previous identification in the literature called “Other RBPs” (Figure 12A).

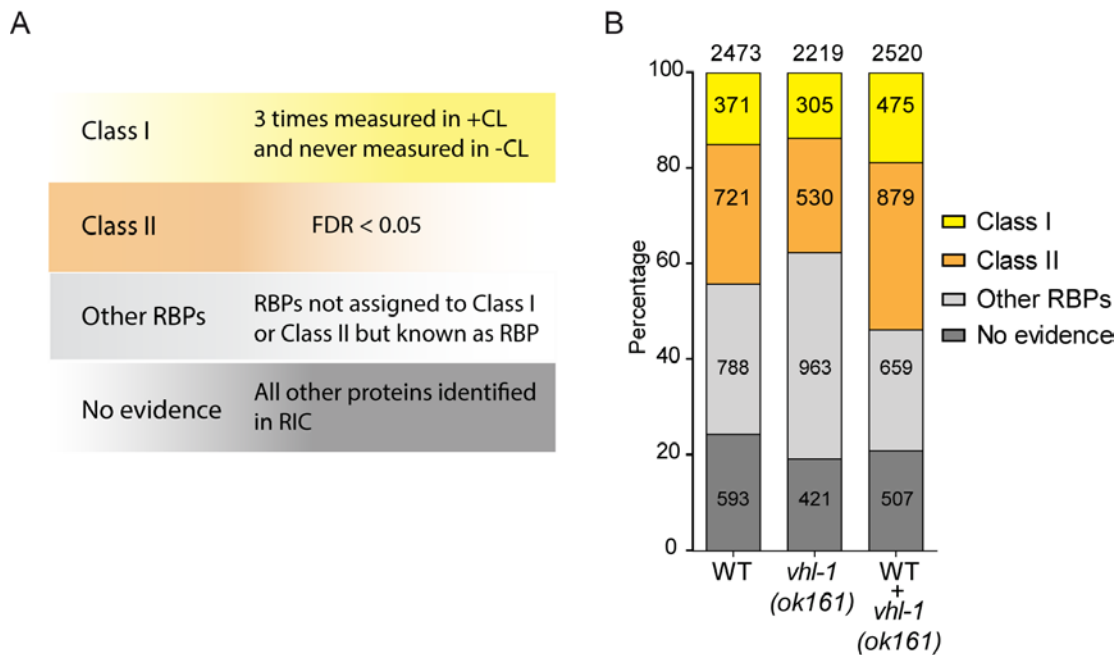


Figure 12: Classification of the wild-type and *vhl-1(ok161)* RBPome.

A. Definition of RBP classes. Proteins measured exclusively three times (out of three replicates) in the crosslinked samples and never in the corresponding non-crosslinked samples are in Class I. All proteins with a calculated FDR lower than 0.05 are in Class II. Proteins falling neither into Class I nor Class II but identified before in a published RBPome are in class “Other RBPs”. All other proteins were classified as “No evidence”. **B.** Proteins identified in the wild-type and *vhl-1(ok161)* RIC were assigned to their corresponding classes shown by numbers in a bar. From left to right are shown Proteins identified in the RIC of wild-type, *vhl-1(ok161)* and the merged wild-type and *vhl-1(ok161)* RIC data. The classes are color-coded as followed: Class I (yellow), Class II (orange), Other RBPs (light grey) or No evidence (dark grey). The number on top of each bar is the total number of proteins measured. See also Esmailie et al. 2019.

All proteins falling neither into Class I nor Class II but identified in our screen with previous evidence in one of the published RBPomes available to date are in the class “Other RBPs”. The available RBPomes used in this study include data from various species – i.e. human, mouse, fly and worms (Hentze et al., 2018; Ignarski et al., 2019; Queiroz et al., 2019; Tamburino et al., 2013; Trendel et al., 2019; Urdaneta et al., 2019). All the other proteins identified in the RIC not falling into Class I, Class II or Other RBPs were classified as “No evidence” (Figure 12A). These classifications revealed that we identified, in wild-type, 1880 RBPs out of 2473 total identified proteins (Figure 12B). In *vhl-1(ok161)* mutants we identified 1798 out of 2219 to be RBPs (Figure 12B). To get an impression of the quality of our data we merged the datasets from wild-type and *vhl-1(ok161)*. RBPs classified differently between WT

and *vhl-1(ok161)* mutants (e.g. class I in *vhl-1(ok161)* and class II in WT) were assigned to Class II having in total 1354 RBPs assigned to Class I or Class II (Figure 12B).

5.1.7 Annotation enrichment analysis of proteins identified in RIC

Using the criteria described above, more than 75% of the identified proteins in RIC are RBPs. To provide further evidence, we performed annotation enrichment analysis using the combined Class I and II RBPs of wild-type and *vhl-1(ok161)* (Figure 13).

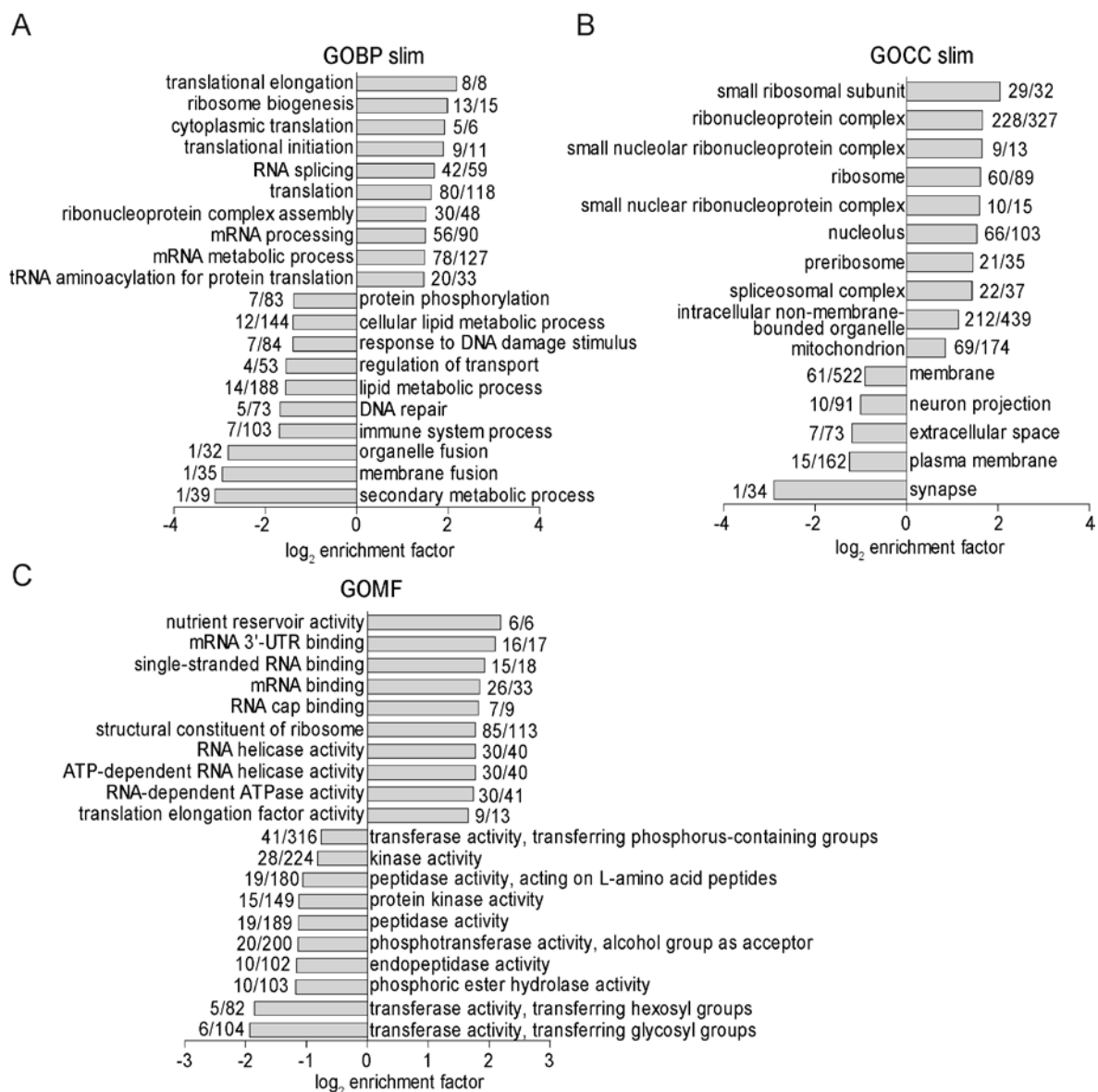


Figure 13: GO-term enrichment of RIC proteins.

A. GO-term enrichment of molecular function (GOMF) using the combined Class I and II RIC of wild-type and *vhl-1(ok161)*. **B.** GO-term enrichment of biological processes slim (GOBP) using the combined Class I and II RIC of wild-type and *vhl-1(ok161)*. **C.** GO-term enrichment of cellular compartments slim (GOCC) using the combined Class I and II RIC of wild-type and *vhl-1(ok161)*. The number next to each bar represents the number of proteins falling into the category followed by the number of category sizes. See also Esmailie et al. 2019.

The total set of pooled proteins identified in both RIC and proteome experiments were used as a background. The UniProt IDs were annotated using Perseus software for Gene Ontology (GO), PFAM and SMART. Gene set enrichment analysis was calculated using the Fisher exact test (Perseus standard settings, FDR<0.05 (Tyanova et al. 2016)). Plotting the top enriched and depleted terms of molecular function, biological processes slim and cellular compartment slim showed that the vast majority of terms is associated with RNA including *mRNA binding*, *ribonucleoprotein complex*, *translational elongation*, *RNA splicing* and *RNA helicase activity* (Figure 13A, B and C). We analysed the GO terms of molecular function in terms of *RNA binding* versus *DNA binding* in more detail. In comparison to the proteome, we were able to determine that the term *RNA binding* occurs more often in Class I and II proteins than in the proteome (Figure 14). In contrast the term *DNA binding* was more present in the proteome compared to the Class I and II proteins.

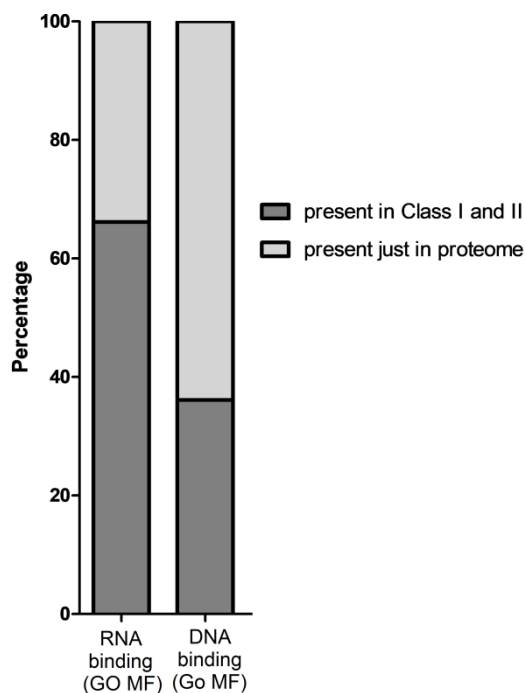
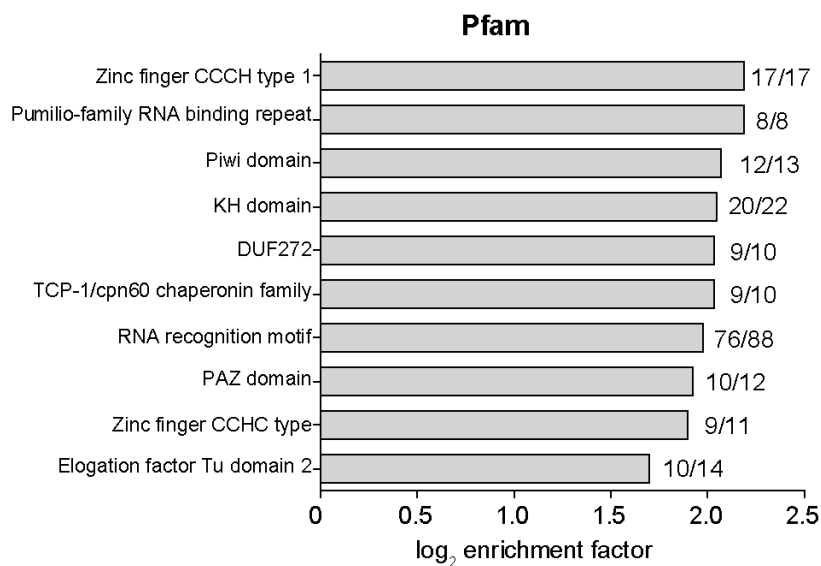


Figure 14: Comparison of the GO terms *RNA binding* and *DNA binding*.

GO-term enrichment of molecular function (GOMF) terms *RNA binding* and *DNA binding* using the combined Class I and II RIC of wild-type and *vhl-1(ok161)*.

Besides, we performed a domain enrichment analysis using Pfam and Smart (Figure 15A and B). Under the most enriched domains, we identified Zink finger, PUF, Piwi and RRM domains which are all well known to be RNA binding domains. Taken together the GO-term and domain enrichment analysis showed that the proteins identified in the RIC are RNA binding associated with regards to GO-terms and domains.

A



B

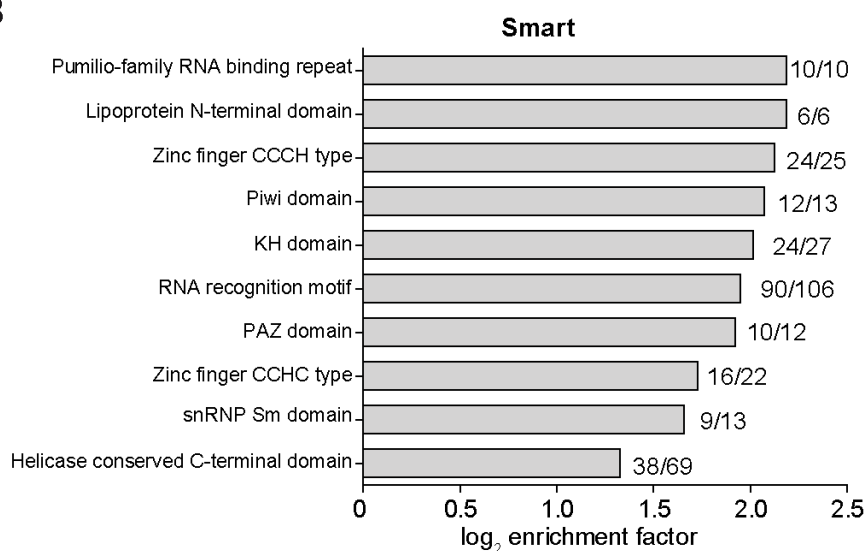


Figure 15: Domain enrichment of RIC proteins.

A. PFAM analysis using the combined Class I and II RIC of wild-type and *vhl-1(ok161)*. **B.** SMART analysis using the combined Class I and II RIC of wild-type and *vhl-1(ok161)*. The number next to each bar represents the number of proteins falling into the category followed by the number of category sizes. See also Esmailie et al. 2019.

5.2 Identification of novel RBPs

5.2.1 Comparative analysis of published RNA interactomes

To elucidate whether our study had identified previously unknown RBPs we compared our list of Class I and Class II proteins with previously published datasets summarized by Hentze et al. (Hentze et al. 2018). These datasets comprise RIC experiments from human, mouse, fly, worm and yeast. Interestingly, about 20% of

RBPs in our dataset were identified in the fly, worm and yeast dataset whereas about 50% of RBPs in our dataset were identified in mouse and human (Figure 16A). Combining all of these datasets 70% of the RBPs in our dataset had previously been identified. We wondered how the only published *C. elegans* RIC dataset from Matia-Gonzales et al. overlapped with our findings and how both datasets matched to the combined data of human, mouse, fly and yeast. The comparison revealed that Matia-Gonzales et al. identified 594 RBPs whereas we identified 1354 RBPs using Class I and II (Figure 16B). Out of the 594 RBPs identified by Matia-Gonzales et al. 364 (61%) RBPs were included in the 1354 RBPs identified in our dataset. Both, the Matia-Gonzales et al. (*C. elegans*) dataset and our dataset have an overlap of 67% to the combined data of human, mouse, fly and yeast (Figure 16B).

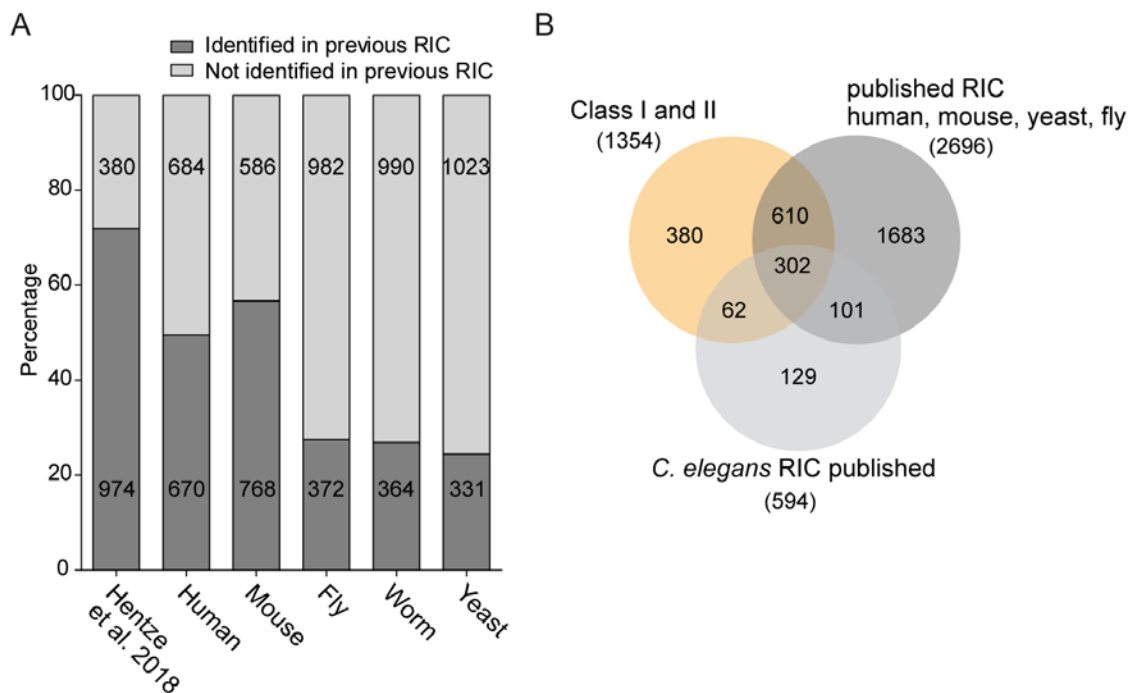


Figure 16: Comparisons of Class I and Class II RBPs with previously published RIC datasets.

A. Bar diagram showing the number of Class I and Class II RBPs identified in the previously published dataset (dark grey) or not identified (light grey). **B.** Venn diagram depicting the overlap of Class I and Class II RBPs with the published *C. elegans* RIC and other RIC datasets. The numbers in the circles show the overlap of proteins with each dataset. See also Esmailie et al. 2019.

5.2.2 Comparison of RIC with novel techniques

The limitation of the RIC experiment is the pulldown of RNA primarily with a poly-A tail. There is evidence that RIC can pulldown also other RNA species by RNA-RNA

contacts (Piñeiro et al. 2018). However, RIC relies on the capture of polyadenylated RNA. Newly developed techniques allow for purification of all RNA species and identification of bound proteins (Queiroz et al. 2019; Trendel et al. 2019; Urdaneta and Beckmann 2019). To this end, we compared our data with the data of XRNAX, OOPS and PTex (Figure 17A). The comparison revealed that 66% of the 1354 RBPs identified in our dataset were also identified as RBPs in the dataset generated by XRNAX, OOPS or PTex. 475 RBPs out of 1354 RBPs are found in all four datasets. Interestingly, of the 453 RBPs identified in our dataset that were not identified in the data generated by the new techniques 147 of them were identified in other RIC experiments. To complete the analysis we compared our data to a prediction-based RBP study in *C. elegans* (Tamburino et al. 2013). These RBPs are identified by RNA binding domain detection in the protein sequence. Here we found that 28% of our RBPs were predicted before as RBPs (Figure 17B).

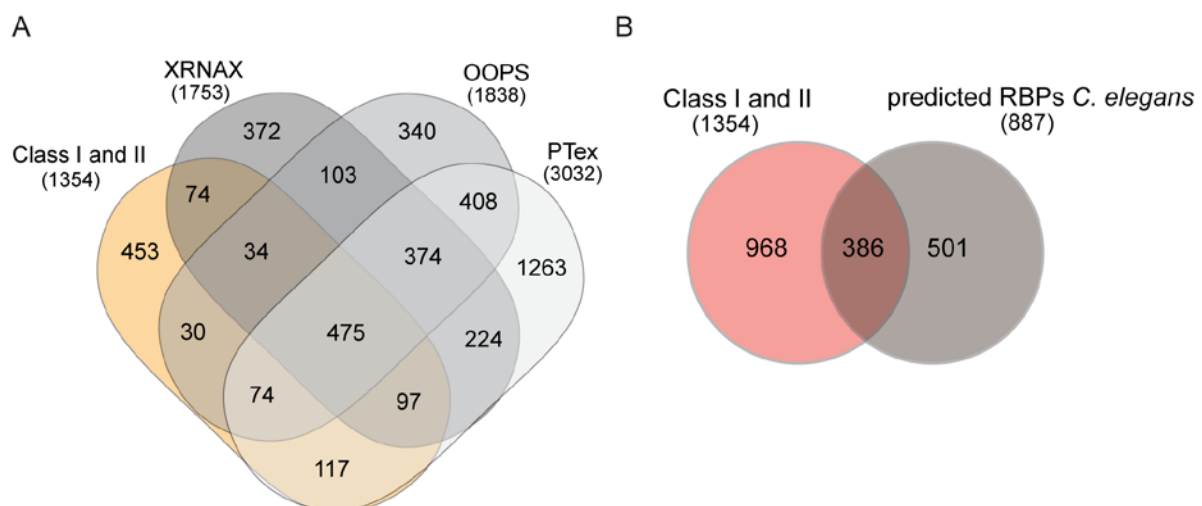


Figure 17: Comparisons of Class I and Class II RBPs with novel techniques and predicted RBPs.

A. Venn diagram comparing 1354 Class I and Class II RBPs to 1753 RBPs identified by XRNAX, 1838 RBPs identified by OOPS and 3032 RBPs identified by PTex (Queiroz et al. 2019; Trendel et al. 2019; Urdaneta and Beckmann 2019). **B.** Venn diagram comparing 1354 Class I and Class II RBPs to 887 RBPs predicted by protein domain analysis in *C. elegans* (Tamburino et al. 2013). See also Esmailie et al. 2019.

5.2.3 The identification of 270 novel RBPs in *C. elegans*

The comparison of RIC experiments of various organisms as well as the comparison of different techniques with our RIC dataset showed a notable overlap. Next, to have a global view of identified RBPs in our dataset, we merged all data comparisons shown in Figures 16 and 17. The identified RBPs in the data used for comparison are based on the experimental identification of RBPs and RNA binding domain analysis. We showed that 1084 RBPs in our dataset had been identified as RBPs previously. The analysis also showed that 270 RBPs had not been known to have RNA-binding capacity before (novel RBPs, Figure 18). Out of the 270 novel RBPs, 92 are conserved in humans whereas 178 are worm specific genes.

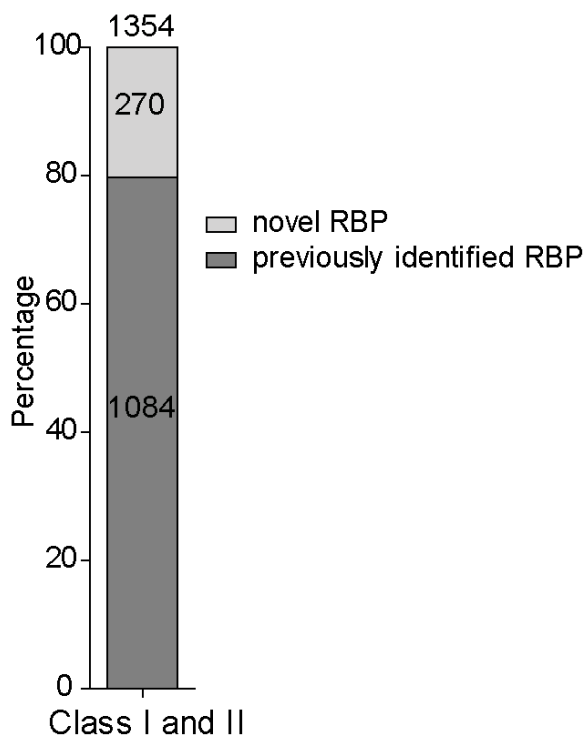


Figure 18: Identification of novel RBPs.

The bar diagram shows the number of proteins previously identified as RBP (1084, dark grey) and novel RBPs (270, light grey). The total number of RBPs (1354) identified in this study is displayed on top of the bar. See also Esmailie et al. 2019.

5.3 Proteome analysis of wild-type and *vhl-1(ok161)*

5.3.1 Proteome data analysis and quality check

The analysis of wild-type and *vhl-1(ok161)* RIC led to the identification of RBPs in both conditions. We were able to distinguish known RBPs from novel RBPs. In the next step, we wanted to know how the activation of hypoxia signaling alters the whole-worm proteome of wild-type and *vhl-1(ok161)* worms since this would be the

actual basis to comparing the individual RBPomes. We used aliquots from the RIC input samples and analysed them by mass spectrometry (see Figure 7). This approach revealed a nice genotype-dependent clustering in the PCA (Figure 19A). Visualizing the dataset in a heat map again confirmed a separation of wild-type and *vhl-1(ok161)* samples (Figure 19B).

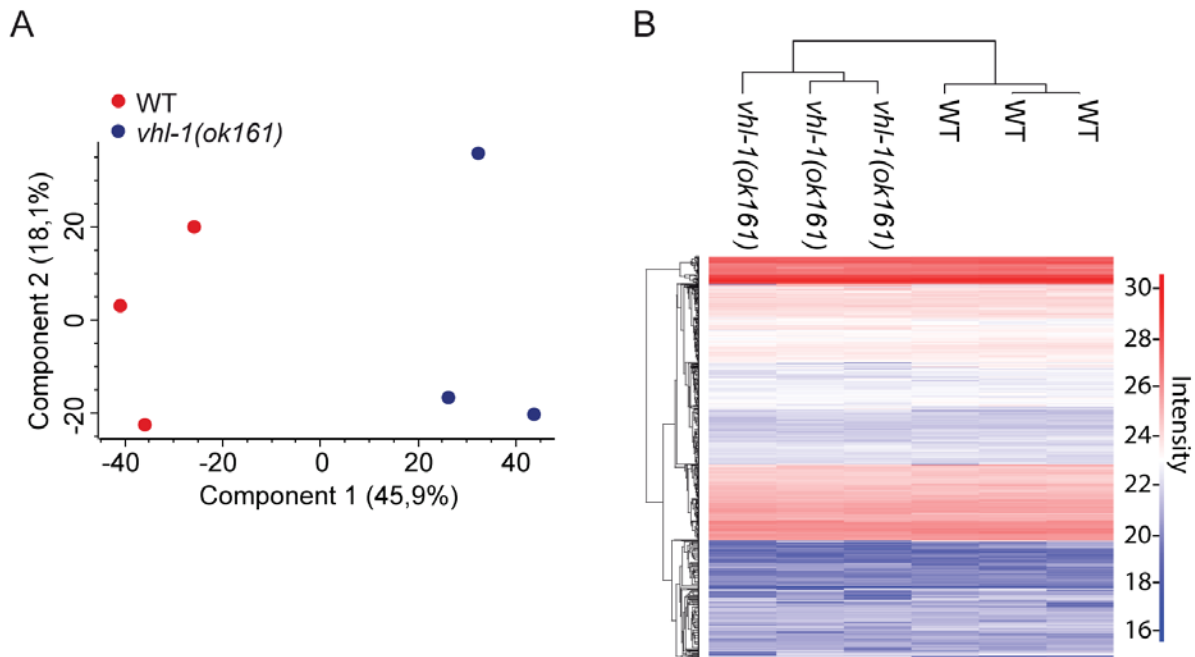


Figure 19: PCA and heat map analysis of wild-type and *vhl-1(ok161)* proteome.

A. PCA of wild-type (red dots) and *vhl-1(ok161)* (blue dots) proteome samples. **B.** Heat map analysis of wild-type and *vhl-1(ok161)* proteome samples. The iBAQ intensity scale goes from 16 (blue) over 23 (white) to 30 (red). See also Esmailie et al. 2019.

5.3.2 Proteome analysis reveals activation of the hypoxia signaling pathway in *vhl-1(ok161)* mutant worms

After the quality check of the proteomes, we wanted to know if the protein levels of known HIF-1 targets are regulated in the *vhl-1(ok161)* worms as expected. Therefore, we marked all known HIF-1 targets (Dengler et al. 2014; Ortiz-Barahona et al. 2010; Shen et al. 2005) in the proteome including HIF-1 itself (Figure 20). Seven target genes and HIF-1 itself were significantly enriched in the *vhl-1(ok161)* mutant. Indicating that HIF-1 is indeed stabilized in *vhl-1(ok161)* mutant worms.

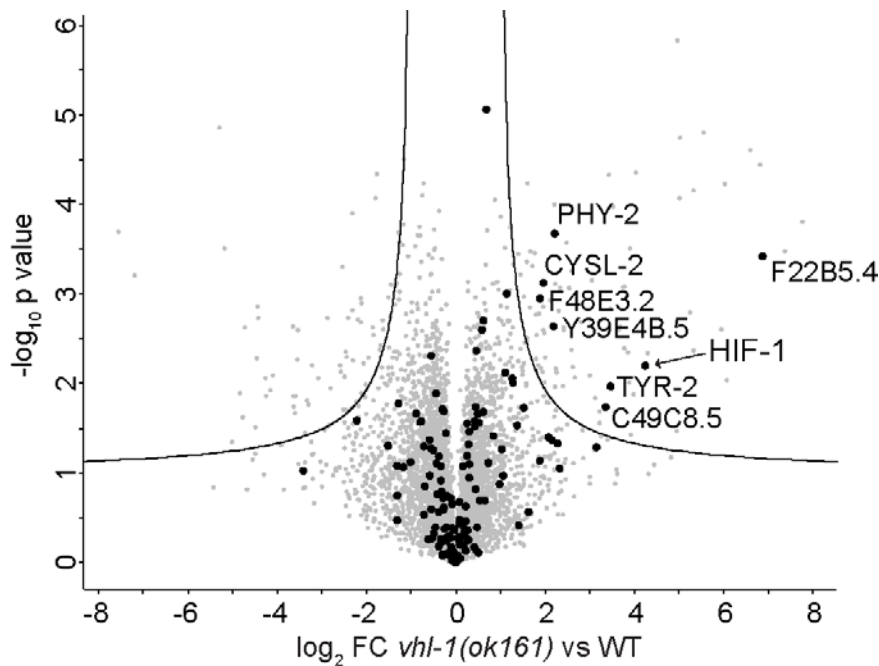


Figure 20: Analysis of HIF-1 and its target genes in wild-type and *vhl-1(ok161)* proteome.

Volcano plot shows \log_2 FC change of the wild-type proteome versus the *vhl-1(ok161)* proteome against the $-\log_{10}$ p-value of the wild-type proteome compared to the *vhl-1(ok161)* proteome. HIF-1 target genes (Dengler et al. 2014; Ortiz-Barahona et al. 2010; Shen et al. 2005) are marked as black dots. Significant HIF-1 target genes are indicated with their names. HIF-1 is also marked with an arrow. See also Esmailie et al. 2019.

5.3.3 Annotation enrichment analysis of the proteome

GO-term enrichment analysis of the proteome of wild-type and *vhl-1(ok161)* showed *CoA desaturase activity*, *response to biotic stimulus* and *immune system process* as the most enriched terms in biological processes and molecular function (Figure 21A). Analysis of the GO-terms of cellular compartment revealed two enriched terms, namely *lysosome* and *vacuole* (Figure 21B). For the domain analysis, we used Pfam. Here fatty acid desaturase and CUB domain were the most enriched terms (Figure 21C).

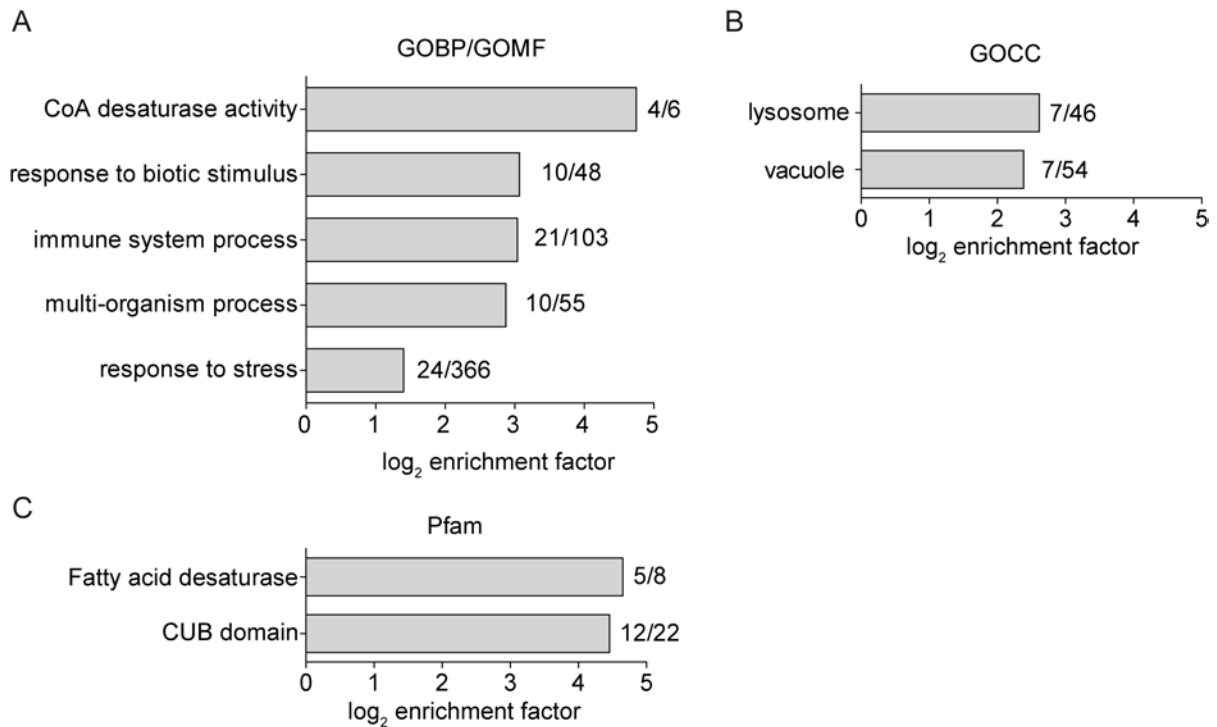


Figure 21: GO-term enrichment analysis of wild-type and *vhl-1(ok161)* proteome.

For each bar diagram, the log₂ enrichment factor is represented on the X-axis. The number next to each bar represents the number of proteins falling into each category followed by the category size. **A.** GO-term analysis of biological processes and molecular function. **B.** GO-term analysis of cellular compartments. **C.** Domain analysis using Pfam. See also Esmailie et al. 2019.

5.4 Analysis of the mode of regulation of RBPs in wild-type and *vhl-1(ok161)*

5.4.1 The hypoxia signaling pathway regulates the abundance of RBPs

We identified 1354 RBPs in the wild-type and *vhl-1(ok161)* RIC and wondered how the identified RBPs are regulated on the proteome level. To this end, we marked all the 1354 RBPs depicted in the volcano plot of the proteome (Figure 22A). Ten (ASP-3, CTSA-2, C41G7.6, GLD-3, H28G03.1, MEX-1, OAT-1, PHY-2, R08E5.3, Y37A1B.5) of the RBPs were significantly upregulated whereas two (COL-8 and F55H12.4) were significantly down-regulated in *vhl-1(ok161)* worms.

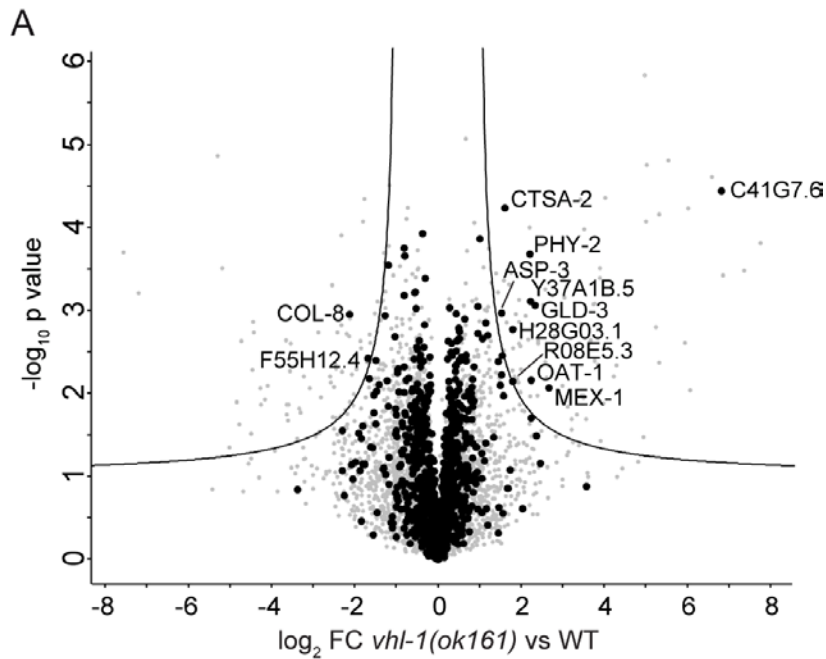


Figure 22: Identification of RBPs in the proteome of wild-type and *vhl-1(ok161)*.

A. Volcano plot depicting the proteomes from wild-type and *vhl-1(ok161)*. The \log_2 fold change is plotted against the $-\log_{10}$ p-value. Black marked dots are RBPs whereas significant RBPs are marked also with their name. Grey dots are all other proteins identified in the proteome. See also Esmailie et al. 2019.

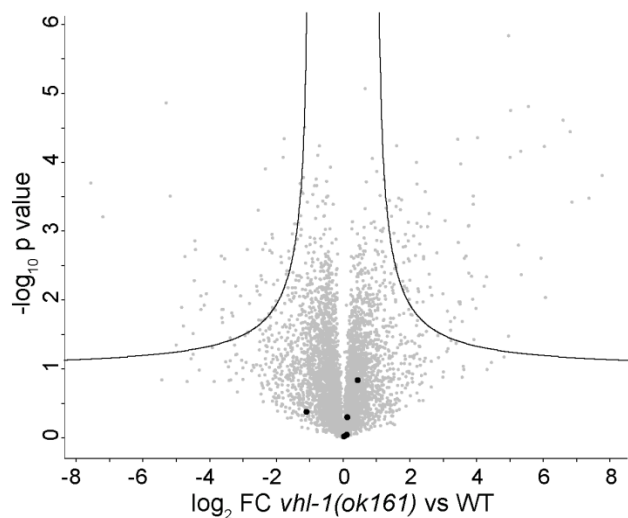
5.4.2 Analysis of RBPs identified exclusively in wild-type or *vhl-1(ok161)* RIC

The RIC analysis identifies RBPs enriched in wild-type or *vhl-1(ok161)* mutant worms but does not allow for a conclusion whether this is due to altered RNA-binding intensity or differential regulation of the protein level of the respective RBP. To identify the mode of regulation of RBPs in the *vhl-1(ok161)* mutant we chose specific criteria to analyse the RBPome. Firstly, we analysed all RBPs which were measured three times in crosslinked samples of one genotype (e.g. wild-type or *vhl-1(ok161)*) but never in the other. This resulted in two lists of RBPs exclusively identified in either wild-type or *vhl-1(ok161)* mutant worms. The analysis revealed five RBPs only measured in *vhl-1(ok161)* crosslinked samples but not in wild-type crosslinked samples (Figure 23A). Analysis of these RBPs in the proteome shows that their abundance is not affected by the mutation (Figure 23B).

A

WB Gene ID	Gene Name	Human Ortholog	RBPome Class	novel RBP	Function
WBGene0006442	<i>tag-65</i>	<i>CHERP</i>	I		calcium homeostasis endoplasmic reticulum protein
WBGene0009498	<i>tat-5</i>	<i>ATP9B;ATP9A</i>	I	+	ATPase phospholipid transporting
WBGene00010730	<i>ensa-1</i>	<i>ARPP19;ENSA</i>	I		protein phosphatase inhibitor
WBGene00015203	<i>B0495.2</i>	<i>CDK11A</i>	I		cyclin dependent kinase
WBGene00022488	<i>orc-3</i>	n.a.	I	+	n.a.

B



C

WB Gene ID	Gene Name	Human Ortholog	RBPome Class	novel RBP	Function
WBGene00002994	<i>lin-5</i>	n.a.	I	+	dynein complex binding
WBGene00008119	<i>C46F11.4</i>	<i>DDX42</i>	I		ATP binding
WBGene00008412	<i>D2030.2</i>	<i>CLPX</i>	I		ATP binding
WBGene00008694	<i>vwa-8</i>	<i>VWA8</i>	I	+	ATP binding
WBGene00009221	<i>acs-2</i>	<i>ACS2</i>	I		acyl-CoA synthetase
WBGene00009259	<i>hpo-34</i>	n.a.	I	+	n.a.
WBGene00009290	<i>F31D4.2</i>	<i>ARMT1</i>	I	+	S-adenosylmethionine-dependent methyltransferase
WBGene00009740	<i>F45H10.3</i>	<i>NDUFA7</i>	I		NADH dehydrogenase
WBGene00010015	<i>atad-3</i>	<i>ATAD3A</i>	I		ATP binding
WBGene00010766	<i>mmps-27</i>	<i>MMP27</i>	I		mitochondrial ribosome binding
WBGene00011743	<i>T13F2.2</i>	<i>SUB1</i>	I		DNA binding
WBGene00012156	<i>ebp-2</i>	<i>MAPRE1</i>	I		microtubule binding
WBGene00012996	<i>pinp-4</i>	<i>PIN4</i>	I		peptidyl-prolyl cis-trans isomerase
WBGene00013040	<i>Y49E10.21</i>	n.a.	I	+	n.a.
WBGene00013477	<i>Y69E1A.5</i>	<i>PEBP1</i>	I		protein kinase binding
WBGene00014108	<i>ZK856.7</i>	n.a.	I	+	n.a.
WBGene00016419	<i>tyr-4</i>	<i>TYR</i>	I	+	metal ion binding
WBGene00018682	<i>aagr-4</i>	<i>GANAB;GANC</i>	I		carbohydrate binding and hydrolyzing O-glycosyl
WBGene00019005	<i>F57B10.8</i>	<i>ABT1</i>	I		RNA binding
WBGene00019478	<i>tag-225</i>	<i>TIMP2;TIMP3;TIMP1;TIMP4</i>	I		metalloendopeptidase inhibitor
WBGene00020104	<i>R148.5</i>	n.a.	I	+	n.a.
WBGene00020112	<i>pf-d-5</i>	<i>PFDN5</i>	I		unfolded protein binding
WBGene00006583	<i>tnc-2</i>	<i>TNNC2</i>	II	+	troponin I binding
WBGene00016415	<i>ampd-1</i>	<i>AMPD2</i>	II		AMP deaminase

D

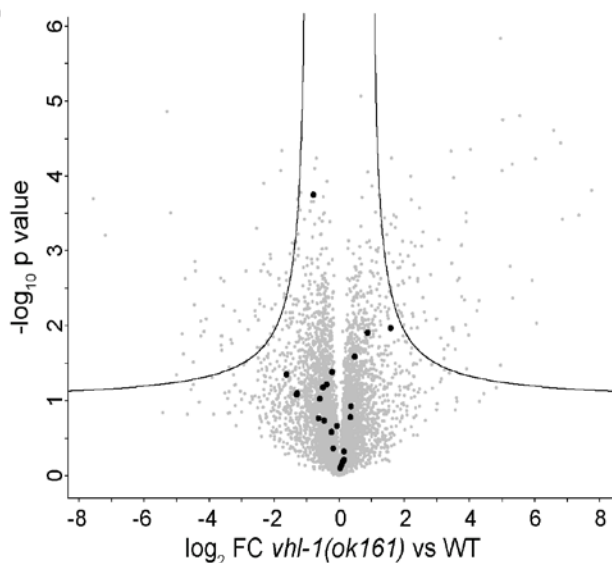


Figure 23: RBPs measured exclusively in either wild-type or *vhl-1(ok161)* analysed in their proteomes.

A. Table of RBPs measured exclusively in *vhl-1(ok161)* samples but never in wild-type samples. **B.** RBPs from table A are marked in black in the volcano plot of the proteomes from wild-type and *vhl-1(ok161)*. The \log_2 fold change is plotted against the $-\log_{10}$ p-value. **C.** Table of RBPs measured exclusively in wild-type samples but not in *vhl-1(ok161)* samples. **D.** RBPs from table C are marked in black in the volcano plot of the proteome of wild-type and *vhl-1(ok161)*. The \log_2 fold change is plotted against the $-\log_{10}$ p-value. See also Esmailie et al. 2019.

Interestingly, analysis of the RBPs exclusively measured in wild-type crosslinked samples but not measured in *vhl-1(ok161)* crosslinked samples identified twenty four RBPs (Figure 23C). All of these RBPs are also not differentially regulated in the proteome (Figure 23D), indicating that in the *vhl-1(ok161)* mutant the RBP binding capacity is changed but not the abundance.

5.4.3 Identification of the mode of regulation of RBPs in wild-type and *vhl-1(ok161)* RIC

Focussing on RBPs which were measured three times in crosslinked samples of one genotype is one way to analyse the data regarding modulation by hypoxia-signaling. Another way is to directly correlate the \log_2 fold changes of crosslinked versus non-crosslinked samples in the RIC and compare both genotypes. We plotted *vhl-1(ok161)* \log_2 fold changes against wild-type \log_2 fold changes (Figure 24A). To identify RBPs which were enriched in wild-type or *vhl-1(ok161)* we calculated the 95% prediction interval (grey lines, Figure 24A). All proteins above the interval and marked in red are RBPs enriched in the wild-type whereas all lines below the line marked in blue are enriched in *vhl-1(ok161)* (Figure 24A and Table 20). All proteins outside the 95% prediction interval (above or below the line) marked in grey are not in Class I or Class II. Analysing both the red and blue marked RBPs in the proteome revealed that all except for one protein - H28G03.1 - are not regulated on the protein level but only regarding RNA-binding (Figure 24B and C).

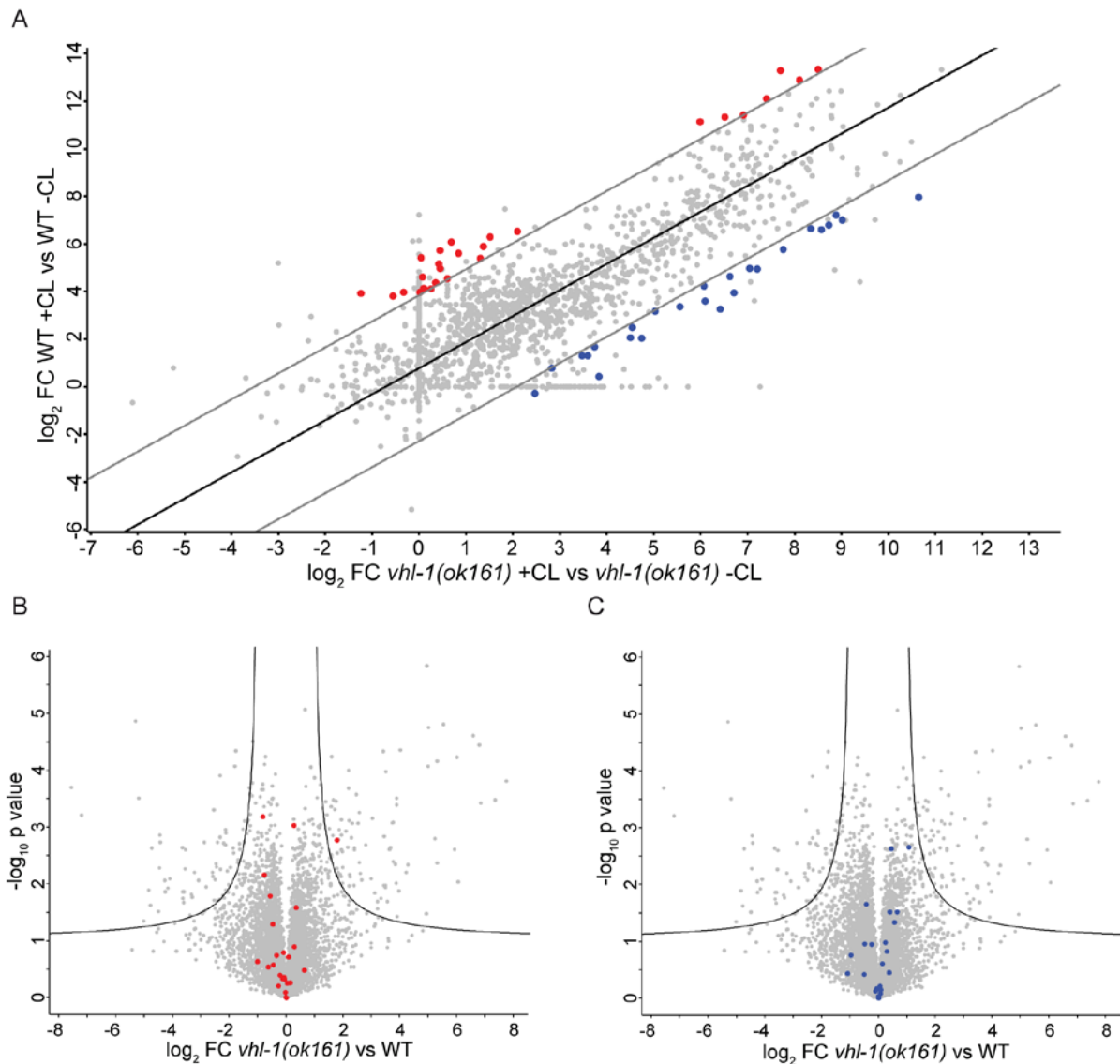


Figure 24: Identification of mode of regulation of RBPs in wild-type and *vhl-1(ok161)*.

A. The scatterplot depicts the RIC of wild-type and *vhl-1(ok161)* mutant worms. The \log_2 FC of crosslinked versus non-crosslinked *vhl-1(ok161)* data against \log_2 FC of crosslinked versus non-crosslinked wild-type data was plotted. The grey lines show the calculated 95% interval. Red marked dots represent RBPs enriched in wild-type whereas blue marked dots represent RBPs enriched in *vhl-1(ok161)*. Protein information of red and blue marked RBPs in Table 20 and http://shiny.cecad.uni-koeln.de:3838/celegans_rbpome. **B.** Red marked RBPs from A. depicted in the wild-type and *vhl-1(ok161)* proteome data. The \log_2 fold change is plotted against the $-\log_{10}$ p-value. **C.** Blue marked RBPs from A. depicted in the wild-type and *vhl-1(ok161)* proteome data. The \log_2 fold change is plotted against the $-\log_{10}$ p-value. See also Esmailie et al. 2019.

Table 20: Overview of RBPs above and below the 95% prediction interval.

WB Gene ID	Gene Name	Human Ortholog	RBPome Class	novel RBP	95% prediction interval
WBGene00012904	<i>tiar-2</i>	<i>TIA1;TIAL1</i>	II		above
WBGene00015943	<i>tiar-1</i>	<i>TIA1;TIAL1</i>	II		above
WBGene00016489	<i>fubl-3</i>	<i>FUBP3;KHSRP;FUBP1</i>	II		above
WBGene00019249	<i>H28G03.1</i>	<i>HNRNPA2B1;HNRNPA1</i>	II		above
WBGene00022253	<i>hrpf-2</i>	<i>HNRNPH1;HNRNPH2</i>	II		above
WBGene00015547	<i>ain-1</i>	n.a.	II	+	above
WBGene00003994	<i>pgl-3</i>	n.a.	II		above
WBGene00021921	<i>rbm-39</i>	<i>RBM39;RBM23</i>	II		above
WBGene00004386	<i>rnp-3</i>	<i>SNRPA;SNRPB2</i>	II		above
WBGene00022368	<i>Y92H12BR.2</i>	n.a.	II	+	above
WBGene00001336	<i>qars-1</i>	<i>QARS</i>	II		above
WBGene00000377	<i>cct-1</i>	<i>TCP1</i>	II		above
WBGene00000381	<i>cct-6</i>	<i>CCT6A;CCT6B</i>	II		above
WBGene00006876	<i>vab-10</i>	<i>DST;MACF1</i>	II		above
WBGene00020166	<i>T02G5.7</i>	<i>ACAT1;ACAA2;ACAT2</i>	II		above
WBGene00004461	<i>rpn-5</i>	<i>PSMD12</i>	II		above
WBGene00018271	<i>F41C3.5</i>	<i>CTSA;CPVL</i>	II		above
WBGene00015687	<i>chdp-1</i>	n.a.	II	+	above
WBGene00003391	<i>mog-3</i>	<i>CWC25;CWC25</i>	II		above
WBGene00018892	<i>cir-1</i>	<i>CIR1</i>	II		above
WBGene00000869	<i>cyc-1</i>	<i>CYC1</i>	II		above
WBGene00003053	<i>lmp-1</i>	n.a.	II		above
WBGene00003989	<i>pfn-1</i>	<i>PFN4</i>	II		above
WBGene00006914	<i>vha-5</i>	<i>ATP6VOA1;ATP6VOA4</i>	II		above
WBGene00009084	<i>F23B12.7</i>	<i>CEBPZ</i>	II		below
WBGene00003598	<i>nhl-2</i>	<i>TRIM24;TRIM28</i>	II		below
WBGene00018710	<i>F52G3.1</i>	<i>PRRC2C</i>	II		below
WBGene00000772	<i>cpb-3</i>	<i>CPEB1;CPEB1</i>	II		below
WBGene00003026	<i>lin-41</i>	<i>TRIM71</i>	II		below
WBGene00006887	<i>vav-1</i>	<i>VAV3;VAV1;VAV2</i>	II		below
WBGene00003367	<i>mix-1</i>	<i>SMC2</i>	II		below
WBGene00008502	<i>skih-2</i>	<i>SKIV2L</i>	II		below
WBGene00014165	<i>puf-12</i>	<i>PUM3</i>	II		below
WBGene00001029	<i>dnj-11</i>	<i>DNAJC2</i>	II		below
WBGene00003596	<i>ngp-1</i>	<i>GNL2</i>	II		below
WBGene00007050	<i>utp-20</i>	<i>UTP20</i>	II		below
WBGene00007617	<i>rrbs-1</i>	<i>RRS1</i>	II		below
WBGene00017997	<i>mrpl-1</i>	<i>MRPL1</i>	II		below
WBGene00022021	<i>Y61A9LA.10</i>	<i>BMS1</i>	II		below
WBGene00012244	<i>mrps-11</i>	<i>MRPS11;RPS14</i>	II		below
WBGene00001856	<i>hil-5</i>	<i>HIST1H1E</i>	II		below
WBGene00022042	<i>icd-2</i>	<i>NACA2;NACA;NACAD</i>	II		below
WBGene00006725	<i>ubl-1</i>	<i>RPS27A</i>	II		below
WBGene00000680	<i>col-106</i>	<i>SFTPD</i>	II	+	below
WBGene00021430	<i>Y38F2AR.12</i>	<i>OPLAH</i>	II	+	below
WBGene00012198	<i>W02B8.2</i>	<i>CIT</i>	II		below
WBGene00020718	<i>mrps-2</i>	<i>MRPS2</i>	II		below
WBGene00006937	<i>wah-1</i>	<i>AIFM1</i>	II		below
WBGene00010002	<i>F53F8.5</i>	<i>C19orf47</i>	II		below
WBGene00021377	<i>Y37E11B.5</i>	<i>DUS3L</i>	II		below
WBGene00021555	<i>Y45G5AM.2</i>	<i>XPNPEP1</i>	II		below
WBGene00006584	<i>tmi-1</i>	<i>TNNI1</i>	II		below

5.5 Hypoxia-signaling associated RBPs have an impact on *C. elegans* lifespan

5.5.1 Establishing the lifespan machine in *C. elegans*

The in-depth analysis of the wild-type and *vhl-1(ok161)* RIC revealed 80 RBPs which have differential RNA binding capacity in either wild-type or *vhl-1(ok161)* (Figures 23 and 24). It is known that *vhl-1(ok161)* worms have an extended lifespan compared to the wild-type worms (Müller et al. 2009). We wondered if one or more of the RBPs identified in our analysis may be involved in lifespan extension. To answer this question, lifespan experiments in *C. elegans* are required. These experiments are laborious and time consuming, especially when run in a larger number of knockout strains or RNAi conditions. To enhance lifespan analysis, we decided to establish the lifespan machine developed by Nicholas Stroustrup in our group (Figure 25A, Stroustrup et al 2013). The lifespan machine is based on commercially available scanners, which are used to scan the plates containing worms in a specified time interval. This allows for the inclusion of much larger numbers of worms per condition compared to manual screens and a much more frequent scoring of mortality. Unfortunately, the scanners could not be used as purchased. Some of the scanners had to be converted and other components had to be built (see methods part 4.2.1.7). On the other hand, there is no software that could be downloaded instantly to the PC. Many individual software packages had to be installed beforehand, connected to each other and run on a PC with the Linux operating system. On that computer the Worm Browser and the Image Server was then installed (Stroustrup et al. 2013). Image processing cuts the acquired images into plate pictures and identifies worms through contrast thresholding and morphology analysis. Movement analysis reconstructs each worm path and determines their time of death based on ceased movement. Afterwards the automatically generated survival data in the Worm Browser software is analysed and falsely identified objects are excluded manually. Also, the time point of death of each worm can be adjusted if incorrectly marked by the software. To visualize the resulting table into time-survival curves GraphPad Prism was used (Figure 25B).

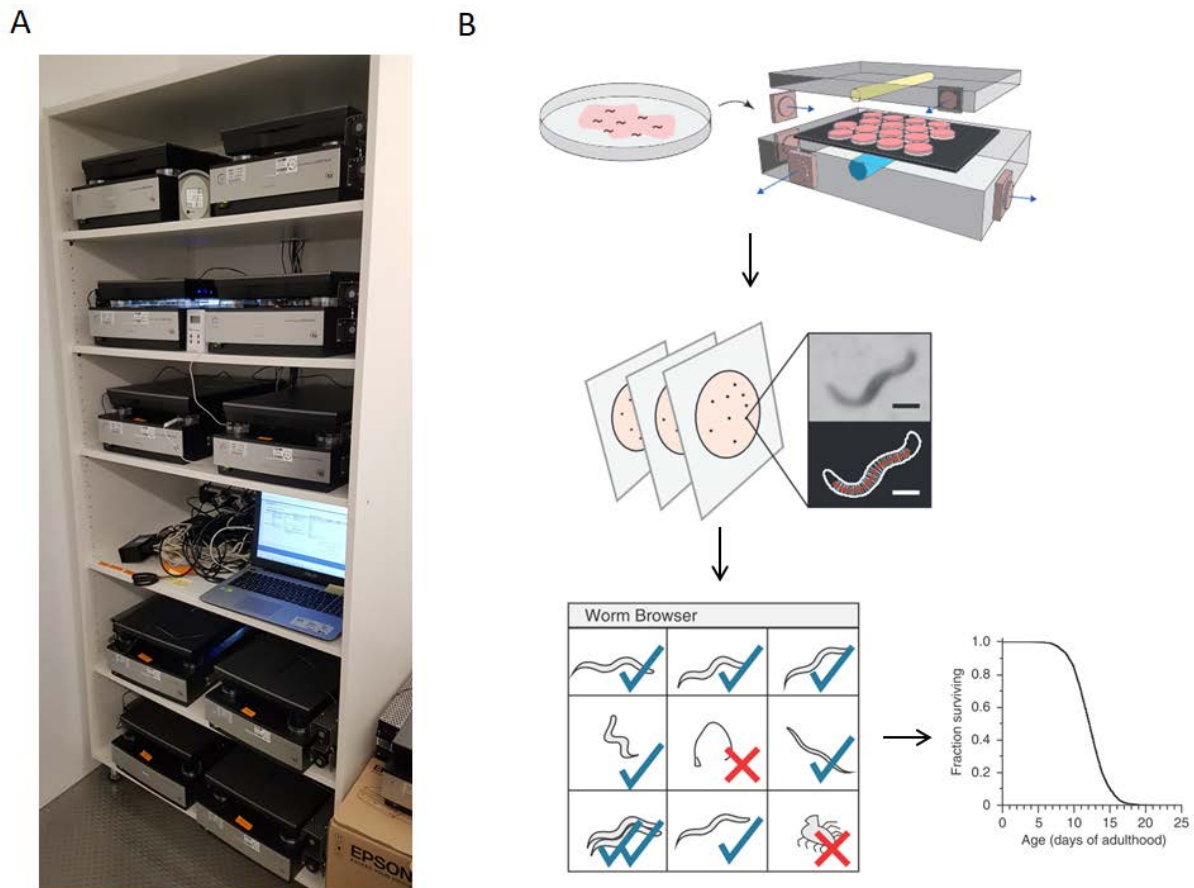


Figure 25: Overview of the lifespan machine.

A. The lifespan machine in the Nephrolab Cologne. Ten scanners are placed in a temperature-controlled room. In the middle of the cupboard is a laptop running the acquisition server to monitor all the scanners. **B.** Agarose plates with worms inside are placed in the scanner by placing them upside down. The scanner is mounted with fans on their side. The airflow of the fans is indicated by the blue arrows. After scans are completed images are overlaid and worms are identified by the software. The Worm Browser software allows confirming or refusing the identified worms. Completing the analysis the software transforms the data into a survival curve. Images modified from (Stroustrup et al. 2013).

5.5.2 Lifespan analysis of long-lived mutants

After setting up the lifespan machine we went on to test the performance of the device. All of the following lifespan assays were performed at 20°C in a temperature-controlled room. We first checked the lifespan of wild-type worms (Figure 26A). The median lifespan of the wild-type worms showed a similar range compared to previous manual results in our lab as well as data from other groups (D. H. Mitchell et al. 1979; Müller et al. 2009). We used 349 worms for the lifespan analysis and a scan interval of 30 minutes. To show that we were able to detect differential effects on lifespan we checked the lifespan of long-lived *vhl-1(ok161)* and *daf-2(e1370)* (Figure 26B and C). For *vhl-1(ok161)* it has been shown that the median lifespan extension is

about 3 days (Müller et al. 2009). Inhibition of insulin signaling by *daf-2* knockout is one of the best established settings of longevity with a lifespan more than twice as long as wild-type (Kenyon et al. 1993). As expected, in both experiments the mutant worms showed an increased lifespan comparable to published data.

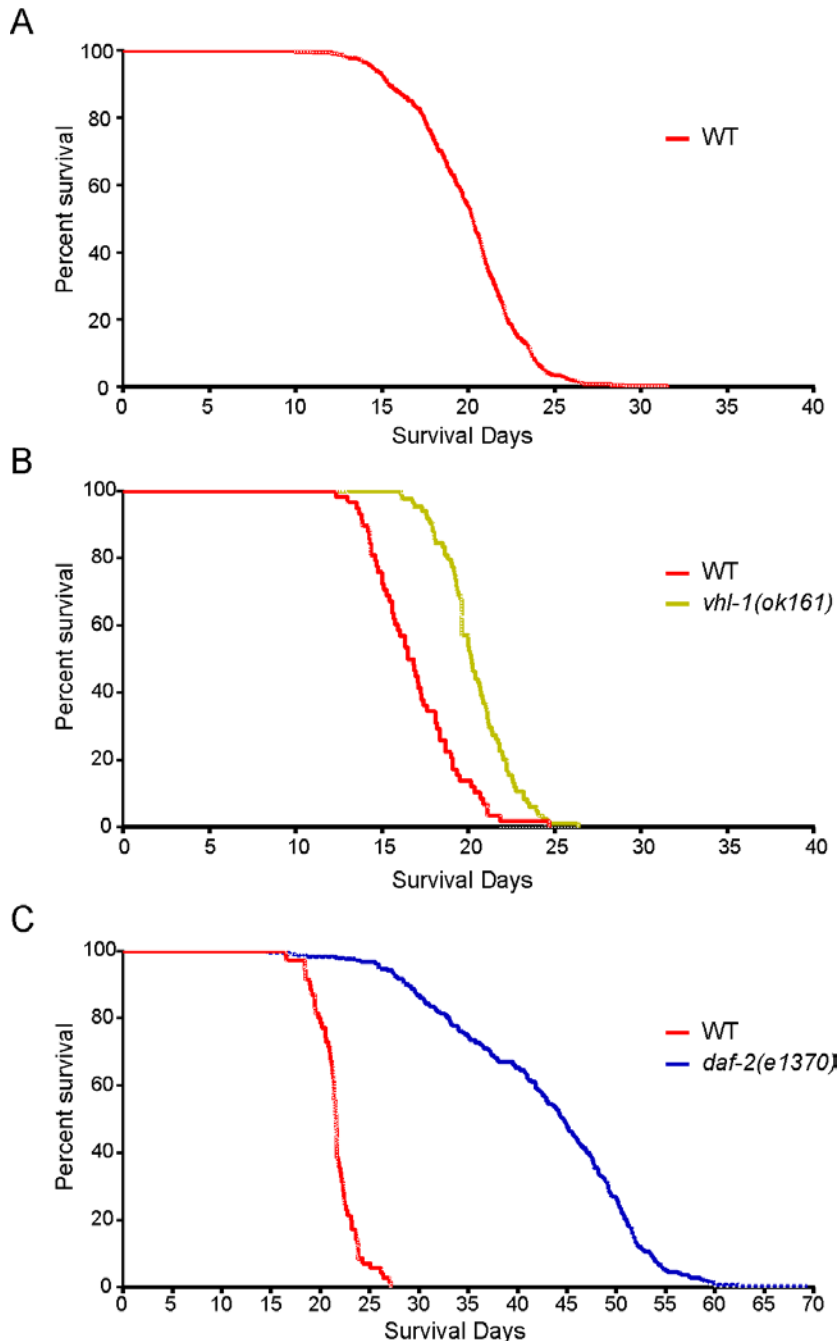


Figure 26: Automated lifespan analysis of *C. elegans* mutants.

A. Lifespan analysis of wild-type worms. 349 worms were analysed and have a median lifespan of 20 days. **B.** Lifespan analysis of wild-type (red, WT) and *vhl-1(ok161)* (yellow). 58 worms were analysed for wild-type and 84 worms for *vhl-1(ok161)*. The median lifespan for wild-type is 16.5 days and for *vhl-1(ok161)* 20 days. **C.** Lifespan analysis of wild-type (red) and *daf-2(e1370)* (blue). 70 worms were analysed for wild-type and 242 worms for *daf-2(e1370)*. The median lifespan for wild-type is 21 days and for *daf-2(e1370)* 46 days (see also Table 12).

5.5.3 Lifespan analysis of worms fed on RNAi in the lifespan machine set-up

The first analyses using the lifespan machine indicated that the machine was fully functional (Figure 26A-C). To analyse the effect of the RBPs on lifespan extension we designed an RNAi lifespan experiment. Commercially available RNAi libraries cover most of the coding genome of *C. elegans* including most the RBPs we wanted to analyse. However, before starting the analysis it appeared essential to show that the machine would provide reliable results for worms grown on HT115 *E. coli* that are used for the expression of dsRNA required for RNAi. We analysed wild-type worms fed bacteria expressing RNAi against *daf-2* mRNA (Figure 27A).

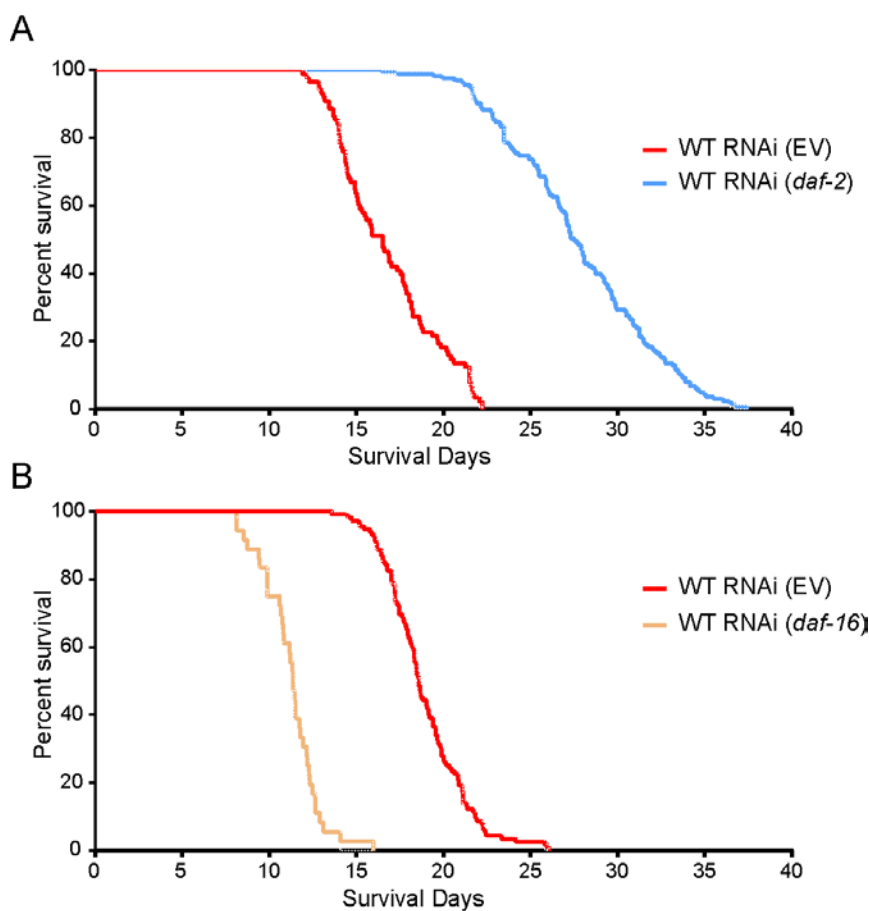


Figure 27: Lifespan analysis of *C. elegans* feed on RNAi.

A. Lifespan analysis of wild-type worms feed with bacteria expressing empty vector (EV) RNAi (red) or *daf-2* RNAi (blue). 88 worms were analysed for EV RNAi and 163 worms for *daf-2* RNAi. The median lifespan for EV RNAi is 16.5 days and for *daf-2* RNAi 27.5 days. **B.** Lifespan analysis of wild-type feed with bacteria expressing empty vector RNAi (red) or *daf-16* RNAi (orange). 115 worms were analysed for EV RNAi and 36 worms for *daf-16* RNAi. The median lifespan for EV RNAi is 18.5 days and for *daf-16* RNAi 11 days (see also Table 12).

We observed an increased lifespan, as showed before (Kenyon et al. 1993; Müller et al. 2009). Lifespan extension through inhibition of insulin signaling depends on the

FOXO transcription factor DAF-16 and knockdown of *daf-16* in wild-type leads to a shortened lifespan (Kenyon et al. 1993). Therefore, we fed worms with bacteria expressing RNAi against *daf-16* mRNA and were able to reproduce the known phenotypes (Figure 27B). These data confirm that the lifespan machine can analyse worms fed with bacteria expressing RNAi and be used to analyse the lifespan of the 80 RBPs knockdowns.

5.5.4 Knockdown of RBPs regulates *C. elegans* lifespan

The RBPs we wanted to focus were derived from the in-depth analysis of the RIC and proteome of wild-type and *vhl-1(ok161)* mutant worms (Figures 23 and 24). In a first pilot screen, we examined 8 of them on the lifespan machine (Figure 28A).

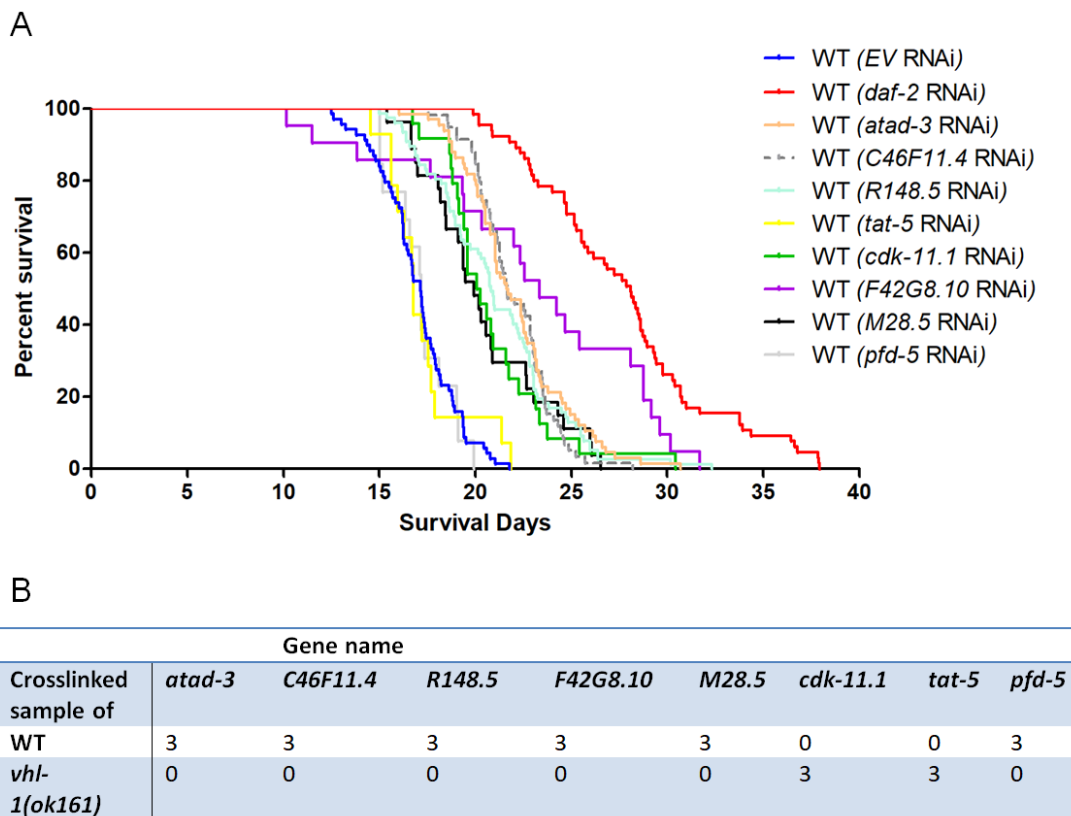


Figure 28: Lifespan analysis of RBP knockdown in *C. elegans*.

A. Lifespan analysis of wild-type (WT) feed with bacteria expressing RNAi against: empty vector (EV), *daf-2*, *atad-3*, *C46F11.4*, *R148.5*, *F42G8.10*, *M28.5*, *cdk-11.1*, *tat-5* and *pfd-5*. For each RNAi knockdown N > 50 worms. The median lifespan in days are for EV (17.14), *daf-2* (28.10), *atad-3* (21.66), *C46F11.4* (21.66), *R148.5* (20.83), *cdk-11.1* (20.16), *tat-5* (16.79), *pfd-5* (17.18), *F42G8.10* (23.35) and *M28.5* (19.94). The experiment was performed once (see also Table 12). **B.** Overview of the RBPs tested in lifespan analysis. The numbers indicate detection of the RBPs in the crosslinked RIC samples of wild-type and *vhl-1(ok161)* mutant worms. *atad-3*, *C46F11.4*, *R148.5*, *F42G8.10*, *M28.5* and *pfd-5* were measured three times in wild-type crosslinked samples and never in *vhl-1(ok161)* crosslinked samples. *cdk-11.1* and *tat-5* were measured three times in *vhl-1(ok161)* crosslinked samples and never in wild-type crosslinked samples.

The knockdown of 6 of these RBPs showed an increased lifespan compared to the wild-type. Interestingly, F42G8.10 RNAi showed an increase of six days median survival compared to the wild-type whereas the other five showed an increase of 2 to 4 days. Analysis of the RIC revealed that five of the six lifespan increasing RBPs were identified exclusively in the wild-type crosslinked samples and one of them exclusively in the *vhl-1(ok161)* crosslinked samples (Figure 28B).

5.5.5 CRISPR-Cas9 based Genome editing in *C. elegans*

Using the lifespan machine we were able to identify RBPs potentially increasing the lifespan of wild-type worms upon downregulation. It is still unclear how these RBPs increase the lifespan. The identification of the RNA targets of these RBPs would be a first step towards testable hypotheses on how these RBPs potentially regulate the lifespan extension. The identification of RNA bound to RBPs is possible by cross-linking and immunoprecipitation (CLIP) experiments (Ule et al. 2003). One of the crucial steps of CLIP is the isolation of a specific protein using immunoprecipitation protocols. In *C. elegans*, there are few validated antibodies against endogenous proteins available. To overcome this limitation we decided to use CRISPR-Cas9 technology in the worm as reported before (Paix et al. 2017). We designed DNA oligos to fuse a 3xFLAG tag to endogenous RBPs N-terminally. We injected CRISPR-Cas9 mix (*dpy-10* ssODN and crRNA, *pqn-53* ssODN and crRNA, Cas9, tracrRNA, KCl and HEPES pH 7.4) into the germline of the worm to tag *pqn-53* (for details see Methods). *pqn-53* contains a prion-like domain which is found in RNA binding proteins and it localizes to the nucleus (Hennig et al. 2015). In the analysed RIC it is defined as Class II RBP in both wild-type and *vhl-1(ok161)* mutant worms and is therefore a good candidate to establish CRISPR-Cas9. The insertion of *dpy-10* ssODN and crRNA into the CRISPR-Cas9 mix will cause a dumpy phenotype in the progeny of injected worms. Therefore successful injection was confirmed by the identification of the dumpy phenotype on the plates (Figure 29A). Worms showing a dumpy phenotype were isolated and a 3 primer based PCR showed their heterozygosity for an insertion when a second band at high 270 base pair appeared (Figure 29B). Heterozygous worms were singled and the progeny of these worms were screened for homozygosity by PCR. Worms supposed to be homozygous for insertion were confirmed by sequencing for successful insertion (Figure 29C). The expression of the successfully integrated FLAG tag was confirmed by western

blotting (Figure 29D). The time frame from injection to the new strain was three weeks. Therefore it is feasible to generate a considerably larger number of tagged RBP strains in the future.

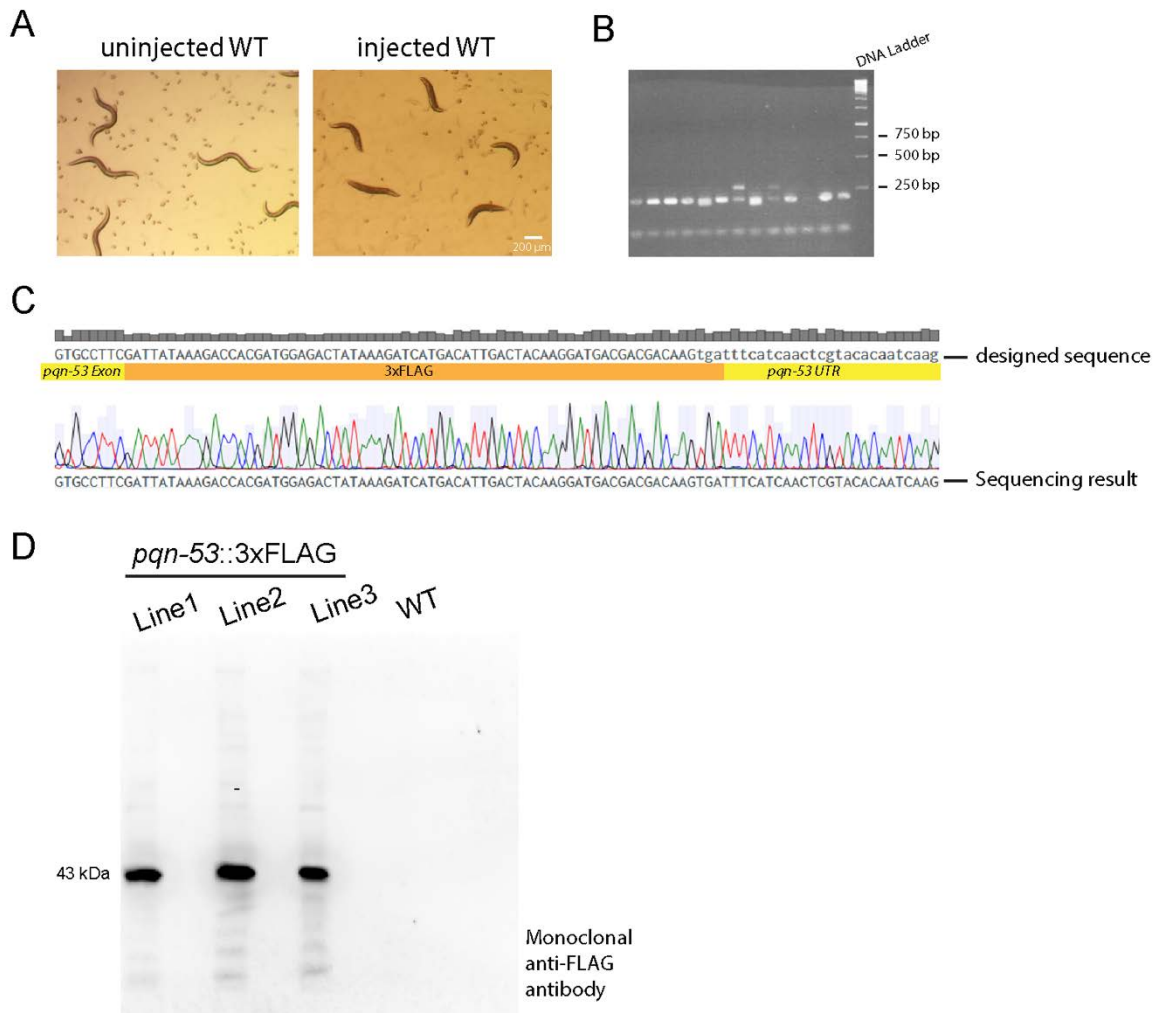


Figure 29: Genome editing using CRISPR-Cas9.

A. Images of *C. elegans* after injection with CRISPR-Cas9 mix (*dpy-10* ssODN and crRNA, *pqn-53* ssODN and crRNA, Cas9, tracrRNA, KCl and HEPES pH 7.4). Wild-type worms injected show dumpy phenotype in the F1 generation (right) compared to not injected worms (left). The scale depicts 200 μ m. **B.** PCR analysis of the F1 generation after injection. Worms with insertion show in addition of a band 200 bp band a 270 bp band (red boxes). **C.** Sequence analysis of worms with homozygous insertions is checked for the correct sequence of the FLAG insertion. The sequence on the top row shows the expected sequence upon FLAG insertion whereas the bottom row shows the sequencing result of *pqn-53:3xFLAG* line 1. **D.** Western blot analysis of three different strains generated by CRISPR-Cas9. *pqn-53:3xFLAG* has a size of 43 kDa. As a negative control wild-type worms were used.

6 Discussion

Preconditioning protocols have the potential to increase stress resistance in the kidney and thereby prevent AKI. One promising preconditioning protocol is the activation of the hypoxia signaling pathway. The key gene in the hypoxia signaling pathway is HIF. Although this pathway is well studied it has not been possible yet to transfer the findings to the clinical setting. Therefore, we aimed to gain a better understanding of the hypoxia signaling pathway. We focused on a group of important post-transcriptional regulator proteins, RBPs. The exceptional features of RBPs to bind RNA and to determine its fate make RBPs a key regulator in several pathways including the hypoxia signaling pathway (Masuda et al. 2009). How the hypoxia signaling pathway affects the RBP landscape is not yet understood. Therefore we set out to investigate the global impact of the hypoxia signaling pathway regarding RBPome.

6.1 *vhl-1(ok161)* mutant phenotype and its impact in RIC

When growing *vhl-1(ok161)* mutant worms we observed that they appear shorter compared to the wild-type worms. Microscopy revealed that they also have an increased width. Both characteristics are a typical phenotype in *C. elegans* reported as dumpy. This phenotype is caused by defects in the extracellular matrix (ECM) of the worms (McMahon et al. 2003). Interestingly, it was previously shown that human VHL can bind directly to collagen IV alpha 2 (G. Kurban et al. 2008). Additionally, inactivated VHL leads to remodeling of fibronectin and collagen IV resulting in highly vascularized tumors with increased invasive ability (G. Kurban et al. 2008; Ghada Kurban et al. 2006). It was also found that lifespan in *C. elegans* is partly linked to collagen which is the main component of ECM (Ewald et al. 2015). The upregulation of a single collagen gene can lead to an increased lifespan in the worm. Besides, it is known that *vhl-1(ok161)* mutant worms live longer compared to the wild-type worms (Mehta et al. 2009; Müller et al. 2009; Y. Zhang et al. 2009). Together these results suggest a direct link between the lifespan extension of *vhl-1(ok161)* mutant worms and potential changes in the ECM. The fact that the *vhl-1(ok161)* mutant worms show a dumpy phenotype comes with a couple of problems regarding the comparison to wild-type worms. In our RIC experiment, we used equal numbers of wild-type and *vhl-1(ok161)* mutant worms. RNA and protein analyses revealed that the RNA and protein content is reduced in *vhl-1(ok161)* mutant worms compared to wild-type

worms even when the same worm number was extracted. An explanation for this reduction of RNA and protein content could be the smaller body size of *vhl-1(ok161)* mutant worms. Besides, changes in the worm cuticle (as indicated by the dumpy phenotype) could lead to differences in the efficiency of RNA and protein extraction. To compensate for this imbalance regarding the whole proteome we normalized the data to protein amount after measurement of wild-type and *vhl-1(ok161)* mutant. However, normalization would not have easily been possible for the corresponding RIC experiment. To overcome this challenge in the RIC experiment, we saturated the beads with RNA indicated by the measured RNA yield after pulldown which should make the results independent from the differences between the two strains. Nonetheless we cannot exclude a resulting bias introduced into the comparison between wild-type worms and *vhl-1(ok161)* mutant worms completely. More confirmatory experiments regarding single RBPs differentially regulated by hypoxia signaling will be required to address this aspect conclusively. Here, immunoprecipitation of specific proteins in combination with polynucleotide kinase assays or RNAseq (in the sense of crosslinking and immunoprecipitation) will be helpful in the future. These experiments will be enabled by the CRISPR-based introduction of Flag-tags as established in my project.

6.2 The complexity of RIC protocols

We performed RIC by using wild-type and *vhl-1(ok161)* mutant worms and identified in total 2473 proteins for wild-type and *vhl-1(ok161)* mutant worms. We chose intensity-based absolute quantification (iBAQ) as our analysis strategy due to the expected large difference regarding the number of proteins measured between crosslinked and non-crosslinked samples. For the proteome, we wanted to keep the comparability to the RBPome as high as possible and consequently used iBAQs as well. Performing PCA and hierarchical clustering we came to the conclusion to exclude one non-crosslinked sample for each wild-type and *vhl-1(ok161)* mutant worms as the number of proteins measured was unexpectedly high for these samples. Additionally, the corresponding crosslinked samples revealed fewer proteins measured than in the non-crosslinked outliers. This is most likely explained by contamination with whole worm lysates underlining that these samples needed to be excluded as outliers. We are aware that three biological replicates are favourable for statistical analyses. Nonetheless, our statistical approach allowed for the

identification of a high number of significantly enriched RBPs showing that two non-crosslinked controls were sufficient for our purpose. Furthermore, earlier RIC experiments have shown that reliable datasets can be built on two biological replicates (Baltz et al. 2012; Castello et al. 2012; Liepelt et al. 2016; S. F. Mitchell et al. 2013). Castello et al. used two UVC crosslinked and non-crosslinked samples and compared these to one UVA crosslinked and non-crosslinked sample pre-treated with 4SU revealing comparable results (Castello et al. 2012). Liepelt et al. pooled their non-crosslinked replicates from different conditions (+/- LPS) for all downstream analyses considering the stable results in non-crosslinked samples between conditions (Liepelt et al. 2016). As expected in the non-crosslinked samples, most proteins are washed off due to lack of covalent bonds. In our dataset, 502 proteins were exclusively detected only in crosslinked samples making it impossible to perform any statistics with these proteins as they are not measured in the non-crosslinked samples. Obviously, these proteins are very likely to be indeed RBPs and were defined as such in our analyses. Taken together, we detected 1354 RBPs for wild-type and *vhl-1(ok161)* mutant worms in the RIC. Our analysis indicates that at least 6.8% of protein coding genes in *C. elegans* encode RBPs. That number exceeds the predicted 4.4% (Tamburino et al. 2013) showing the restrictions of computational RBP prediction algorithms.

6.3 Interspecies data comparison

To get a deeper understanding of both the quality and the content of our dataset we compared it to published RIC datasets. To date, the only other RBPome performed in *C. elegans* was published by Matia-González et al. (Matia-González et al. 2015). The overlap between our dataset and that from Matia-González et al. is approximately 26 percent. The limited overlap with the previous study characterizing the worm RBPome is most likely due to differences in the experimental setup regarding mass spectrometry and more importantly, the choice of controls. Matia-Gonzalez et al. used RNase ONE treated and poly(A) competitor controls, whilst we employed non-crosslinked controls. Additionally, we used exclusively young adult worms whereas they used either a mixed worm stage population or L4 stage worms. Also, we identified 1354 RBPs whereas they identify 594 RBPs. To further extend the analysis we compared our dataset with datasets that include human, worms, mouse and were summarized by Hentze et al. (Hentze et al. 2018). Since our dataset is based on *C.*

C. elegans, we converted gene identifiers into their orthologues from human, mouse, fly and yeast. This came with the additional challenge that the conservation of gene sets differs between these organisms. Consequently, many cases of RBPs identified in one of the datasets but not found in ours may be the result of a lack of (known) conservation. To complete the comparisons we also used data coming from novel approaches that identify RBPs from total RNA (Queiroz et al. 2019; Trendel et al. 2019; Urdaneta and Beckmann 2019). The number of identified RBPs in these novel approaches was higher possibly due to the fact that these protocols do not enrich for polyA-tailed RNA binding but reveal RBPs bound to all different types of RNA. More than 65 percent of our identified RBPs were covered by these datasets. Although the overlap of our data with the *C. elegans* dataset by Matia-González et al. is 26 percent, the comparison to RBPomes from other species revealed that 80 percent of our RBPome were already known as RBPs (Hentze et al. 2018; Ignarski et al. 2019; Queiroz et al. 2019; Trendel et al. 2019; Urdaneta et al. 2019). In addition, the fact that many classical RBDs were identified in our dataset by domain enrichment analysis shows that we actually identified RBPs. Taking this into consideration and the fact that we have an increased detection of RBPs compared to Matia-Gonzalez shows our RIC was more sensitive possibly due to differences in the protocol and due to technological progress in the field of mass spectrometry. In addition to the increasing choice and improvement of technologies, the characterization of RBPs in specific biological settings such as hypoxia will also increase the number of proteins identified. Proteins that are only expressed under these specific conditions can only be identified as RBPs under these circumstances. For instance, performing a RIC using mIMCD-3 cells maintained under either normoxic conditions or six hours under hypoxic conditions resulted in six RBPs that were identified exclusively in hypoxic conditions (Ignarski et al. 2019). Moreover, two RBPs were exclusively identified upon induction of germline apoptosis in *C. elegans* (Matia-González et al. 2015). However, only a few studies have used specific biological conditions to carry out RIC to date. In our dataset, we noticed that the novel RBPs identified either exclusively in wild-type or *vhl-1(ok161)* mutants are overrepresented by 38 percent compared to the entire dataset by 20 percent. That finding speaks again for RIC experiments in certain biological conditions to identify all RBPs. Since efficient crosslinking is a crucial step in RIC, not all type of samples are appropriate for this technique. As soon as a certain thickness of the sample is reached, crosslinking gets inefficient. As a

result, primarily cell monolayers have been used for these experiments limiting our understanding of biological processes in RBP regulation to this rather artificial setting. Since, *C. elegans* is transparent and has a diameter of 50 μm (Maguire et al. 2011), crosslinking does indeed reach sufficient efficiency and RIC can be performed. This enables an insight into the RBPome in a living model organism. As an alternative to UVC crosslinking performed in our study, irradiation with UVA in combination with a photoreactive ribonucleoside analog such as 4SU can be used (Baltz et al. 2012; Beckmann 2017; Castello et al. 2012; Ignarski et al. 2019). 4SU is incorporated into newly transcribed RNA and can also be used for instance to analyse the half-life and degradation of an RNA (Tani and Akimitsu 2012). It allows to globally identify the RNA segments that are crosslinked by the mRNA-bound proteome (Baltz et al. 2012). Unfortunately, it has been shown that *C. elegans* absorbs little of the 4SU compared to HEK239 cells (Jungkamp et al. 2011). In addition, 4SU itself shows certain toxicity and therefore may have an impact on the results (Lozzio and Wigler 1971). The efficient crosslinking of organs is just as challenging. So far RIC was not performed on whole organs. However, in CLIP experiments and in the novel approach that identify RBPs (PTex) mouse-brain tissue was used (Licatalosi et al. 2008; Ule et al. 2003; Urdaneta et al. 2019). Before irradiation the mouse-brain was disrupted by cryogenic grinding resulting in efficient crosslinking (Urdaneta et al. 2019). Another recent study improved RIC UV-crosslinking efficiency in leaves with a possibility to adapt that approach to animal organs (Bach-Pages et al. 2020). The constant improvement of the RIC method will make it possible to use all types of samples in the future and thus to identify new RBPs.

6.4 The impact of hypoxia signaling on the RBP landscape

The main goal of my thesis was to understand how the hypoxia signaling pathway influences the RBP landscape. To that end, we compared the RIC data of wild-type worms to *vhl-1(ok161)* mutant worms. The stabilization of *HIF-1* in *vhl-1(ok161)* mutant worms leads to the activation of various target genes. We hypothesized that RBPs exist among these target genes. The analysis of the proteome of wild-type and *vhl-1(ok161)* mutant worms showed that 12 out of 1354 of the identified RBPs are differentially regulated upon *HIF-1* stabilization. Interestingly, among these proteins *PHY-2* was upregulated and *COL-8* was downregulated in *vhl-1(ok161)* mutant worms. Both are collagen related genes involved in the formation of the

extracellular matrix (Cox et al. 1989; Friedman et al. 2000). The finding may link RBPs to the ECM phenotype observed in *vhl-1(ok161)* mutant worms. How ECM formation and ECM components may be functionally linked to RBPs is not clear at the moment and will require future studies. The majority of RBPs do not seem to be regulated at the protein level but rather at the level of RNA binding. A group of RBPs that appeared especially interesting to us were those proteins which were exclusively detected in RIC from either wild-type or *vhl-1(ok161)* crosslinked samples. We identified exclusively in *vhl-1(ok161)* crosslinked samples *tag-65*, *tat-5*, *ensa-1*, *cdk-11.1* and *orc-3*. Both *tat-5* and *orc-3* are novel RBPs without classical RBD and therefore belong to the enigmRBPs. *tat-5* human ortholog is *ATPase phospholipid transporting 9A (ATP9A)*. In *C. elegans* *tat-5* was shown to be involved in the regulation of extracellular vesicles release and this finding has been confirmed in mammals (Naik et al. 2019; Wehman et al. 2011). The human ortholog of *tag-65* is the *calcium homeostasis endoplasmic reticulum protein (CHERP)*. It modulates intracellular Ca^{2+} homeostasis and was observed as splicing regulator as a U2-related protein (Laplante et al. 2000; Wang et al. 2019). The human orthologue *ensa-1* is *cAMP regulated phosphoprotein 19 (ARPP19)* and *endosulfine alpha (ENSA)*. Together they are important for the control of mitosis and its M- and S-phases (Castro and Lorca 2018). The human orthologue of *Cdk-11.1* is *CDK11A* and similar to *ensa-1* human orthologs it is involved in cell cycle regulation (Liu et al. 2017). *orc-3* is not conserved in humans but there is evidence that it is involved in *C. elegans* germ-line development (Hanazawa et al. 2001). The fact that nothing of their protein function indicates RNA binding capacity is typical for enigmRBPs (Beckmann et al. 2015). A special group of these enigmRBPs are the metabolic enzymes. One well-characterized example is the iron regulatory protein 1 (IRP1) (Anderson et al. 2012). IRP1 binds to iron-responsive elements (IREs) in the 5' or 3' untranslated regions of mRNAs and can block mRNA translation (5' UTR binding) or leads to mRNA stabilization (3' UTR binding). Thus IRP1 controls mRNAs encoding proteins involved in iron homeostasis and thereby maintain intracellular iron levels (Anderson et al. 2012; Hentze et al. 2010). However, RNA may also affect enzymes by changing their activity, complex formation or stability. Other possibilities of RNA/enzyme interactions have been proposed, it is imaginable that RNA binding blocks the catalysis performed by an enzyme or that RNA binding is needed to bridge between complex subunits (Castello et al. 2015). These possible modes of action exerted by RNA to

regulate enzymes still need to be tested. Even though the 5 proteins were exclusively identified in *vhl-1(ok161)* samples there is no link to hypoxia signaling found in the literature. This could be due to the fact that these proteins were also not regulated in the proteome so that they do not stand out in a “normal” analysis. Consequently, RIC adds another layer of complexity to our understanding of this pathway and an insight into how RNA-binding of these proteins changes upon hypoxia as well as the consequences of RNA-binding to cellular biology would be extremely interesting. A study by our laboratory that performed a RIC in hypoxia-treated mIMCD-3 cells has also shown that the RNA binding of RBPs changes rather than the occurrence of the RBPs (Ignarski et al. 2019). In total 12 proteins were identified in their RIC that reaches significant exclusively in one condition and therefore assigned as RBP. Six of them in mIMCD-3 cells treated with normoxia and six of them in mIMCD-3 cells treated with hypoxia. The comparison to my data showed that two of these twelve RBPs have a similar pattern. The protein *SDAD1* in mouse is labeled as RBP exclusively in hypoxic mIMCD-3 cells and its *C. elegans* ortholog *pro-3* is only found in the *vhl-1(ok161)* mutant worms. *SDAD1* has been shown to promote proliferation of colon cancer cells by reducing apoptosis (Zeng et al. 2017). On the other hand, *TCP1* in the mouse was labeled as RBP only in normoxic mIMCD-3 cells and its *C. elegans* ortholog *cct-1* was found in RIC only in wild-type worms. *TCP1* is a type II chaperonin that sequestered and folded newly synthesized or misfolded proteins in a ATP dependent manner (Showalter et al. 2020). Interestingly, one study shows that *TCP1* can be associated with the recovery from AKI (Blanco-Gozalo et al. 2020) and could be a viable target for therapeutic development.

6.5 The *C. elegans* lifespan machine

Since the link between hypoxia-regulated RBPs and stress resistance mediated by hypoxic preconditioning is at the heart of our research interest moving on to a phenotype analysis based on our RIC data was the logical next step. In *C. elegans* stress resistance is coupled with lifespan extension. Often, increased stress resistance is directly proportional to an increased lifespan in worms for the majority of pathways studied to date (Zhou et al. 2011). We wanted to study if the regulation of one of the identified RBPs in the *vhl-1(ok161)* mutant worms is also involved in increased lifespan. To this end, we first initiated establishment of the lifespan machine (Stroustrup et al. 2013). We were able to install 10 scanners in the

laboratory. 14 plates (6 mm) with 50 worms each fit on each scanner. This enables us to carry out lifespan analyses with 7000 worms at the same time. When setting up the machine we first solved obvious problems such as the heat generated by each scan by equipping them with fans. We also sealed the plates so that they did not dry out and reduced bacterial contamination. We tested the lifespan machine by using wild-type, *vhl-1(ok161)* and *daf-2* mutants. Noticeably, the lifespan curves of the wild-type differ between experiments. That can be explained by the different number of worms used in each experiment. We noticed that the number of worms influences the pattern of the curve. When using more worms we had more data points for each time point making the curve more continuous. Unfortunately, a high number of worms are not always guaranteed due to the number of strains used and exclusion of plates due to contamination. Considering the great opportunity and simplification of lifespan experiments linked to the lifespan machine the capacity of the machine was fully utilized soon after its establishment. Consequently another 15 scanners are currently being planned to extend the lifespan machine. That would allow us to analyse the lifespans of 17500 worms at the same time. The lifespan machine can be handled by a single scientist. Consequently, the number of experiments possible for one scientist is greatly enhanced by this device enabling fast lifespan screening. Although the lifespan machine offers many advantages over manual counting, unfortunately FUdRs need to be supplemented into the NGM agar. FUdR sterilizes the worm that no offspring can arise that is eaten up the food. Unfortunately, FUdR treatment itself can affect the lifespan of mutant worms but not the lifespan of wild-type worms (Aitlhadj and Stürzenbaum 2010; Park et al. 2017). An alternative to FUdR would be to use RNAi to prevent progeny. A possibility would be an RNAi construct targeting *mex-3* that has already been used successfully in Stroustrup lab. *MEX-3* is important for the anterior–posterior asymmetry in embryos and therefore upon downregulation leads to embryonic lethality (Draper et al. 1996). Further, the data generated by the lifespan machine can potentially be used beyond the mere analysis of nematode lifespan. This phenotype is evaluated by registration of movement and the worm position on the plate. This data could also be used to analyse the movement patterns of the worms including a number of additional phenotypic assays such as chemotaxis or osmotic avoidance that are based on movement.

6.6 RBPs involved in *C. elegans* lifespan

We then went on to perform the first pilot lifespan screen of RBPs identified in my project. Knockdown of *atad-3*, *C46F11.4*, *R148.5*, *cdk-11.1*, *F42G8.10* and *M28.5* increased the lifespan of wild-type worms. As described before *cdk-11.1* human ortholog is *CDK11A* and was exclusively detected in *vhl-1(ok161)* mutant worms. Knockdown of *cdk-11.1* is linked to slow growth (Pothof et al. 2003). We observed the same in *vhl-1(ok161)* mutants and slow growth is frequently observed in long-lived strains (Y. Lee et al. 2016). *C46F11.4* human ortholog is the DEAD box protein *Ddx42*. *Ddx42* and is known to interact with the apoptosis inducer ASPP2 (Uhlmann-Schiffler et al. 2009). For *C46F11.4* an RNAi screen indicates extension of the lifespan of a short lived mutant (Xie and Roy 2012). *atad-3* is involved in mitochondrial iron and heme homeostasis (van den Ecker et al. 2015). It has been shown that *atad-3* RNAi promotes longevity in *C. elegans* confirming our results (Hoffmann et al. 2012). The human ortholog of *atad-3*, *ATAD3A* has been found to be overexpressed in various types of cancer (Teng et al. 2019) which could point towards a potential role as a factor ensuring growth and survival. The human ortholog of *M28.5* is *SNU13*. *SNU13* is one of the four core proteins of C/D small nucleolar RNPs (snoRNPs) that are involved in post-transcriptional modifications (Quinternet et al. 2016). Interestingly, the human orthologues of *F42G8.10*, *NDUFB11* are implicated in microphthalmia (van Rahden et al. 2015). The deletion of *VHL* in retinal pigment epithelium was also linked to microphthalmia (Lange et al. 2012). Taken together, our screen identifies highly interesting RBP candidates that may be involved in increased stress resistance and longevity upon activation of hypoxia signaling. Epistasis experiments with *vhl-1/hif-1* will now be needed to further corroborate this link. Before studying the RBPs identified in our screen, a validation of their actual RNA binding capacity should be carried out. A well-established method is immunoprecipitation and radioactive labeling of co-purified RNA (PNK assay) (Tawk et al. 2017). This has already been successfully carried out on HEK293T cells in our laboratory (Ignarski et al. 2019). In *C. elegans* we were able to perform successfully an immunoprecipitation of an FLAG tagged RBP and are now working to carry out the PNK assay. As soon as RBPs are confirmed of their RNA binding capacity, it would be of great importance to identify the RNA targets using CLIP protocols (Jungkamp et al. 2011).

6.7 Future perspectives to elucidate RBPs in AKI

Our results show that RBPs are regulated by the hypoxia signaling pathway and that their RNA binding capacity is affected by this pathway. This is particularly interesting since one of these RBPs could also have the potential – like hypoxia itself - to prevent AKI. That modulation of these RBPs has already a beneficial effect in the organisms as we could show by an increased lifespan of the worms. So far it remains open whether this increased lifespan is also dependent on the activation of the hypoxia signaling pathway. Nonetheless, modulation of these specific RBPs could be a targeted way to activate stress resistance in the future. To move closer to this goal, knowledge on the actual transcripts bound by these RBPs would be crucial. As discussed before CLIP experiments could answer this question (Ule et al. 2003). Once the RNA targets are known binding to these targets can be modulated using antisense oligos targeting the binding sites (Van Nostrand et al. 2016). On the one hand, this approach would allow to elucidate which binding events are indeed involved in the increase of stress resistance. On the other hand, antisense therapies have become a new option in clinical care and considering the rapidly increasing number of such therapies that have been approved in the last years, this can get a first step towards clinical translation. However, transferring these results to mammals is obviously a key step that has to be performed beforehand. Here, experiments in cell culture using human and mouse cells can be used to show that the RBP is influenced by hypoxia on the one hand and that the binding of the RBP to the target RNA is conserved on the other. If these results are satisfactory, the hypotheses need to be tested in murine AKI models (e.g. ischemia-reperfusion or cisplatin toxicity (Hesketh et al. 2014; Späth et al. 2019; Xu et al. 2015)) modulating the RBP of choice either using antisense oligos or genetic interventions (e.g. mutation of the RNA-binding domain). Obviously, the way towards clinical translation will be a long one. Nonetheless, the molecular understanding gained in models like the ones used in this project is the crucial step to start such endeavors and creating entirely new opportunities. Such novel strategies are urgently awaited since – despite research on AKI for many decades – classical approaches have not yielded any targeted therapeutic or preventive measures.

7 Conclusion

Preconditioning protocols have the potential to prevent AKI. Unfortunately, these protocols cannot be used in the clinic yet because too little is known about their molecular mechanisms. One of the underlying mechanisms of these preconditioning protocols is the activation of the hypoxia signaling pathway. HIF activation as the center of the hypoxia signaling pathways has a profound impact on cellular biology. However, it is not known which factors play the most important role regarding stress resistance. In the scope of this thesis we were able to generate proteome and RBPome datasets of wild-type and *vhl-1(ok161)* mutant worms using RIC. Our data suggest that the hypoxia signaling pathway modulates the RBPome landscape. In particular, it seems that the RNA binding capacity rather than the protein abundance of the RBPs is changed. Similar observation has already taken place in cell culture as well. *C. elegans* can now be used to examine the hypoxia-inducible factor signaling and its modulation of the RBPs further by using RNA interference and mutant strains highlighting the worm as a good model organism. In total, we identified 80 RBPs that were modulated by the hypoxia signaling pathway. The lifespan machine established in scope of this work will make it possible to examine the lifespan of worms upon knockdown of all of these RBPs in the near future. However, of the eight RBPs that we have analysed so far, six have already shown that they actually play a role in extending the lifespan. In summary, we can say that our results have not only expanded the repertoire of RBPs in general, but also filled the gap of which RBPs are modulated by the hypoxia signaling pathway. This enables to select candidates that can be examined further, which in turn means a major step towards our understanding of the modulation of the hypoxia signaling pathway for future applications in the clinic.

8 References

- Aitlhadj, L., and S. R. Stürzenbaum. 2010. The use of FUDR can cause prolonged longevity in mutant nematodes. *Mechanisms of Ageing and Development*, 131(5):364–365.
- Anderson, C. P., L. Shen, R. S. Eisenstein, and E. A. Leibold. 2012. Mammalian iron metabolism and its control by iron regulatory proteins☆. *Biochimica et Biophysica Acta*, 1823(9):1468–1483.
- Bach-Pages, M., F. Homma, J. Kourelis, F. Kaschani, S. Mohammed, M. Kaiser, R. A. L. van der Hoorn, A. Castello, and G. M. Preston. 2020. Discovering the RNA-Binding Proteome of Plant Leaves with an Improved RNA Interactome Capture Method. *Biomolecules*, 10(4):661.
- Baltz, A. G., M. Munschauer, B. Schwanhäusser, A. Vasile, Y. Murakawa, M. Schueler, N. Youngs, D. Penfold-Brown, K. Drew, M. Milek, E. Wyler, R. Bonneau, M. Selbach, C. Dieterich, and M. Landthaler. 2012. The mRNA-bound proteome and its global occupancy profile on protein-coding transcripts. *Molecular Cell*, 46(5):674–690.
- Beckmann, B. M. 2017. RNA interactome capture in yeast. *Methods (San Diego, Calif.)*, 118–119:82–92.
- Beckmann, B. M., R. Horos, B. Fischer, A. Castello, K. Eichelbaum, A.-M. Alleaume, T. Schwarzl, T. Curk, S. Foehr, W. Huber, J. Krijgsveld, and M. W. Hentze. 2015. The RNA-binding proteomes from yeast to man harbour conserved enigmRBPs. *Nature Communications*, 6:10127.
- Blanco-Gozaolo, V., A. G. Casanova, S. M. Sancho-Martínez, M. Prieto, Y. Quiros, A. I. Morales, C. Martínez-Salgado, C. Agüeros-Blanco, A. Benito-Hernández, M. A. Ramos-Barron, C. Gómez-Alamillo, M. Arias, and F. J. López-Hernández. 2020. Combined use of GM2AP and TCP1-eta urinary levels predicts recovery from intrinsic acute kidney injury. *Scientific Reports*, 10(1):11599.
- Brennan, C. M., and J. A. Steitz. 2001. HuR and mRNA stability. *Cellular and Molecular Life Sciences: CMLS*, 58(2):266–277.
- Brenner, S. 1974. The genetics of *Caenorhabditis elegans*. *Genetics*, 77(1):71–94.

- Butter, F., M. Scheibe, M. Mörl, and M. Mann. 2009. Unbiased RNA–protein interaction screen by quantitative proteomics. *Proceedings of the National Academy of Sciences of the United States of America*, 106(26):10626–10631.
- Castello, A., B. Fischer, K. Eichelbaum, R. Horos, B. M. Beckmann, C. Strein, N. E. Davey, D. T. Humphreys, T. Preiss, L. M. Steinmetz, J. Krijgsveld, and M. W. Hentze. 2012. Insights into RNA biology from an atlas of mammalian mRNA-binding proteins. *Cell*, 149(6):1393–1406.
- Castello, A., M. W. Hentze, and T. Preiss. 2015. Metabolic Enzymes Enjoying New Partnerships as RNA-Binding Proteins. *Trends in Endocrinology and Metabolism*, 26(12):746–757.
- Castro, A., and T. Lorca. 2018. Greatwall kinase at a glance. *Journal of Cell Science*, 131(20).
- Chandrasekar, B., J. F. Nelson, J. T. Colston, and G. L. Freeman. 2001. Calorie restriction attenuates inflammatory responses to myocardial ischemia-reperfusion injury. *American Journal of Physiology. Heart and Circulatory Physiology*, 280(5):H2094-2102.
- Chawla, L. S., and P. L. Kimmel. 2012. Acute kidney injury and chronic kidney disease: an integrated clinical syndrome. *Kidney International*, 82(5):516–524.
- Cho, S.-J., I.-F. Teng, M. Zhang, T. Yin, Y.-S. Jung, J. Zhang, and X. Chen. 2015. Hypoxia-inducible factor 1 alpha is regulated by RBM38, a RNA-binding protein and a p53 family target, via mRNA translation. *Oncotarget*, 6(1):305–316.
- Cléry, A., M. Blatter, and F. H.-T. Allain. 2008. RNA recognition motifs: boring? Not quite. *Current Opinion in Structural Biology*, 18(3):290–298.
- Coffman, T. M. 2014. The inextricable role of the kidney in hypertension. *The Journal of Clinical Investigation*, 124(6):2341–2347.
- Costa, D., M. Scognamiglio, C. Fiorito, G. Benincasa, and C. Napoli. 2019. Genetic background, epigenetic factors and dietary interventions which influence human longevity. *Biogerontology*, 20(5):605–626.

- Cox, G. N., C. Fields, J. M. Kramer, B. Rosenzweig, and D. Hirsh. 1989. Sequence comparisons of developmentally regulated collagen genes of *Caenorhabditis elegans*. *Gene*, 76(2):331–344.
- Cramer, P. 2019. Organization and regulation of gene transcription. *Nature*, 573(7772):45–54.
- Dengler, V. L., M. Galbraith, and J. M. Espinosa. 2014. Transcriptional regulation by hypoxia inducible factors. *Critical Reviews in Biochemistry and Molecular Biology*, 49(1):1–15.
- Draper, B. W., C. C. Mello, B. Bowerman, J. Hardin, and J. R. Priess. 1996. MEX-3 Is a KH Domain Protein That Regulates Blastomere Identity in Early *C. elegans* Embryos. *Cell*, 87(2):205–216.
- Edgar, R. S., and W. B. Wood. 1977. The nematode *Caenorhabditis elegans*: a new organism for intensive biological study. *Science (New York, N.Y.)*, 198(4323):1285–1286.
- Eltzschig, H. K., and T. Eckle. 2011. Ischemia and reperfusion--from mechanism to translation. *Nature Medicine*, 17(11):1391–1401.
- Endre, Z. H. 2011. Renal ischemic preconditioning: finally some good news for prevention of acute kidney injury. *Kidney International*, 80(8):796–798.
- Epstein, A. C., J. M. Gleadle, L. A. McNeill, K. S. Hewitson, J. O'Rourke, D. R. Mole, M. Mukherji, E. Metzen, M. I. Wilson, A. Dhanda, Y. M. Tian, N. Masson, D. L. Hamilton, P. Jaakkola, R. Barstead, J. Hodgkin, P. H. Maxwell, C. W. Pugh, C. J. Schofield, and P. J. Ratcliffe. 2001. *C. elegans* EGL-9 and mammalian homologs define a family of dioxygenases that regulate HIF by prolyl hydroxylation. *Cell*, 107(1):43–54.
- Esmaille, R., M. Ignarski, K. Bohl, T. Krüger, D. Ahmad, L. Seufert, B. Schermer, T. Benzing, R.-U. Müller, and F. Fabretti. 2019. Activation of Hypoxia-Inducible Factor Signaling Modulates the RNA Protein Interactome in *Caenorhabditis elegans*. *iScience*, 22:466–476.
- Evans, T. 2006. Transformation and microinjection. *WormBook*.

- Ewald, C. Y., J. N. Landis, J. Porter Abate, C. T. Murphy, and T. K. Blackwell. 2015. Dauer-independent insulin/IGF-1-signalling implicates collagen remodelling in longevity. *Nature*, 519(7541):97–101.
- Farrar, A. 2018. Acute Kidney Injury. *The Nursing Clinics of North America*, 53(4):499–510.
- Feigerlová, E., and S.-F. Battaglia-Hsu. 2017. Role of post-transcriptional regulation of mRNA stability in renal pathophysiology: focus on chronic kidney disease. *FASEB Journal: Official Publication of the Federation of American Societies for Experimental Biology*, 31(2):457–468.
- Fire, A., S. Xu, M. K. Montgomery, S. A. Kostas, S. E. Driver, and C. C. Mello. 1998. Potent and specific genetic interference by double-stranded RNA in *Caenorhabditis elegans*. *Nature*, 391(6669):806–811.
- Fontana, L., L. Partridge, and V. D. Longo. 2010. Extending healthy life span--from yeast to humans. *Science (New York, N.Y.)*, 328(5976):321–326.
- Friedman, L., J. J. Higgin, G. Moulder, R. Barstead, R. T. Raines, and J. Kimble. 2000. Prolyl 4-hydroxylase is required for viability and morphogenesis in *Caenorhabditis elegans*. *Proceedings of the National Academy of Sciences*, 97(9):4736–4741.
- Galbán, S., Y. Kuwano, R. Pullmann, J. L. Martindale, H. H. Kim, A. Lal, K. Abdelmohsen, X. Yang, Y. Dang, J. O. Liu, S. M. Lewis, M. Holcik, and M. Gorospe. 2008. RNA-binding proteins HuR and PTB promote the translation of hypoxia-inducible factor 1alpha. *Molecular and Cellular Biology*, 28(1):93–107.
- Go, A. S., G. M. Chertow, D. Fan, C. E. McCulloch, and C. Hsu. 2004. Chronic kidney disease and the risks of death, cardiovascular events, and hospitalization. *The New England Journal of Medicine*, 351(13):1296–1305.
- Grishok, A. 2005. RNAi mechanisms in *Caenorhabditis elegans*. *FEBS Letters*, 579(26):5932–5939.
- Hafner, M., M. Landthaler, L. Burger, M. Khorshid, J. Hausser, P. Berninger, A. Rothballer, M. Ascano, A.-C. Jungkamp, M. Munschauer, A. Ulrich, G. S. Wardle, S. Dewell, M. Zavolan, and T. Tuschl. 2010. Transcriptome-wide

- identification of RNA-binding protein and microRNA target sites by PAR-CLIP. *Cell*, 141(1):129–141.
- Halbeisen, R. E., A. Galgano, T. Scherrer, and A. P. Gerber. 2008. Post-transcriptional gene regulation: from genome-wide studies to principles. *Cellular and Molecular Life Sciences: CMLS*, 65(5):798–813.
- Hall, T. M. T. 2005. Multiple modes of RNA recognition by zinc finger proteins. *Current Opinion in Structural Biology*, 15(3):367–373.
- Hanazawa, M., M. Mochii, N. Ueno, Y. Kohara, and Y. Iino. 2001. Use of cDNA subtraction and RNA interference screens in combination reveals genes required for germ-line development in *Caenorhabditis elegans*. *Proceedings of the National Academy of Sciences*, 98(15):8686–8691.
- Harris, A. L. 2002. Hypoxia--a key regulatory factor in tumour growth. *Nature Reviews. Cancer*, 2(1):38–47.
- Hasan, A., C. Cotobal, C. D. S. Duncan, and J. Mata. 2014. Systematic analysis of the role of RNA-binding proteins in the regulation of RNA stability. *PLoS Genetics*, 10(11):e1004684.
- Hennig, S., G. Kong, T. Mannen, A. Sadowska, S. Kobelke, A. Blythe, G. J. Knott, K. S. Iyer, D. Ho, E. A. Newcombe, K. Hosoki, N. Goshima, T. Kawaguchi, D. Hatters, L. Trinkle-Mulcahy, T. Hirose, C. S. Bond, and A. H. Fox. 2015. Prion-like domains in RNA binding proteins are essential for building subnuclear paraspeckles. *The Journal of Cell Biology*, 210(4):529–539.
- Hentze, M. W., A. Castello, T. Schwarzl, and T. Preiss. 2018. A brave new world of RNA-binding proteins. *Nature Reviews. Molecular Cell Biology*, 19(5):327–341.
- Hentze, M. W., M. U. Muckenthaler, B. Galy, and C. Camaschella. 2010. Two to tango: regulation of Mammalian iron metabolism. *Cell*, 142(1):24–38.
- Hesketh, E. E., A. Czopek, M. Clay, G. Borthwick, D. Ferenbach, D. Kluth, and J. Hughes. 2014. Renal ischaemia reperfusion injury: a mouse model of injury and regeneration. *Journal of Visualized Experiments: JoVE*, (88).
- Hoffmann, M., S. Honnen, E. Mayatepek, W. Wätjen, W. J. H. Koopman, O. Bossinger, and F. Distelmaier. 2012. MICS-1 interacts with mitochondrial

- ATAD-3 and modulates lifespan in *C. elegans*. *Experimental Gerontology*, 47(3):270–275.
- Hughes, C. S., S. Foehr, D. A. Garfield, E. E. Furlong, L. M. Steinmetz, and J. Krijgsveld. 2014. Ultrasensitive proteome analysis using paramagnetic bead technology. *Molecular Systems Biology*, 10:757.
- Hwangbo, D.-S., H.-Y. Lee, L. S. Abozaid, and K.-J. Min. 2020. Mechanisms of Lifespan Regulation by Calorie Restriction and Intermittent Fasting in Model Organisms. *Nutrients*, 12(4).
- Ignarski, M., C. Rill, R. W. J. Kaiser, M. Kaldirim, R. Neuhaus, R. Esmailie, X. Li, C. Klein, K. Bohl, M. Petersen, C. K. Frese, M. Höhne, I. Atanassov, M. M. Rinschen, K. Höpker, B. Schermer, T. Benzing, C. Dieterich, F. Fabretti, and R.-U. Müller. 2019. The RNA-Protein Interactome of Differentiated Kidney Tubular Epithelial Cells. *Journal of the American Society of Nephrology: JASN*, 30(4):564–576.
- Jiang, H., R. Guo, and J. A. Powell-Coffman. 2001. The *Caenorhabditis elegans* hif-1 gene encodes a bHLH-PAS protein that is required for adaptation to hypoxia. *Proceedings of the National Academy of Sciences of the United States of America*, 98(14):7916–7921.
- Joo, J. D., M. Kim, V. D. D’Agati, and H. T. Lee. 2006. Ischemic preconditioning provides both acute and delayed protection against renal ischemia and reperfusion injury in mice. *Journal of the American Society of Nephrology: JASN*, 17(11):3115–3123.
- Jungkamp, A.-C., M. Stoeckius, D. Mecnas, D. Grün, G. Mastrobuoni, S. Kempa, and N. Rajewsky. 2011. In vivo and transcriptome-wide identification of RNA binding protein target sites. *Molecular Cell*, 44(5):828–840.
- Kaelin, W. G. 2005. Proline hydroxylation and gene expression. *Annual Review of Biochemistry*, 74:115–128.
- Kaelin, W. G., and P. J. Ratcliffe. 2008. Oxygen sensing by metazoans: the central role of the HIF hydroxylase pathway. *Molecular Cell*, 30(4):393–402.
- Kamath, R. S., and J. Ahringer. 2003. Genome-wide RNAi screening in *Caenorhabditis elegans*. *Methods (San Diego, Calif.)*, 30(4):313–321.

- Kazan, H., D. Ray, E. T. Chan, T. R. Hughes, and Q. Morris. 2010. RNAcontext: a new method for learning the sequence and structure binding preferences of RNA-binding proteins. *PLoS Computational Biology*, 6:e1000832.
- KDIGO for AKI. 2012. *Kidney International Supplements*, 2(1):1.
- Kenyon, C., J. Chang, E. Gensch, A. Rudner, and R. Tabtiang. 1993. A *C. elegans* mutant that lives twice as long as wild type. *Nature*, 366(6454):461–464.
- König, J., K. Zarnack, G. Rot, T. Curk, M. Kayikci, B. Zupan, D. J. Turner, N. M. Luscombe, and J. Ule. 2010. iCLIP reveals the function of hnRNP particles in splicing at individual nucleotide resolution. *Nature Structural & Molecular Biology*, 17(7):909–915.
- Kurban, G., E. Duplan, N. Ramlal, V. Hudon, Y. Sado, Y. Ninomiya, and A. Pause. 2008. Collagen matrix assembly is driven by the interaction of von Hippel-Lindau tumor suppressor protein with hydroxylated collagen IV alpha 2. *Oncogene*, 27(7):1004–1012.
- Kurban, Ghada, V. Hudon, E. Duplan, M. Ohh, and A. Pause. 2006. Characterization of a von Hippel Lindau pathway involved in extracellular matrix remodeling, cell invasion, and angiogenesis. *Cancer Research*, 66(3):1313–1319.
- Kwon, S. C., H. Yi, K. Eichelbaum, S. Föhr, B. Fischer, K. T. You, A. Castello, J. Krijgsveld, M. W. Hentze, and V. N. Kim. 2013. The RNA-binding protein repertoire of embryonic stem cells. *Nature Structural & Molecular Biology*, 20(9):1122–1130.
- Lange, C. A. K., U. F. O. Luhmann, F. M. Mowat, A. Georgiadis, E. L. West, S. Abrahams, H. Sayed, M. B. Powner, M. Fruttiger, A. J. Smith, J. C. Sowden, P. H. Maxwell, R. R. Ali, and J. W. B. Bainbridge. 2012. Von Hippel-Lindau protein in the RPE is essential for normal ocular growth and vascular development. *Development (Cambridge, England)*, 139(13):2340–2350.
- Laplante, J. M., F. O'Rourke, X. Lu, A. Fein, A. Olsen, and M. B. Feinstein. 2000. Cloning of human Ca²⁺ homeostasis endoplasmic reticulum protein (CHERP): regulated expression of antisense cDNA depletes CHERP, inhibits intracellular Ca²⁺ mobilization and decreases cell proliferation. *The Biochemical Journal*, 348 Pt 1:189–199.

- Lee, F. C. Y., and J. Ule. 2018. Advances in CLIP Technologies for Studies of Protein-RNA Interactions. *Molecular Cell*, 69(3):354–369.
- Lee, S. R., and J. Lykke-Andersen. 2013. Emerging roles for ribonucleoprotein modification and remodeling in controlling RNA fate. *Trends in Cell Biology*, 23(10):504–510.
- Lee, Y., W. Hwang, J. Jung, S. Park, J. J. T. Cabatbat, P.-J. Kim, and S.-J. V. Lee. 2016. Inverse correlation between longevity and developmental rate among wild *C. elegans* strains. *Aging (Albany NY)*, 8(5):986–994.
- Lerner, M. R., and J. A. Steitz. 1979. Antibodies to small nuclear RNAs complexed with proteins are produced by patients with systemic lupus erythematosus. *Proceedings of the National Academy of Sciences of the United States of America*, 76(11):5495–5499.
- Li, C., J. Lu, and B. Zhang. 2012. Development of a novel chronic intermittent hypoxia chamber. *Sleep & Breathing = Schlaf & Atmung*, 16(1):177–179.
- Licatalosi, D. D., A. Mele, J. J. Fak, J. Ule, M. Kayikci, S. W. Chi, T. A. Clark, A. C. Schweitzer, J. E. Blume, X. Wang, J. C. Darnell, and R. B. Darnell. 2008. HITS-CLIP yields genome-wide insights into brain alternative RNA processing. *Nature*, 456(7221):464–469.
- Liepelt, A., I. S. Naarmann-de Vries, N. Simons, K. Eichelbaum, S. Föhr, S. K. Archer, A. Castello, B. Usadel, J. Krijgsveld, T. Preiss, G. Marx, M. W. Hentze, D. H. Ostareck, and A. Ostareck-Lederer. 2016. Identification of RNA-binding Proteins in Macrophages by Interactome Capture. *Molecular & Cellular Proteomics: MCP*, 15(8):2699–2714.
- Liu, T., Y. Wu, X. Dong, C. Pan, G. Du, J. Yang, W. Wang, X. Bao, P. Chen, M. Pan, and C. Lu. 2017. Identification and characterization of the BmCyclin L1-BmCDK11A/B complex in relation to cell cycle regulation. *Cell Cycle*, 16(9):861–868.
- Lozzio, C. B., and P. W. Wigler. 1971. Cytotoxic effects of thiopyrimidines. *Journal of Cellular Physiology*, 78(1):25–32.

- Maguire, S. M., C. M. Clark, J. Nunnari, J. K. Pirri, and M. J. Alkema. 2011. The *C. elegans* Touch Response Facilitates Escape from Predacious Fungi. *Current Biology*, 21(15):1326–1330.
- Masuda, K., K. Abdelmohsen, and M. Gorospe. 2009. RNA-binding proteins implicated in the hypoxic response. *Journal of Cellular and Molecular Medicine*, 13(9A):2759–2769.
- Matia-González, A. M., E. E. Laing, and A. P. Gerber. 2015. Conserved mRNA-binding proteomes in eukaryotic organisms. *Nature Structural & Molecular Biology*, 22(12):1027–1033.
- McMahon, L., J. M. Muriel, B. Roberts, M. Quinn, and I. L. Johnstone. 2003. Two Sets of Interacting Collagens Form Functionally Distinct Substructures within a *Caenorhabditis elegans* Extracellular Matrix. *Molecular Biology of the Cell*, 14(4):1366–1378.
- Mehta, R., K. A. Steinkraus, G. L. Sutphin, F. J. Ramos, L. S. Shamieh, A. Huh, C. Davis, D. Chandler-Brown, and M. Kaeberlein. 2009. Proteasomal regulation of the hypoxic response modulates aging in *C. elegans*. *Science (New York, N.Y.)*, 324(5931):1196–1198.
- Mello, C. C., J. M. Kramer, D. Stinchcomb, and V. Ambros. 1991. Efficient gene transfer in *C. elegans*: extrachromosomal maintenance and integration of transforming sequences. *The EMBO Journal*, 10(12):3959–3970.
- Mitchell, D. H., J. W. Stiles, J. Santelli, and D. R. Sanadi. 1979. Synchronous growth and aging of *Caenorhabditis elegans* in the presence of fluorodeoxyuridine. *Journal of Gerontology*, 34(1):28–36.
- Mitchell, J. R., M. Verweij, K. Brand, M. van de Ven, N. Goemaere, S. van den Engel, T. Chu, F. Forrer, C. Müller, M. de Jong, W. van IJcken, J. N. M. IJzermans, J. H. J. Hoeijmakers, and R. W. F. de Bruin. 2010. Short-term dietary restriction and fasting precondition against ischemia reperfusion injury in mice. *Aging Cell*, 9(1):40–53.
- Mitchell, S. F., S. Jain, M. She, and R. Parker. 2013. Global analysis of yeast mRNPs. *Nature Structural & Molecular Biology*, 20(1):127–133.

- Moore, M. J. 2005. From birth to death: the complex lives of eukaryotic mRNAs. *Science (New York, N.Y.)*, 309(5740):1514–1518.
- Moore, P. K., R. K. Hsu, and K. D. Liu. 2018. Management of Acute Kidney Injury: Core Curriculum 2018. *American Journal of Kidney Diseases: The Official Journal of the National Kidney Foundation*, 72(1):136–148.
- Müller, R.-U., F. Fabretti, S. Zank, V. Burst, T. Benzing, and B. Schermer. 2009. The von Hippel Lindau tumor suppressor limits longevity. *Journal of the American Society of Nephrology: JASN*, 20(12):2513–2517.
- Naik, J., C. M. Hau, L. ten Bloemendaal, K. S. Mok, N. Hajji, A. M. Wehman, S. Meisner, V. Muncan, N. J. Paauw, H. E. de Vries, R. Nieuwland, C. C. Paulusma, and P. J. Bosma. 2019. The P4-ATPase ATP9A is a novel determinant of exosome release. *PLoS ONE*, 14(4).
- Niranjanakumari, S., E. Lasda, R. Brazas, and M. A. Garcia-Blanco. 2002. Reversible cross-linking combined with immunoprecipitation to study RNA-protein interactions in vivo. *Methods (San Diego, Calif.)*, 26(2):182–190.
- Orphanides, G., and D. Reinberg. 2002. A unified theory of gene expression. *Cell*, 108(4):439–451.
- Ortiz-Barahona, A., D. Villar, N. Pescador, J. Amigo, and L. del Peso. 2010. Genome-wide identification of hypoxia-inducible factor binding sites and target genes by a probabilistic model integrating transcription-profiling data and in silico binding site prediction. *Nucleic Acids Research*, 38(7):2332–2345.
- Paix, A., A. Folkmann, and G. Seydoux. 2017. Precision genome editing using CRISPR-Cas9 and linear repair templates in *C. elegans*. *Methods (San Diego, Calif.)*, 121–122:86–93.
- Park, H.-E. H., Y. Jung, and S.-J. V. Lee. 2017. Survival assays using *Caenorhabditis elegans*. *Molecules and Cells*, 40(2):90–99.
- Piñeiro, D., M. Stoneley, M. Ramakrishna, J. Alexandrova, V. Dezi, R. Juke-Jones, K. S. Lilley, K. Cain, and A. E. Willis. 2018. Identification of the RNA polymerase I-RNA interactome. *Nucleic Acids Research*, 46(20):11002–11013.

- Pocock, J. M., and D. G. Nicholls. 1998. Exocytotic and nonexocytotic modes of glutamate release from cultured cerebellar granule cells during chemical ischaemia. *Journal of Neurochemistry*, 70(2):806–813.
- Pothof, J., G. van Haften, K. Thijssen, R. S. Kamath, A. G. Fraser, J. Ahringer, R. H. A. Plasterk, and M. Tijsterman. 2003. Identification of genes that protect the *C. elegans* genome against mutations by genome-wide RNAi. *Genes & Development*, 17(4):443–448.
- Praitis, V., E. Casey, D. Collar, and J. Austin. 2001. Creation of low-copy integrated transgenic lines in *Caenorhabditis elegans*. *Genetics*, 157(3):1217–1226.
- Provenzano, R., A. Besarab, C. H. Sun, S. A. Diamond, J. H. Durham, J. L. Cangiano, J. R. Aiello, J. E. Novak, T. Lee, R. Leong, B. K. Roberts, K. G. Saikali, S. Hemmerich, L. A. Szczech, K.-H. P. Yu, and T. B. Neff. 2016. Oral Hypoxia-Inducible Factor Prolyl Hydroxylase Inhibitor Roxadustat (FG-4592) for the Treatment of Anemia in Patients with CKD. *Clinical Journal of the American Society of Nephrology: CJASN*, 11(6):982–991.
- Puelles, V. G., W. E. Hoy, M. D. Hughson, B. Diouf, R. N. Douglas-Denton, and J. F. Bertram. 2011. Glomerular number and size variability and risk for kidney disease. *Current Opinion in Nephrology and Hypertension*, 20(1):7–15.
- Queiroz, R. M. L., T. Smith, E. Villanueva, M. Marti-Solano, M. Monti, M. Pizzinga, D.-M. Mirea, M. Ramakrishna, R. F. Harvey, V. Dezi, G. H. Thomas, A. E. Willis, and K. S. Lilley. 2019. Comprehensive identification of RNA-protein interactions in any organism using orthogonal organic phase separation (OOPS). *Nature Biotechnology*, 37(2):169–178.
- Quinternet, M., M.-E. Chagot, B. Rothé, D. Tiotiu, B. Charpentier, and X. Manival. 2016. Structural Features of the Box C/D snoRNP Pre-assembly Process Are Conserved through Species. *Structure (London, England: 1993)*, 24(10):1693–1706.
- Rao, U. V., and H. N. Wagner. 1972. Normal weights of human organs. *Radiology*, 102(2):337–339.
- Rocak, S., and P. Linder. 2004. DEAD-box proteins: the driving forces behind RNA metabolism. *Nature Reviews. Molecular Cell Biology*, 5(3):232–241.

- Scherrer, T., N. Mittal, S. C. Janga, and A. P. Gerber. 2010. A screen for RNA-binding proteins in yeast indicates dual functions for many enzymes. *PloS One*, 5(11):e15499.
- Shen, C., D. Nettleton, M. Jiang, S. K. Kim, and J. A. Powell-Coffman. 2005. Roles of the HIF-1 hypoxia-inducible factor during hypoxia response in *Caenorhabditis elegans*. *The Journal of Biological Chemistry*, 280(21):20580–20588.
- Showalter, A. E., A. C. Martini, D. Nierenberg, K. Hosang, N. A. Fahmi, P. Gopalan, A. S. Khaled, W. Zhang, and A. R. Khaled. 2020. Investigating Chaperonin-Containing TCP-1 subunit 2 as an essential component of the chaperonin complex for tumorigenesis. *Scientific Reports*, 10(1):798.
- Smith, T., E. Villanueva, R. M. L. Queiroz, C. S. Dawson, M. Elzek, E. C. Urdaneta, A. E. Willis, B. M. Beckmann, J. Krijgsveld, and K. S. Lilley. 2020. Organic phase separation opens up new opportunities to interrogate the RNA-binding proteome. *Current Opinion in Chemical Biology*, 54:70–75.
- Späth, M. R., M. P. Bartram, N. Palacio-Escat, K. J. R. Hoyer, C. Debes, F. Demir, C. B. Schroeter, A. M. Mandel, F. Grundmann, G. Ciarimboli, A. Beyer, J. N. Kizhakkedathu, S. Brodesser, H. Göbel, J. U. Becker, T. Benzing, B. Schermer, M. Höhne, V. Burst, J. Saez-Rodriguez, P. F. Huesgen, R.-U. Müller, and M. M. Rinschen. 2019. The proteome microenvironment determines the protective effect of preconditioning in cisplatin-induced acute kidney injury. *Kidney International*, 95(2):333–349.
- Stroustrup, N., B. E. Ulmschneider, Z. M. Nash, I. F. López-Moyado, J. Apfeld, and W. Fontana. 2013. The *Caenorhabditis elegans* Lifespan Machine. *Nature Methods*, 10(7):665–670.
- Strowitzki, M. J., E. P. Cummins, and C. T. Taylor. 2019. Protein Hydroxylation by Hypoxia-Inducible Factor (HIF) Hydroxylases: Unique or Ubiquitous? *Cells*, 8(5).
- Sulston, J. E., D. G. Albertson, and J. N. Thomson. 1980. The *Caenorhabditis elegans* male: postembryonic development of nongonadal structures. *Developmental Biology*, 78(2):542–576.
- Sulston, J. E., and H. R. Horvitz. 1977. Post-embryonic cell lineages of the nematode, *Caenorhabditis elegans*. *Developmental Biology*, 56(1):110–156.

- Tamburino, A. M., S. P. Ryder, and A. J. M. Walhout. 2013. A compendium of *Caenorhabditis elegans* RNA binding proteins predicts extensive regulation at multiple levels. *G3 (Bethesda, Md.)*, 3(2):297–304.
- Tani, H., and N. Akimitsu. 2012. Genome-wide technology for determining RNA stability in mammalian cells. *RNA Biology*, 9(10):1233–1238.
- Tawk, C., M. Sharan, A. Eulalio, and J. Vogel. 2017. A systematic analysis of the RNA-targeting potential of secreted bacterial effector proteins. *Scientific Reports*, 7(1):9328.
- Teng, Y., L. Lang, and C. Shay. 2019. ATAD3A on the Path to Cancer. *Advances in Experimental Medicine and Biology*, 1134:259–269.
- Timmons, L., D. L. Court, and A. Fire. 2001. Ingestion of bacterially expressed dsRNAs can produce specific and potent genetic interference in *Caenorhabditis elegans*. *Gene*, 263(1–2):103–112.
- Trendel, J., T. Schwarzl, R. Horos, A. Prakash, A. Bateman, M. W. Hentze, and J. Krijgsveld. 2019. The Human RNA-Binding Proteome and Its Dynamics during Translational Arrest. *Cell*, 176(1–2):391-403.e19.
- Tyanova, S., T. Temu, P. Sinitcyn, A. Carlson, M. Y. Hein, T. Geiger, M. Mann, and J. Cox. 2016. The Perseus computational platform for comprehensive analysis of (prote)omics data. *Nature Methods*, 13(9):731–740.
- Uhlmann-Schiffler, H., S. Kiermayer, and H. Stahl. 2009. The DEAD box protein Ddx42p modulates the function of ASPP2, a stimulator of apoptosis. *Oncogene*, 28(20):2065–2073.
- Ule, J., K. B. Jensen, M. Ruggiu, A. Mele, A. Ule, and R. B. Darnell. 2003. CLIP identifies Nova-regulated RNA networks in the brain. *Science (New York, N.Y.)*, 302(5648):1212–1215.
- Uno, M., and E. Nishida. 2016. Lifespan-regulating genes in *C. elegans*. *Npj Aging and Mechanisms of Disease*, 2(1):1–8.
- Urdaneta, E. C., and B. M. Beckmann. 2019. Fast and unbiased purification of RNA-protein complexes after UV cross-linking. *Methods (San Diego, Calif.)*.
- Urdaneta, E. C., C. H. Vieira-Vieira, T. Hick, H.-H. Wessels, D. Figini, R. Moschall, J. Medenbach, U. Ohler, S. Granneman, M. Selbach, and B. M. Beckmann.

2019. Purification of cross-linked RNA-protein complexes by phenol-toluol extraction. *Nature Communications*, 10(1):1–17.
- van den Ecker, D., M. Hoffmann, G. Müting, S. Maglioni, D. Herebian, E. Mayatepek, N. Ventura, and F. Distelmaier. 2015. Caenorhabditis elegans ATAD-3 modulates mitochondrial iron and heme homeostasis. *Biochemical and Biophysical Research Communications*, 467(2):389–394.
- Van Nostrand, E. L., G. A. Pratt, A. A. Shishkin, C. Gelboin-Burkhart, M. Y. Fang, B. Sundararaman, S. M. Blue, T. B. Nguyen, C. Surka, K. Elkins, R. Stanton, F. Rigo, M. Guttman, and G. W. Yeo. 2016. Robust transcriptome-wide discovery of RNA-binding protein binding sites with enhanced CLIP (eCLIP). *Nature Methods*, 13(6):508–514.
- van Rahden, V. A., E. Fernandez-Vizarra, M. Alawi, K. Brand, F. Fellmann, D. Horn, M. Zeviani, and K. Kutsche. 2015. Mutations in NDUFB11, encoding a complex I component of the mitochondrial respiratory chain, cause microphthalmia with linear skin defects syndrome. *American Journal of Human Genetics*, 96(4):640–650.
- Vigne, P., and C. Frelin. 2007. Plasticity of the responses to chronic hypoxia and dietary restriction in an aged organism: evidence from the Drosophila model. *Experimental Gerontology*, 42(12):1162–1166.
- Wallace, M. A. 1998. Anatomy and physiology of the kidney. *AORN Journal*, 68(5):800, 803–816, 819–820; quiz 821–824.
- Wang, Q., Y. Wang, Y. Liu, C. Zhang, Y. Luo, R. Guo, Z. Zhan, N. Wei, Z. Xie, L. Shen, G. Wu, W. Wu, and Y. Feng. 2019. U2-related proteins CHERP and SR140 contribute to colorectal tumorigenesis via alternative splicing regulation. *International Journal of Cancer*, 145(10):2728–2739.
- Wehman, A. M., C. Poggioli, P. Schweinsberg, B. D. Grant, and J. Nance. 2011. The P4-ATPase TAT-5 inhibits the budding of extracellular vesicles in C. elegans embryos. *Current Biology: CB*, 21(23):1951–1959.
- Wen, H., Y. Yu, G. Zhu, L. Jiang, and J. Qin. 2015. A droplet microchip with substance exchange capability for the developmental study of C. elegans. *Lab on a Chip*, 15(8):1905–1911.

- White, J. G., E. Southgate, J. N. Thomson, and S. Brenner. 1986. The structure of the nervous system of the nematode *Caenorhabditis elegans*. *Philosophical Transactions of the Royal Society of London. B, Biological Sciences*, 314(1165):1–340.
- Wilkie, G. S., K. S. Dickson, and N. K. Gray. 2003. Regulation of mRNA translation by 5'- and 3'-UTR-binding factors. *Trends in Biochemical Sciences*, 28(4):182–188.
- Xie, M., and R. Roy. 2012. Increased Levels of Hydrogen Peroxide Induce a HIF-1-dependent Modification of Lipid Metabolism in AMPK Compromised *C. elegans* Dauer Larvae. *Cell Metabolism*, 16(3):322–335.
- Xu, Y., H. Ma, J. Shao, J. Wu, L. Zhou, Z. Zhang, Y. Wang, Z. Huang, J. Ren, S. Liu, X. Chen, and J. Han. 2015. A Role for Tubular Necroptosis in Cisplatin-Induced AKI. *Journal of the American Society of Nephrology: JASN*, 26(11):2647–2658.
- Xue, J. L., F. Daniels, R. A. Star, P. L. Kimmel, P. W. Eggers, B. A. Molitoris, J. Himmelfarb, and A. J. Collins. 2006. Incidence and mortality of acute renal failure in Medicare beneficiaries, 1992 to 2001. *Journal of the American Society of Nephrology: JASN*, 17(4):1135–1142.
- Yeo, G. W., N. G. Coufal, T. Y. Liang, G. E. Peng, X.-D. Fu, and F. H. Gage. 2009. An RNA code for the FOX2 splicing regulator revealed by mapping RNA-protein interactions in stem cells. *Nature Structural & Molecular Biology*, 16(2):130–137.
- Yu, Z. F., and M. P. Mattson. 1999. Dietary restriction and 2-deoxyglucose administration reduce focal ischemic brain damage and improve behavioral outcome: evidence for a preconditioning mechanism. *Journal of Neuroscience Research*, 57(6):830–839.
- Zamore, P. D., J. R. Williamson, and R. Lehmann. 1997. The Pumilio protein binds RNA through a conserved domain that defines a new class of RNA-binding proteins. *RNA (New York, N. Y.)*, 3(12):1421–1433.
- Zeng, M., L. Zhu, L. Li, and C. Kang. 2017. miR-378 suppresses the proliferation, migration and invasion of colon cancer cells by inhibiting SDAD1. *Cellular & Molecular Biology Letters*, 22.

- Zhang, X.-L., Z.-W. Yan, W.-W. Sheng, J. Xiao, Z.-X. Zhang, and Z.-B. Ye. 2011. Activation of hypoxia-inducible factor-1 ameliorates postischemic renal injury via inducible nitric oxide synthase. *Molecular and Cellular Biochemistry*, 358(1–2):287–295.
- Zhang, Y., Z. Shao, Z. Zhai, C. Shen, and J. A. Powell-Coffman. 2009. The HIF-1 hypoxia-inducible factor modulates lifespan in *C. elegans*. *PloS One*, 4(7):e6348.
- Zhou, K. I., Z. Pincus, and F. J. Slack. 2011. Longevity and stress in *Caenorhabditis elegans*. *Aging (Albany NY)*, 3(8):733–753.

9 Publications

9.1 Publications in academic journals

Esmaille, R., M. Ignarski, K. Bohl, T. Krüger, D. Ahmad, L. Seufert, B. Schermer, T. Benzing, R.-U. Müller, and F. Fabretti. 2019. Activation of Hypoxia-Inducible Factor Signaling Modulates the RNA Protein Interactome in *Caenorhabditis elegans*. *IScience*, 22:466–476.

Ignarski, M., C. Rill, R. W. J. Kaiser, M. Kaldirim, R. Neuhaus, **R. Esmaille**, X. Li, C. Klein, K. Bohl, M. Petersen, C. K. Frese, M. Höhne, I. Atanassov, M. M. Rinschen, K. Höpker, B. Schermer, T. Benzing, C. Dieterich, F. Fabretti, and R.-U. Müller. 2019. The RNA-Protein Interactome of Differentiated Kidney Tubular Epithelial Cells. *Journal of the American Society of Nephrology: JASN*, 30(4):564–576.

9.2 International conferences

Esmaille R., Ignarski M., Bohl K., Krüger T., Ahmad D., Seufert L., Schermer B., Benzing T., Müller RU and Fabretti F. Activation of hypoxia-inducible factor signaling modulates the RNA protein interactome in *Caenorhabditis elegans*. German Society of Nephrology 2019. (*poster presentation*)

Esmaille R., Ignarski M., Bohl K., Krüger T., Ahmad D., Seufert L., Schermer B., Benzing T., Müller RU and Fabretti F. Activation of hypoxia-inducible factor signaling modulates the RNA protein interactome in *Caenorhabditis elegans*. 35th Ernst Klenk Symposium 2018. (*poster presentation*)

Esmaille R., Ignarski M., Krüger T., Ahmad D., Bohl K., Schermer B., Benzing T., Müller RU and Fabretti F. Activation of hypoxia-inducible factor signaling modulates the RNA protein interactome in *Caenorhabditis elegans*. 24th Annual Meeting of the RNA Society 2019. (*poster presentation*)

Esmaille R., Ignarski M., Krüger T., Neuhaus R., Atanassov I., Dietrich C., Fabretti F. and Müller RU. RNA Binding Proteins in stress resistance – a screen in *C. elegans*. 34th Ernst Klenk Symposium 2018. (*poster presentation*)

Esmaille R., Krüger T., Ignarski M., Neuhaus R., Dietrich C., Fabretti F. and Müller RU. RNA-bindende Proteine als Modulatoren der Stressantwort – eine Analyse in *C. elegans*. and **Esmaille R.**, Chokkalingam M., Petersen M., Bharill P., Beyer A., Schermer B., Benzing T., Fabretti F. and Müller RU. Studium der Rolle des Hypoxie-Signalweges in der Bildung extrazellulärer Matrix unter Verwendung des Nematodenmodells. German Society of Nephrology 2018. (*poster presentation*)

Esmaille R., Krüger T., Ignarski M., Neuhaus R., Dietrich C., Fabretti F. and Müller RU. RNA Binding Proteins in stress resistance – a screen in *C. elegans*. German European Worm Meeting 2018. (*poster presentation*)

Esmaille R., Petersen M., Bharill P., Chokkalingam M., Mishra T., Beyer A., Schermer B., Benzing T., Fabretti F. and Müller RU. Dissecting the role of hypoxia-signaling in extracellular matrix formation of the nematode. Keystone Symposia: Pushing the Limits of Healthspan and Longevity 2018. (*oral presentation*)

Esmaille R., Krüger T., Ignarski M., Neuhaus R., Fabretti F., Dietrich C., Müller RU. RNA Binding Proteins in stress resistance – a screen in *C. elegans*. 21st International *C. elegans* Conference 2017. (*poster presentation*)

Esmaille R., Krüger T., Ignarski M., Neuhaus R., Fabretti F., Dietrich C., Müller RU. RNA Binding Proteins in stress resistance – a screen in *C. elegans*. German Foundation for Aging Research 2017. (*poster presentation*)

Esmaille R., Petersen M., Bharill P., Fabretti F., Chokkalingam M., Mishra T., Beyer A., Schermer B., Benzing T., Müller RU. Role of VHL-1 in extracellular matrix formation in *C. elegans*. European Worm Meeting 2016. (*poster presentation*)

10 Acknowledgment

Firstly, I would like to thank Prof. Dr. Roman-Ulrich Müller, Prof. Dr. Thomas Benzing and Prof. Dr. Bernhard Schermer for giving me the opportunity to perform my doctoral thesis work at the Nephrolab. Especially, I would like to thank Prof. Dr. Roman-Ulrich Müller for his great supervision and strong support. My questions and ideas were always heard and supported at any time.

I would also like to thank Prof. Dr. Björn Schumacher and Prof. Dr. Günter Schwarz for their respective roles as Chair and assessor during my PhD defense.

A very special thanks goes to Francesca Fabretti. She introduced me to the world of molecular biology and was always open to my questions. If there were any problems in an experiment, she found the solution.

I also would like to thank the entire Nephrolab for a wonderful time. Especially: Sabine Bertsch and Priyanka Kohli, who always had time to go for a cup of hot chocolate, Michael Ignarski who, not only introduced me to the world of radioactivity but also to polish beer, Katrin Bohl for all the bioinformatic help, Lisa Seufert for the great distraction during long incubation phases. Very few people were able to follow our intellectual conversations. Martyna Brütting known as Myna, for all the entertaining conversations and that you were laughing about my jokes even if they were bad. Serena Greco-Torres is definitely to be mentioned here. I am infinitely grateful to you for all the plates and reagents that you have provided for me over the last years. I could always rely on you and will miss the time in the worm room picking worms and chat together.

Part of my work included the Lifespan machine and setting it up was a pleasure because of the people I met. Mostly I thank Cyril Statzer for the great help and Nicholas Stroustrup for supporting us to handle the lifespan machine. I also thank Sebastian Bargfrede being a great support regarding lifespan machine and all other technical challenges.

Last but not least, I would like to thank all of my family, especially my mother Rebecca Esmailie and my sister Mariam Esmailie for all the love and support.

I would also like to thank Sonja Bertram who was always by my side and supported me. I can no longer imagine my life without you.

11 Erklärung

Erklärung zur Dissertation gemäß der Promotionsordnung vom 12. März 2020

„Hiermit versichere ich an Eides statt, dass ich die vorliegende Dissertation selbstständig und ohne die Benutzung anderer als der angegebenen Hilfsmittel und Literatur angefertigt habe. Alle Stellen, die wörtlich oder sinngemäß aus veröffentlichten und nicht veröffentlichten Werken dem Wortlaut oder dem Sinn nach entnommen wurden, sind als solche kenntlich gemacht. Ich versichere an Eides statt, dass diese Dissertation noch keiner anderen Fakultät oder Universität zur Prüfung vorgelegen hat; dass sie - abgesehen von unten angegebenen Teilpublikationen und eingebundenen Artikeln und Manuskripten - noch nicht veröffentlicht worden ist sowie, dass ich eine Veröffentlichung der Dissertation vor Abschluss der Promotion nicht ohne Genehmigung des Promotionsausschusses vornehmen werde. Die Bestimmungen dieser Ordnung sind mir bekannt. Darüber hinaus erkläre ich hiermit, dass ich die Ordnung zur Sicherung guter wissenschaftlicher Praxis und zum Umgang mit wissenschaftlichem Fehlverhalten der Universität zu Köln gelesen und sie bei der Durchführung der Dissertation zugrundeliegenden Arbeiten und der schriftlich verfassten Dissertation beachtet habe und verpflichte mich hiermit, die dort genannten Vorgaben bei allen wissenschaftlichen Tätigkeiten zu beachten und umzusetzen. Ich versichere, dass die eingereichte elektronische Fassung der eingereichten Druckfassung vollständig entspricht.“

Teilpublikationen:

Esmailie, R., M. Ignarski, K. Bohl, T. Krüger, D. Ahmad, L. Seufert, B. Schermer, T. Benzing, R.-U. Müller, and F. Fabretti. 2019. Activation of Hypoxia-Inducible Factor Signaling Modulates the RNA Protein Interactome in *Caenorhabditis elegans*. *IScience*, 22:466–476.

10.08.2020, Reza Esmailie,

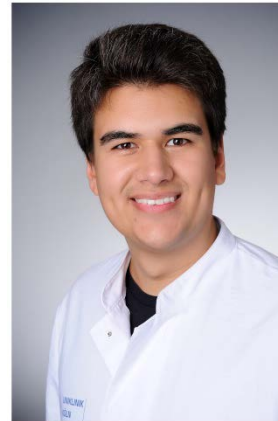


Datum, Name und Unterschrift

12 Curriculum vitae

Persönliche Daten

Nachname: Esmailie
Vorname: Reza
Geburtsdatum: 03. Mai 1988
Geburtsort: Hamburg, Deutschland
Nationalität: Deutsch



Akademische Ausbildung

Seit 08/2015 **Promotion**
Universität zu Köln, Köln, Deutschland
Titel der Dissertation: *Activation of hypoxia-inducible factor signaling modulates the RNA protein interactome in Caenorhabditis elegans.*
Betreuung: Prof. Dr. Müller, Prof. Dr. Schumacher

09/2012 – 07/2015 **Master of Science in Biological Sciences**
Universität zu Köln, Köln, Deutschland
Titel der Masterarbeit: *Elucidating the role of the von Hippel-Lindau tumour suppressor in extracellular matrix formation using C. elegans.*
Betreuer: Prof. Dr. Schermer

10/2008– 09/2012 **Bachelor of Science in Biological Sciences**
Universität zu Köln, Köln, Deutschland
Titel der Bachelorarbeit: *Ubiquitin Dependent DNA Damage Response in Caenorhabditis elegans.*
Betreuer: Prof. Dr. Hoppe

Schulische Ausbildung

1998 – 2007 Gesamtschule Steilshoop, Hamburg, Deutschland
1994 – 1998 Grundschule Edwin-Scharff-Ring, Hamburg, Deutschland